Democratic and Popular Republic of Algeria

Ministry of higher Education and scientific research

University of Echahid Hamma Lakhdar El-Oued

Faculty of Technology

Department of Electrical engineering

THESIS

Presented for obtaining The LMD

Doctorate degrees on telecommunication

Option : System telecommunication

THEME

Millimeter Wave (MMW) communications link for future mobile networks (5G and beyond).

Defended by :

- **BEDDA ZEKRI Abdelbasset**

In front of the jury composed of:

President :	Mr HETTIRI Messaoud	MCA University of Eloued.
Supervisor :	Mr. AJGOU Riadh	MCA University of Eloued.
Examiner :	Mr KHELIL Abdelatif	MCA University of Eloued.
Examiner :	Mr SBAA Salim	Professor University of Biskra
Examiner :	Mr BENARABI Bilal	MCA University of Ouregla
Aid Supervisor:	Mr BEN MAHMOUD Slimane	MCA University of M'sila.

Academic Year : 2021/2022

Acknowledgments

First and foremost, my deep thanks and gratitude to Almighty ALLAH, for His graces and blessings and for giving me strength and ability throughout the years of the PhD to successfully complete my thesis.

I would like to thank very sincerely my thesis supervisor Dr. **AJGOU.Riadh** MCA at El-oued University, for welcoming me in his research team. I would like to express my deep gratitude for the trust that he has placed to me and for his support and advices.

I address my deep appreciation to my co-supervisor Dr **MEFTAH El-hadi** MCA at Chlef University for his relevant advices , explanations , insightful comments, and his support throughout the years of this thesis.

I should like to thank all **members of the Jury** for your invaluable work. Thank you for your effort and for giving me the opportunity to present our work front of you.

At the end of this long-term work, it is with great pleasure that I would like to thank my family: my parents, my sisters, my brothers for their motivation and support, my friend **BEZZAHI Abdelhakim**.

My wife **Asma** and My sons **abdelbari**, **Kheloud** , **Salma** , **Abdelkalek**, **Istabrak**

Thank you for encouraging me and helped me to go successfully through all years.

Abstract

The fifth-generation (5G) wireless communication deployment has already begun. However, some technical problems that need to be updated and further technological improvements are needed. In 5G NR (New Radio), the wide ranges of radio spectrum, from 30 to 300 GHz and 0.1 to 10 THz, referred to as millimeter waves (mm Waves) and sub-terahertz respectively, remain unemployed in wireless communication. These ranges can offer a great opportunity to cope with the huge expansion in data and connectivity in today's mobile society. For this concern, this thesis provides an in-depth statistical study of millimeter wave propagation candidates for 5G/6G systems (28, 38, 60, 73, 100, and 120 GHz) based on different scenarios for outdoor Urban Microcell (UMi) channels with various scenarios especially the geometrical parameters (Co-Pol/X-Pol, SISO/SIMO/MIMO),spatial consistency and also the environmental conditions (LOS/NLOS, rain rate, temperature and humidity for an urban Microcell). The results indicated that the 38 and 73 GHz channels are quite tolerant to the impact of deteriorating environmental conditions and geometrical parameter variations, while the 60, 100 and 120 GHz channels are more affected. In terms of path loss (PL) and path loss exponent (PLE), The results showed that the performance of mmWave channels can be influenced by changing the spatial consistency parameters. the omnidirectional power delay profile (OPDP) showed improved performance over the directional power delay profile (DPDP) for all channels**.**

Keywords: Path loss, mmWaves, Sub-terahertz, LOS/NLOS, OPDP, DPDP , spatial consitency

Résumé

Le déploiement de la communication sans fil de cinquième génération (5G) a déjà commencé. Cependant, certains problèmes techniques doivent être mis à jour et d'autres améliorations technologiques sont nécessaires. En 5G NR (New Radio), les larges gammes du spectre radio, de 30 à 300 GHz et de 0,1 à 10 THz, dénommées respectivement ondes millimétriques (ondes mm) et sub-térahertz, restent sans emploi dans les communications sans fil. Ces gammes peuvent offrir une excellente opportunité pour faire face à l'énorme expansion des données et de la connectivité dans la société mobile d'aujourd'hui. Pour cette préoccupation, cette thèse propose une étude statistique approfondie des candidats à la propagation des ondes millimétriques pour les systèmes 5G/6G (28, 38, 60, 73, 100 et 120 [GHz]) sur la base de différents scénarios pour les microcellules urbaines extérieures. (UMi) avec différents scénarios, notamment les paramètres géométriques (Co-Pol/X-Pol, SISO/SIMO/MIMO), la cohérence spatiale et également les conditions environnementales (LOS/NLOS, taux de pluie, température et humidité pour un microcellule urbaine). Les résultats ont indiqué que les canaux 38 et 73 GHz sont assez tolérants à l'impact de la détérioration des conditions environnementales et des variations de paramètres géométriques, tandis que les canaux 60, 100 et 120 GHz sont plus affectés. En termes de perte de trajet (PL) et d'exposant de perte de trajet (PLE), les résultats ont montré que les performances des canaux mmWave peuvent être influencées en modifiant les paramètres de cohérence spatiale. le profil de retard de puissance omnidirectionnel (OPDP) a montré des performances améliorées par rapport au profil de retard de puissance directionnel (DPDP) pour tous les canaux.

Mots clés : Perte de trajet, ondes millimétrique, sous-Téra Hertz, LOS/NLOS, OPDP, DPDP, cohérence spatiale

الملخص

بدأ بالفعل نشر الاتصالات اللاسلكية من الجيل الخامس ومع ذلك، هناك بعض المشاكل التقنية التي تحتاج إلى تحديث وهناك حاجة إلى مزيد من التحسينات التكنولوجية. في الجيل الخامس لراديو الجديد، تظل النطاقات الواسعة من الطيف الراديوي، من 30 إلى 300 جيجاهرتز و 0.1 إلى 10 تيراهيرتز ، المشار إليها باسم موجات المليمترية (موجات مم) وتيراهيرتز الفرعية على التوالي ، غير مستغلة في مجال الاتصالات اللاسكية. يمكن أن توفر هذه النطاقات فرصة رائعة للتعامل مع التوسع الهائل في البيانات والاتصال في مجتمع المحمول اليوم. لهذا الشيء، توفر هذه الأطروحة دراسة إحصائية متعمقة لانتشار الموجات المليمترية المرشحة لأنظمة الاتصال للجيل الخامس و السادس (28 ، 38 ، 60 ، 73 ، 100 ، و 120 جيجاهرتز) بناءً على سيناريوهات مختلفة للخلية الدقيقة الموجودة في بيئة حضرية بإستعمال السيناريوهات المختلفة و بالخصوص تلك التي تتعلق بالمعلمات الهندسية للهوائي والتوافق المكاني وكذلك الظروف البيئية خط رؤية مباشر وغير مباشر سرعة المطر ودرجة الحرارة والرطوبة لـ ميكروخلية الحضرية .أشارت النتائج إلى أن قنوات 38 و 73 جيجاهرتز تتحمل تأثير الظروف البيئية المتدهورة وتغيرات المعلمات الهندسية، في حين أن القنوات 60 و 100 و 120 جيجاهرتز أكثر تأثراً. من حيث خسارة المسير (PL) وأسّ خسارة المسير (PLE) ، أوضحت النتائج أن أداء قنوات الموجات mmWave يمكن أن يتأثر بتغيير معلمات التوافق المكاني. أظهر صفة تأخير القدرة متعدد الاتجاهات (OPDP) أداءً محسنًا بالنسبة إلى صفة تأخير القدرة الاتجاهي (DPDP) لجميع القنوات.

الكلمات المفتاحية : خسارة المسار ، الموجات ملمترية ، تيراهيرتز الفرعية ، LOS / NLOS، OPDP، DPDP ، الاتساق المكاني.

Publications & communications associated to this thesis

1 International communications

1.1 ZEKRI, Abdelbasset BEDDA, and Riadh AJGOU. "Study of mmWave channels for different scenarios." *2019 6th International Conference on Image and Signal Processing and their Applications (ISPA)*. IEEE, 2019.

1.2 **International Conference paper** ‘’ Impact of Antenna Polarization on a Statistical Channel Modeling in 5G Cellular Communications ’’
oral presentation in International Pluridisciplinary PhD Meeting , IPPM 2020 which was organized 1st Edition, February 23-26, 2020 at the University of El-Oued.

1.3 Zekri, Abdelbasset Bedda, et al. "Analysis of outdoor to indoor penetration loss for mmwave channels." *2020 1st International Conference on Communications, Control Systems and Signal Processing (CCSSP)*. IEEE, 2020.

1.4 Zekri, Abdelbasset Bedda, Riadh Ajgou, and Messaoud Hettiri. "Impact of Azimuth and Elevation Half Power Beam Width on Human Blockage scenarios in mmWave Channels." *2020 1st International Conference on Communications, Control Systems and Signal Processing (CCSSP)*. IEEE, 2020.

2 International Publications

2.1 Zekri, Abdelbasset Bedda, Riadh Ajgou, and El-Hadi Meftah. "Effect of Spatial Consistency Parameters on 5G Millimeter Wave Channel Characteristics." *Progress In Electromagnetics Research B* 93 (2021): 67-86.

2.2 Zekri, Abdelbasset Bedda, Riadh Ajgou, "Statistical Analysis of 5G/6G Millimeter Wave Channels for different scenarios.", "Journal of Communications Technology and Electronics ", Vol. 67 N° 7 (2022).

List of figures

Chapter 01 : Introduction general

Chapter 02 : State of the Art:

Chapter 03 : Statistical Analysis of 5G/6G Millimeter Wave Channels for different scenarios:

Chapter 04 :Analysis of Outdoor to Indoor Penetration Loss for mmWave Channels

Chapter 05 : The impact of azimuth and elevation Half Power Beam Width on Human Blockage scenarios in mmWave Channels

Chapitre 06 : Effect of spatial consistency parameters on 5G Millimeter Wave channel characteristics

List of Table

List of Acronym

ABG : alpha-beta-gamma

AOA : Angle of Arrival.

AOD : Angle of Departure.

BER: Bit Error Rate.

BS: Base Station.

CI : Close In.

CIF : Close In Frequency.

CIR : Channel Impulse Response.

Co-Pol : Coherent Polarization .

CW : Continuous Wave.

DPDP : Directional Power Delay Profile.

D2D : Device to Device.

FCC : Federal Communications Commission.

FI : Floating Intercept

GSCM : Geometry Stochastic Channel Model.

HPBW: Half Power Band Width.

IoT : Internet of Think.

ITU-R : International Telecommunication Union Radio communication

LOS : Line of Sight .

LRS : Link Registration System.

LSPs : Large Scale Parameters.

LTE : Long Term Evolution .

MIMO : Multiple Input Multiple Output.

mmWave : millimeter wave

M2M : machine-to-machine.

METIS : Mobile and Wireless Communications Enablers for the Twenty-Twenty Information Society

MiWEBA : Millimeter- Wave Evolution for Backhaul & Access

MU–MIMO : Multi User Multiple Input Multiple Output.

NYUSIM : New York University Simulator.

NLOS : Non Line Of Sight.

O2I : Outdoor to Indoor

O2I : Outdoor to Indoor

OPDP : Omni Directional Power Delay Profile.

PDP : Power Delay Profile.

PL : Path Loss.

PLE : Path Los Exponent.

QoE: Quality of Experience.

QoS: Quality of Service.

SIRCIM: Simulation of Indoor Radio Channel Impulse Response Models.

SMRCIM: Simulation of Mobile Radio Channel Impulse Response Models

SISO : Single Input Single Output.

SIMO: Single Input Single Output.

SL : Spatial Lobe.

SSCM : Spatial Statistical Channel Model.

RX : Receiver.

RF : Radio Frequency.

RMS : Root Mean Square.

RMa : Rural Macro cell.

TX : transmitter

TCSL : Time Cluster Spatial Lobe.

TC: Time Cluster.

UMi : Urban Micro-cell.

UHF : Ultra High Frequency.

UMa : Urban Macro cell.

USFCC : United States Federal Communications Commission

UE : User Equipment.

UT: User Terminal

V2V : vehicle to vehicle

XPD : Cross Polarization Discrimination.

X-Pol : Cross Polarization.

1U-MIMO : One User Multiple Input Multiple Output.

3GPP : 3rd Generation Partnership Project.

5G: fifth generation.

1 General introduction

1.1 Introduction

During the last two decades, the world has observed the rapid progression of mobile communication technologies from GSM to LTE-A systems [1]. In the last decade, wireless communications have experienced an explosive growth with the demand for higher data rates. As the demand of wireless communication systems for high data rates quickly increases, there is a very big need for more frequency spectrum. Higher frequency spectrum is needed to accommodate the increases in data usage. One of the solution is using millimeter waves (mmWave) where a massive amount of raw bandwidth exists [1], [2], [3]. The Fifth Generation Mobile Network (5G) is the next generation of wireless communications, which will be 10 times faster than that of the traffic compared of today's network. The mmWave technology is one of the emerging technologies in 5G. As the numbers of mobile devices and wireless applications have increased over the years, there is much competition for frequency bands in the existing radio frequency spectrum (below 6 GHz). This causes issues such as slower service, dropped calls, and network congestion. However, the use of mmWave technology allows operation in the 30-300 GHz range. It will provide higher bandwidth for increased data and information transmissions. These frequencies can carry large amounts of data at very high speeds and with very low latency.

In mmWave, there have a massive amount of bandwidth. The large bandwidth opportunity for mmWave is the new frontier for enhanced mobile broadband, internet of things (IoT), machine-to-machine communication (M2M), vehicle to vehicle (V2V), vehicle to everything (V2V), AR/VR devices, cloud gaming systems and so on[3]. However, there are challenges in this technology as these short millimeter waves are correlated with powerful free space path loss [4]. Thus, it becomes essential to understand the physical aspect associated with mmWave propagation. This thesis is fundamentally performed in the physical layer and is an extension and enhancement of the 5G channel simulator, NYUSIM, developed by NYU wireless lab for mmWave indoor and outdoor communications.

1.2 Evolution of 5G Communications

Current 4G system is supposed to be at least five times faster than 3G services and theoretically, it can provide download speeds of up to 100Mbps. 5G offers to take that into multi-gigabits per second. 5G is an unemployed network system that has undoubted high data rate, reliable and low latency than the previous generations According to the Next Generation Mobile Network's 5G white paper[5], 5G connections must be based on 'user experience, system performance, enhanced services, business models and management & operations'.

The 5G New Radio (NR) specification was released by standards body 3GPP in late 2017 - and chips are already being built '5G-ready'. Greater bandwidth provides faster download speeds and the ability to run more complex mobile internet apps [6].

As 5G is still in development, it is not yet open for use by anyone. However, many companies have started designing 5G products and field experimenting them. Nokia Qualcomm, Samsung,Ericsson and BT, with growing numbers of companies forming 5G partnerships and pledging money to continue to research into 5G and its application [7].

1.3 Millimeter Wave

Millimeter Wave technology is being rapidly adopted for users ranging from enterprise level data centers to single consumers with smart phones requiring higher bandwidth[5], the demand for newer technologies to deliver these transmission rates is higher than ever before higher data , Fig 1.1 shows the overview of millimeter wave. It shows the same air interface for access, D2D, and wireless self-backhaul network in mmWave band. These features are the main deployment for mmWave.

Millimeter waves represent the RF Signal spectrum between the frequencies of 30 GHz and 300 GHz with a wavelength between 1–10 millimeters. But in terms of wireless networking and communications equipment, the name mmWave generally corresponds to a few select bands of radio frequencies found around 38, 60 GHz and more. Recently, the high potential 70 GHz and 80 GHz bands have been assigned for the public domain for the purpose of wireless networking and communications. 5G will bring mobility to mmWave communications as the next-gen wireless network attempts to serve more people and even things with a major expansion of mobile services.

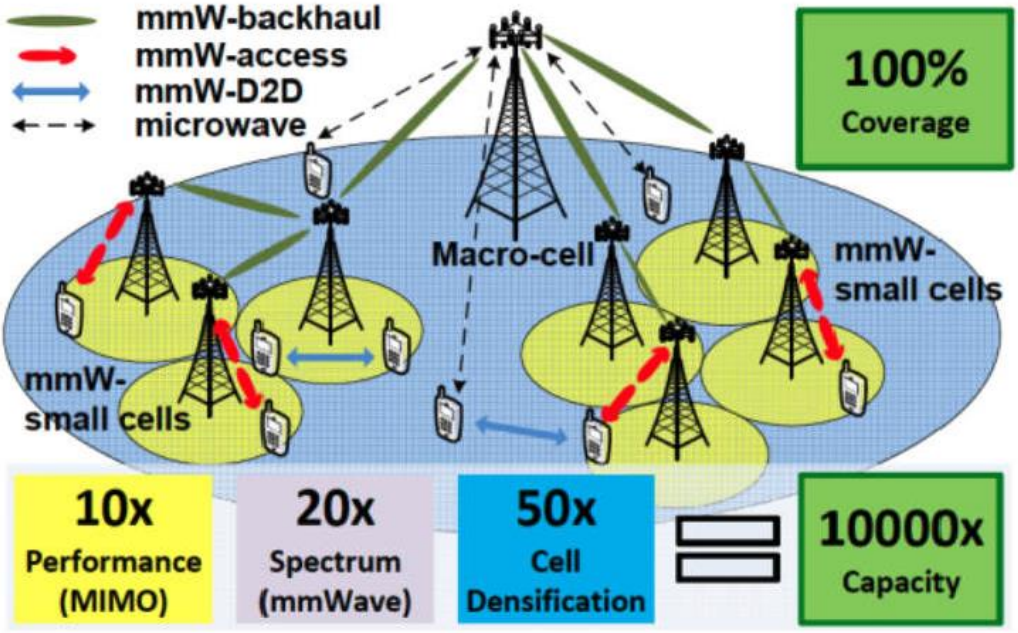

Fig. 1.1 5G Millimeter-wave Networks Overview

1.4 Research Motivation

Channel models and measurements across a extensive range of candidate bands for 5G wireless channels are contemplated. It is motivated by the various propagation and spatial characteristics between different bands and channel models within a various bands. There is numerous challenges to mobilize mmWave communications including coverage, robustness, device size etc. Innovation is required to overcome significant path loss above 28 GHz, to optimize design for User Equipment (UE) etc [8].

Due to its short range of about a kilometer, millimeter wave travels by line of sight, so physical objects like buildings and trees can block its high-frequency wavelengths. Reflections provide alternative paths when LOS blocked, alternative paths in mmWave can have very large receive signal. The main characteristics of mmWave communications are severe attenuation, sparse-scattering environment, and large bandwidth, vulnerability to barriers and antenna misalignment, massive beamforming operation. Motivated by these challenges, this thesis considers mmWave communications and investigates performance analysis of statistical channel for various spectrums.

1.5 Proposed Research Approach

In this thesis, we investigated different factor confronted by 5G/6G Millimeter Wave during propagation in the space:

- Statistical analysis of 5G/6G millimeter wave channels for different scenarios.
- Analysis of outdoor to indoor penetration loss for mmWave channels.
- Impact of azimuth and elevation half power beam width on human blockage scenarios in mmWave channels.
- Effect of spatial consistency parameters on 5G millimeter wave channel characteristics.

The study is based on a novel simulator named NYUSIM [9] [10], which is built upon a statistical channel model for 5G radio communication. It can handle RF bandwidth up to 800 MHz, which is suitable for statistical channel modeling of 5G mmWave based cellular communication. Here, we have considered six operating carrier frequency of 28, 38, 60, 73, 100, 120 [GHz]. The directional, omnidirectional and small-scale power delay profiles (PDPs) have considered.

1.6 Thesis Contribution

An extensive simulation has been carried out to analyze 5G/6G millimeter waves channels statistics with different scenarios. Compared with the existing studies, our key contributions in this thesis can be summarized as follows:

1. An in-depth study of the propagation of different frequency bands using various scenarios was carried out, especially the geometric parameters (Co-Pol / X-Pol, SISO / SIMO / MIMO).
2. The effect of Multi User MIMO (MU–MIMO) on the mmWaves channel characteristics mainly the impact of switching from 1U-MIMO to 2U-MIMO and 2U-MIMO to 4U-MIMO are discussed where in the literature the most researchers have not investigated this study.
3. The effect of switching from LOS to NLOS.

4. Focusing on the analysis of the propagation of frequency bands around 100 [GHz]

(sub-terahertz) that are candidates for 6G systems, taking into account the potential scenarios with additional analysis and details.

5. The performance of mmWave channels can be influenced by changing the spatial consistency parameters.

The contributed spatial analysis could be helpful for modeling and designing the statistical channel model for future 5G/6G mmWave communication. The general aim of this research is to develop a statistical channel modeling of 5G/6G millimeter-wave cellular communication. This thesis is based on statistical channel modeling software developed by NYUWireless known as NYUSIM. Different parameters affecting the channel have been considered in simulation using NYUSIM software developed at NYUWireless. Channel parameters like directional power delay profile (DPDP), omnidirectional power delay profile (OPDP), small-scale power delay profile at different antenna elements are recorded. Scatter plot of path loss as a function of distance for omnidirectional, directional and best direction is also produced with different statistical parameters like path loss, path loss exponent and standard deviation.

1.7 Thesis Organization

The thesis is organized as follows:

Chapter 1 General introduction where we introduce the current and future trends of mobile traffic demand and briefly discusses next generation wireless communication standards. The chapter also reviews research significance, motivations, and contributions of the thesis.

Chapter 2 we present the state of the art , where we review the different channel Models and discusses the 5G Wireless communications technologies where we focus in mmwave Band literature background related to this research. In the end, discusses the literature background related to this research

Chapter 3 present a Statistical analysis of 5G/6G Millimeter Wave Channels for different scenarios.

Chapter 4 presents an Analysis of Outdoor to Indoor Penetration Loss for mmWave Channels.

Chapter 5 explores the Impact of Azimuth and Elevation Half Power Beam Width on Human Blockage scenarios in mmWave Channels.

Chapter 6 we investigate the Effect of Spatial Consistency Parameters on 5G Millimeter Wave Channel Characteristics.

CHAPTER 02

Sate of the art

2 STATE OF THE ART OF CHANNEL MODELS AND SIMULATORS

2.1 Introduction

The construction and implementation of channel models are becoming increasingly important for wireless communication system design, and computer-aided design tools such as channel simulators are essential for performance evaluation of communications systems and for simulating network deployments, before moving forward with new technologies.

There are several channel simulators that have been developed and used by previous researchers [15-21]. For instance, Smith [22] built simulation software for indoor and outdoor propagation channels by making use of the two-ray Rayleigh fading channel model developed by Clarke [23]. Fraunhofer Heinrich Hertz Institute developed a 3-D multi-cell channel model that can accurately predict the performance for an urban macrocell setup with commercial high-gain antennas, upon which a channel simulator has been built that supports features such as time evolution, scenario transitions, and so on [16]. A channel simulator for indoor scenarios was developed for machine-to-machine applications [17]. Rappaport and Seidel developed a measurement-based statistical indoor channel model named SIRCIM (Simulation of Indoor Radio Channel Impulse Response Models) for the early development of WiFi [4] and the corresponding simulation software to generate channel impulse responses (CIRs) for indoor channels operating from 10 MHz to 60 GHz. A similar open-source RF propagation simulator is SMRCIM (Simulation of Mobile Radio Channel Impulse Response Models), that was useful for simulating outdoor channels [19-20]. Another software simulation program, called BERSIM [21], developed by Fung et al., was able to simulate mobile radio communication links and calculate average bit error rate (BER) and bit-by-bit error patterns, that was useful for evaluating link quality in real time without requiring any radio frequency hardware. More detailed descriptions and comparisons of several popular channels models are provided below.

2.2 SIRCIM Channel Model and Simulator

The SIRCIM model, which is a statistical radio channel impulse response model, was developed based on propagation measurements in indoor factory and open plan office scenarios at 1.3 [GHz] [4] in both LOS and obstructed (OBS) topographies. The model can describe the distribution of the number of multipath components in a particular multipath delay profile, the distribution of the number of multipath components received within a local area, the probability of receiving each multipath component at a particular excess delay, the distributions of the amplitudes, phases, and time delays of multipath components received within a local area, and the probability of receiving a multipath component at small scale locations. The computer simulator SIRCIM, which is built based upon the aforementioned channel impulse response model, is able to recreate multipath power delay profiles (PDPs) and continuous-wave (CW) fading profiles that are representative of measured results. SIRCIM allows the prediction of arriving signals at a receiver from one (or many) transmitters by performing convolutions of transmitted signals with simulated channels.

2.3 SMRCIM Channel Model and Simulator

The SMRCIM channel model and simulator are aimed for outdoor environments including urban microcell (UMi) and suburban scenarios [19], which can generate realistic channels based on extensive measured data. The software package SMRCIM belongs to Wireless Valley Communications, Inc. SMRCIM accurately models various types of multipath, including flat-fading, small delay spreads, and very large delay spreads, which are usually encountered in an urban cellular scenario, and it also models the spatial correlation in small-aperture two-element arrays [19]. SMRCIM has been utilized to generate empirically derived random multipath channel for examining the performance of various techniques in CDMA systems [8].

2.3.1 QuaDRiGa Channel Model and Simulator

QuaDRiGa is developed at the Fraunhofer Heinrich Hertz Institute to enable the modeling of MIMO radio channels for specific network configurations, such as indoor, satellite or heterogeneous configurations. The QuaDRiGa channel model is geometry-based stochastic channel model, which collects features created in SCM(e) and WINNER channel models along with novel modeling approaches which provide features to enable quasi-deterministic multi-link tracking of users (receiver) movements in changing environments. It supports 3D propagation, 3D antenna patterns, time evolving channel traces, scenario transitions and variable terminal speeds. In the QuaDRiGa channel model, it is assumed that the base stations are fixed, the mobile terminals are moving, and scattering clusters are fixed as well and the time evolution of the radio channel is deterministic. QuaDRiGa also supports massive MIMO modeling enabled through a new multi-bounce scattering approach and spherical wave propagation. It will be continuously extended with features required by 5G and frequencies beyond 6 [GHz]. The QuaDRiGa channel model is supported by data from extensive channel measurement campaigns at 10/28/43/60/82 [GHz] performed by the same group.

2.3.2 COST 2100 Channel Model

The COST 2100 channel model [14] is a geometry-based stochastic channel model for MIMO systems that is built on the framework of the earlier COST 259 and 273 models [25], which covers aspects such as multi-user, multi-cellular, and cooperative operation in MIMO systems. The most distinguishing feature of the COST 2100 channel model lies in that it is a cluster-based model which is not constrained by large-scale parameters (LSPs), and the environment is described independent of the mobile station location. Specifically, the COST 2100 channel model defines a large number of clusters with consistent stochastic parameters throughout the simulation environment according to the base station location, as well as the mobile station location, and determining the scattering from the visible clusters at each channel instance, and synthesizes the LSPs based on the cluster scattering. There are two key modeling concepts: *visibility region* and *cluster* [14]. A visibility region denotes a circular region given a fixed size in the simulation area, which determines the visibility of only one cluster. When the mobile station enters a visibility region, the related cluster smoothly increases its visibility. A cluster is represented by an ellipsoid in space as viewed from the base station and from the mobile station, which is characterized with specific positions and orientations toward the base station and mobile station[14].

2.3.3 METIS Channel Models

The METIS channel models consist of a map-based model, a stochastic model, and a hybrid model as a combination of both [11]. The map-based model is based on ray tracing using a simplified 3D geometric description of the propagation environment and thus inherently accounts for major propagation mechanisms such as diffraction, specular reflection, diffuse scattering, blocking, etc. Channel realizations are generated with an implementation of the map-based model and are compared to the measurement results in some selected scenarios by analyzing propagation parameter statistics [11]. The stochastic model extends the geometry based stochastic channel model (GSCM), which has been further developed from WINNER/3GPP, in order to provide multi-dimensional shadowing maps with low complexity, mmWave parameters, direct sampling of the power angular spectrum, and frequency dependent path loss models [11]. The hybrid model provides a flexible and scalable channel modelling framework that tries to imbalance between the simulation complexity and realism. The METIS channel models are intended for the frequency range from sub-1 [GHz] to 86 [GHz] and beyond, bandwidths greater than 500 MHz, massive MIMO, extremely large arrays even beyond stationarity interval, direct device-to-device (D2D), machine-to-machine (M2M) and vehicular- to-vehicular (V2V) communications, spatial consistency between topologies and between users (e.g., birth-death process and/or visibility regions for clusters).

2.3.4 MiWEBA Channel Model

The MiWEBA channel model is a quasi-deterministic channel model aimed for millimeter-wave outdoor mobile access links of small cell base stations with a typical cell radius of several hundred meters [26]. The MiWEBA channel model is developed based on a measurement campaign conducted at 60 [GHz] with an RF bandwidth of 250 MHz on a plaza in downtown Berlin, Germany. The quasi- deterministic channel model is a combination of a geometry-based method for a limited number of multipath components and a stochastic approach, and builds on the representation of the mmWave channel impulse response comprised of a few quasi-deterministic strong rays, a number of relatively weak random rays originating from the static surfaces reflections, and flashing rays originating from moving cars, buses, and other dynamic objects reflections [26]. The key benefit of the quasi-deterministic modeling approach compared to pure statistical models is its inherent support for spatial consistency, since it takes into account the positions of the transmitter and receiver. In the MiWEBA channel model, the propagation loss is calculated by the Friis equation, taking additional losses from the oxygen absorption into consideration. The parameters of reflected rays are calculated based upon the Fresnel equations, plus additional losses due to surface roughness [26]. The quasi-deterministic modeling approach requires a precise description of the scenario, thus it is only applicable to the specific scenario investigated and cannot be extended to other scenarios.

2.3.5 WINNER II Channel Model

The WINNER family is a set of geometry-based stochastic channel models. The channel parameters are determined stochastically, based on statistical distributions extracted from channel measurements. The WINNER II channel model is applicable for link-level and system-level simulations of local area, metropolitan area, and wide area wireless communication systems [27]. The channel model is antenna independent, i.e., different antenna configurations and different element patterns can be inserted. The channel parameters are determined stochastically, based on statistical distributions extracted from channel measurement. Channel realizations are generated by summing contributions of rays with specific channel parameters like delay, power, angle-of-arrival and angle-of-departure. The channel model is applicable to any wireless system operating in 2 - 6 [GHz] frequency range with up to 100 MHz RF bandwidth. As the WINNER II channel model is devised for cellular communication between a fixed base station and a mobile user terminal, it is not adequate for situations where both link ends can be at arbitrary locations, or even ultra-dense deployment, where closely located base stations see partly the same environment. Another known defect of the WINNER approach is the lack of support for spherical waves and consistent modeling of closely located users. In particular, it yields poor realism for cases that need high spatial resolution such as massive MIMO and pencil beamforming.

2.3.6 ITU-R IMT-Advanced Channel Model

The ITU working party 5D has recently been developing a recommendation on the framework and objectives of the future development of IMT for 2020 and beyond. The ITU-R IMT-Advanced channel model is a geometry-based stochastic channel model [28], which is known as a double directional channel model. The modeling methodologies of the ITU-R IMT-Advanced channel model are similar to those in the 3GPP channel model to be described in the following subsection.

2.3.7 3GPP Channel Model

The 3GPP channel model is also a geometry-based stochastic spatial channel model developed based on the 2D channel models from ITU and WINNER II, and has been extended to 3D, which is also inspired by the extension from 2D to 3D channel model published as part of WINNERII/WINNER+ [29]. The channel model is suitable for link-level and system-level simulations to estimate realistic channels between a base station, and one or more UEs, that account for empirical correlations between large-scale parameters. The large-scale parameters denote the omnidirectional RMS delay spread, the azimuth spread, the shadow fading, and the Rician K-factor (for LOS channels), and were shown to exhibit significant correlation for a given base-to-mobile link. It is assumed that each multipath component can be represented by a planar wavefront, characterized by small-scale parameters such as path delays, powers, AoAs, and AoDs, extracted from measurement-based statistical distributions. In the 3GPP channel model, a *cluster* is defined as a group of multipath components traveling close in both the temporal and spatial domains, and a *ray* is defined as a multipath component within a cluster. A joint delay-angle clustering approach is adopted in the 3GPP channel model, such that a group of traveling multipaths must depart and arrive from a unique AoD-AoA angle combination centered around a mean propagation delay. The 3GPP TR 38.901 Release 14 channel model [30] is targeted for carrier frequency range from 0.5 [GHz] to 100 [GHz] and large channel bandwidths (up to 10% of the carrier frequency), and takes into account mmWave propagation aspects such as blocking and atmosphere attenuation. The channel model is also aimed to accommodate user terminal mobility with mobile speeds up to 500 km/h, and develop a methodology considering that model extensions to D2D and V2V may be developed in future work. One of the most prominent blemish of the

3GPP channel model is the unrealistically large number of clusters, which might be proper to model sub-6 [GHz] channels, but is not suitable for modeling mmWave channels that exhibit sparsity [31, 32,33].

2.3.8 Statistical Spatial Channel Model by NYU

NYU WIRELESS conducted mmWave measurements from 2012 through 2017 [32, 34, 35, 36], having acquired a total of over 1 Terabytes of data, at frequencies from 28 to 73 [GHz] in various outdoor environments in UMi, UMa, and RMa environments. as presented in Section 2.1. A 3D SSCM [31] has been developed based upon the measured data, which is comprised of similar modeling steps to the 3GPP channel model [30] such as LOS probability model, large-scale path loss model, large-scale parameters, and small-scale parameters, but with different modeling approaches and/or parameters in each step. For instance, for the large-scale path loss model, the CI model is utilized that has solid physical basis and provides lower computational complexity, higher prediction accuracy and higher parameter stability than the ABG model, as demonstrated in [8] and Chapter 4 of this technical report. For multipath clustering, the time-cluster-spatial-lobe (TCSL) clustering approach is proposed that extends the existing ultra-high frequency (UHF) 3GPP model through the additional model parameters of directional RMS lobe angular spreads for spatial lobes [31].

In the SSCM, TCs are composed of multipath components traveling close in time, and arriving from potentially different directions in a short propagation time window. SLs denote primary directions of departure (or arrival) where energy arrives over several hundred nanoseconds [31]. Per the definitions given above, a TC contains multipath components traveling close in time, but may arrive from different SL angular directions, such that the temporal and spatial statistics are decoupled and can be recovered separately. Similarly, an SL may contain many multipath components arriving (or departing) in a space (angular cluster) but with different time delays. This distinguishing feature is obtained from real- world propagation measurements [36] which have shown that multipath components belonging to the same TC can arrive at distinct spatial pointing angles and that energy arriving or departing in a particular pointing direction can span hundreds or thousands of nanoseconds in propagation delay, detectable due to high-gain steerable directional antennas. The TCSL clustering scheme models the directionality of mmWave channels via separate TCs that have time-delay statistics, and via SLs that represent the strongest directions of multipath arrival and departure [31]. The TCSL framework is physically based (e.g., it uses a fixed inter-cluster void interval to represent the minimum propagation time between possible obstructions causing reflection, scattering, or diffraction), and is derived from field observations based on about 1 Terabytes of measured data over many years, and can be used to extract TC and SL statistics for any measurement or ray-tracing data sets [31]. Fig. 2.1 illustrates an omnidirectional PDP, where there are four multipath taps which are grouped into two time clusters with exponentially decaying amplitudes. The four multipath taps are then grouped into two AOA spatial lobes, as shown in Fig. 2.2.

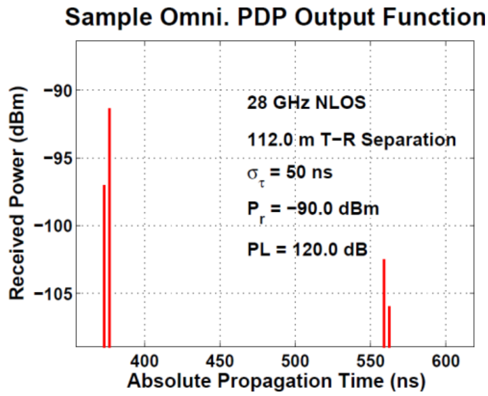

Fig 2.1: Example of an omnidirectional PDP with four multipath taps [31].

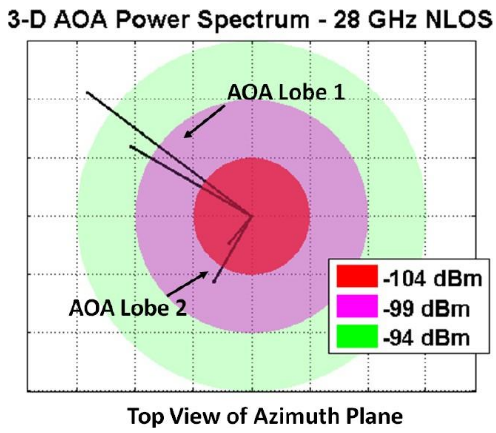

Fig 2.2: Example of an AOA power spectrum with four multipath taps [31].

2.4 5G Communications and Technologies

The next generation (5G) technologies need to be a paradigm shift which includes very high carrier frequency with massive bandwidth, high density of base stations and devices, and very large numbers of antennas. This section overviews the upcoming 5G technology.

2.4.1 5G: Basic Overview

The next (5th) generation wireless network will address the evolution beyond mobile internet to massive IoT (Internet of Things) for the horizon 2019/2020. The main evolution compared with today's 4G and 4.5G (LTE advanced) is that beyond data speed improvements, new IoT and critical communication use cases will require new types of improved performance.

As described in Chapter 1, the increasing internet data traffic has driven the capacity demands for currently deployed 3G and 4G wireless technologies; intensive research toward 5th generation wireless communication networks is thus progressing on many fronts, since 5G technology is expected to be in use even before 2020 (for examples, the South Korean market leader, SK Telecom, signed a very ambitious agreement with Ericsson to develop 5G technology in time to demonstrate a network at 2018 Winter Olympics in Pyeongchang [37]).

2.4.2 5G Key Enabling Technologies

5G networks will be designed to bring the level of performance needed for massive IoT. It will enable a perceived fully ubiquitous connected world. Groundbreaking innovations will drive 5G technologies to reach the fantastic speeds, near-wire line latencies, ubiquitous connectivity with uniform Quality of Experience (QoE), and the strength to connect massive amounts of devices with each other, all working in harmony to provide the user with an immersive experience [26], even while the user is on the move. Future 5G systems will comprise fundamentally new designs to promote wireless capacity utilizing new frequency bands, advanced spectrum efficiency enhancement methods in the legacy band, and seamless synthesis of licensed and unlicensed bands. Figure 2.3 exposes an overview of the key enabling technologies that will permit to reach the 5G main requirements. Consequently, the massively immense capacity demands of the 5G systems will be directed by the following technologies.

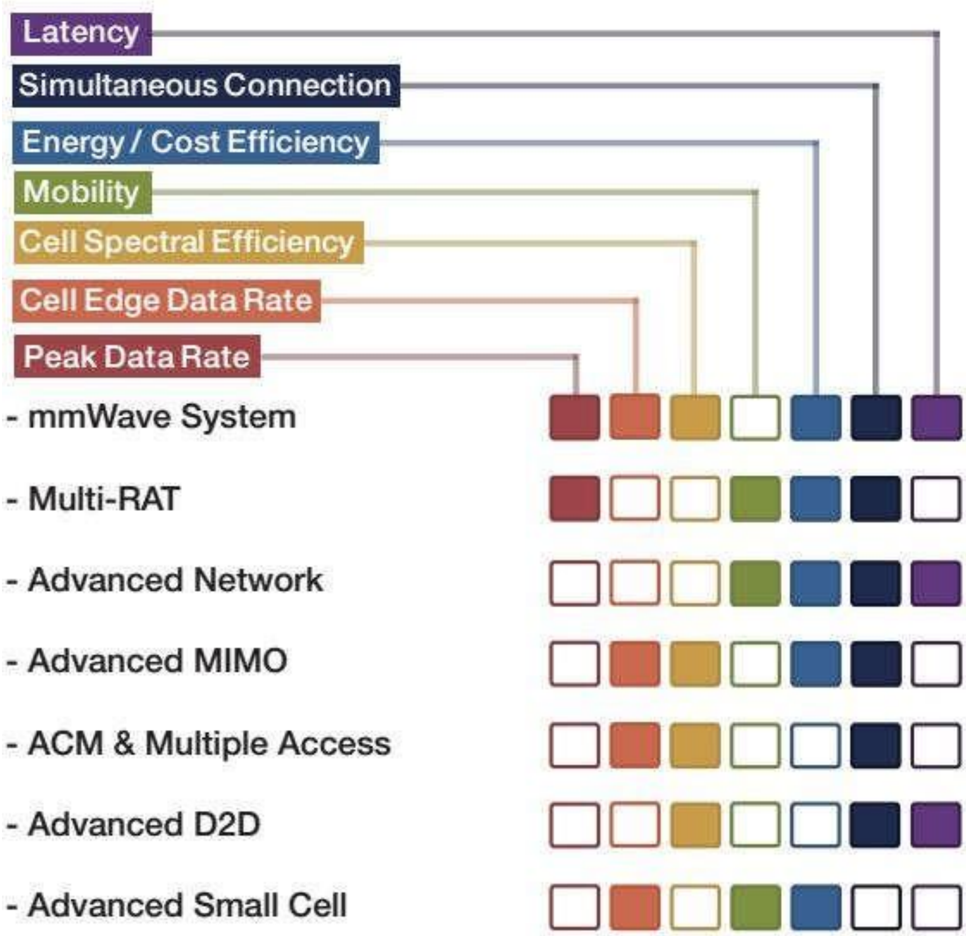

Fig. 2.3 Overview of 5G Key Enabling Technologies. Figure from [36].

2.5 Millimeter Wave Communications

Millimeter wave wireless technology presents the potential to offer bandwidth delivery comparable to that of fiber optics, but without the financial and logistic challenges of deploying fiber the millimeter-wave band refers to the frequency range from 30 [GHz] to 300 [GHz] (or often from 10 [GHz] to 300 [GHz]), which is the highest electromagnetic radiation radio frequency band, with wavelengths ranging from 1 to 100mm [39].

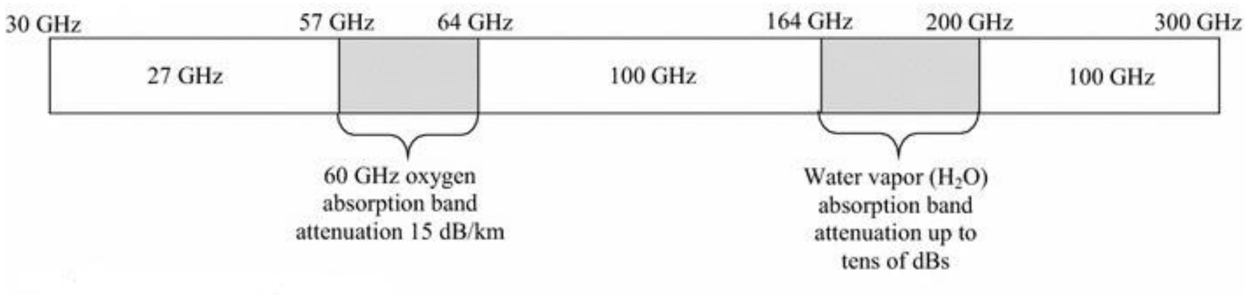

Fig 2.4 Millimeter wave spectrum [36]

However, in the context of wireless communication, the term generally corresponds to a few bands of spectrum near 38, 60 and 94 [GHz], and more recently to a band between 70 [GHz] and 90 [GHz] (also referred to as E-Band), that have been allocated for the purpose of wireless communication in the public domain. Although this new band has gained prominent interest in 5G cellular systems, there are several concerns about its transmission characteristics, as demonstrated in the next subsection.

2.5.1 Millimeter Wave Propagation Characteristics

✓ Free-space Losses

Transmission loss of millimeter wave is accounted by free space loss. If both the transmit and receive antenna apertures are held constant, the link budget actually increases with the frequency, mitigating the higher noise floor associated with broader signal bandwidths. Therefore, the use of higher frequencies should not have any inherent disadvantage compared to lower frequencies, in terms of free space loss.

Again, also MIMO BF gain contributes lessening this high path loss effect, improving an acceptable transmission range.

✓ Atmospheric Losses

Atmospheric gaseous losses of millimeter-wave transmissions due to oxygen molecule (O_2) and water vapor (H_2O) absorption[18][47], actually only at some frequencies (respectively around 60 [GHz] and 180 [GHz], as in Figure 2.5), results in high attenuation of the radio signal.

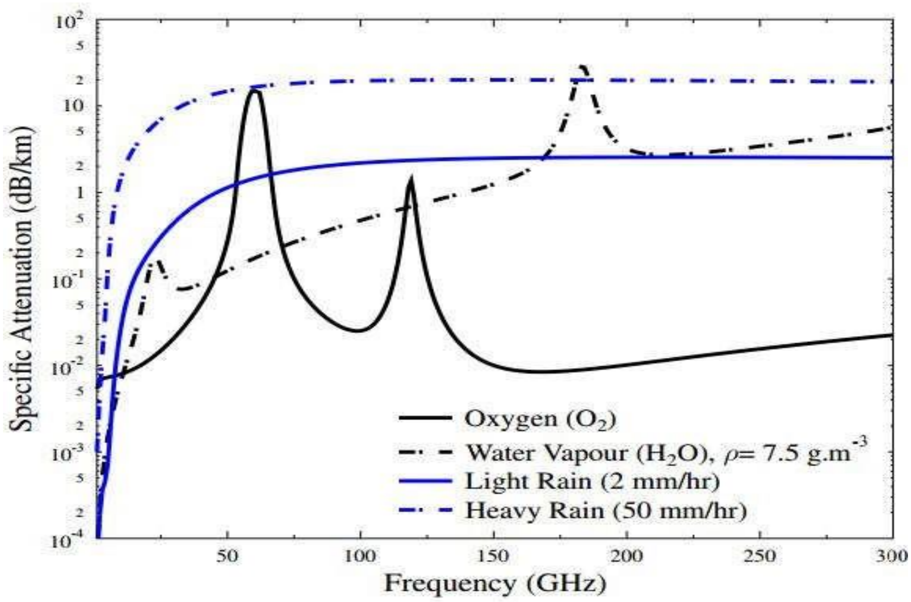

Fig 2.5 Specific attenuation curves of O_2, H_2O and rain at sea level [18],[41]

In Figure 2.5, the O_2 absorption curve maximum are observed at the 60 [GHz] and 119 [GHz] frequencies, at a record of 15 dB/km and 1.4 dB/km loss, respectively. However, by operating at short distances the oxygen absorption loss can be further reduced. For example, by reducing the cell range from 1 km to 100 m, the O_2 absorption at 60 [GHz] and 119 [GHz] drops to only 1.5 dB and 0.14 dB, respectively [42].

Furthermore, it is depicted in Figure 2.5 that H_2O molecules can resonate at 23 [GHz], 183 [GHz] and 323 [GHz], which are associated with a loss of 0.18 dB/km, 28.35 dB/km and 38.6 dB/km, respectively. Hence, atmospheric attenuation imposes an insignificant impact on mmWave signals, especially when transmitting over short distances.

✓ Rain-Induced Fading

Millimeter wave propagation is also affected by rain. Raindrops are roughly the same size as the radio wavelengths and, therefore, cause scattering of the radio signal [43]. The attenuation (dB per km) can be calculated from rain rates (mm per hour), and the curves are plotted in Figure 2.6. Fortunately, the most intense rain tends to fall in selected countries of the world and happens in short bursts, while light rain yields just a little attenuation [40]. Considering today's cell sizes in urban environments are on the order of

200 meters [44], rain attenuation will present a minimal impact on mmWave propagation.

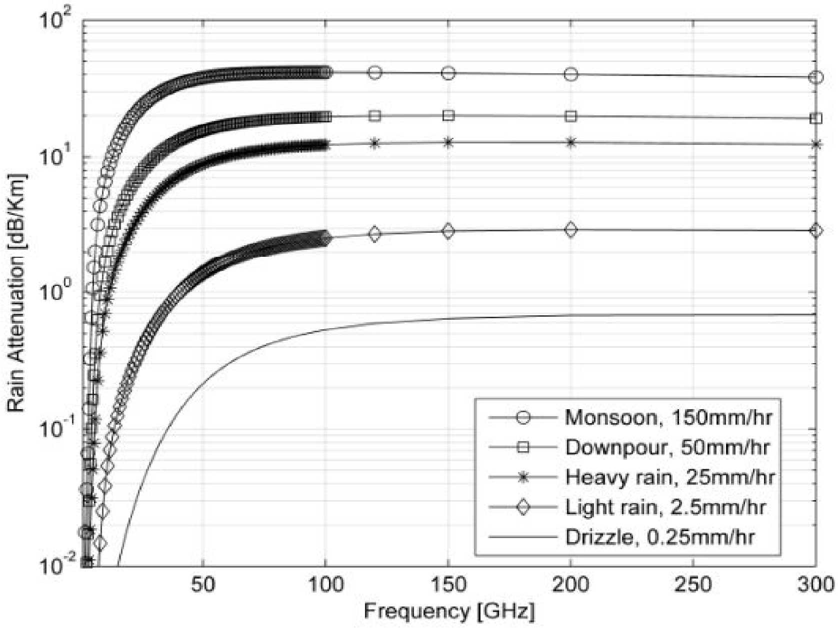

Fig 2.6 Rain attenuations at 1-300 [GHz] frequencies [31].

✓ Foliage Attenuation

While signals at lower frequencies can penetrate more easily through buildings, mmW signals do not penetrate most solid materials very well, due to their small wavelengths. For example, as reported in [40], these signals would not be able to penetrate through solid buildings made of brick or concrete (but they might eventually reach inside the buildings through glass windows and doors). High attenuations for certain materials may aid in keeping mmWave signals transmitted from outdoor base stations restricted to streets and other outdoor structures. Vegetation presence between the transmitter and receiver adds extra attenuation to the signal and it may severely affect the Quality of Service (QoS) of a wireless communication system [42]. The indoor coverage in this case can be provided by other means such as using indoor Wi- Fi or femtocell solutions. Also, foliage losses at millimeter wave frequencies are notable. In fact, foliage loss may be restricting propagation impairment in some cases [43]. As we can see in Figure 2.7, at 80 [GHz] frequency and 10 meters foliage penetration, the loss can be about 23.5 dB, which is about 15 dB higher compared to the loss at 3 [GHz] frequency [40].

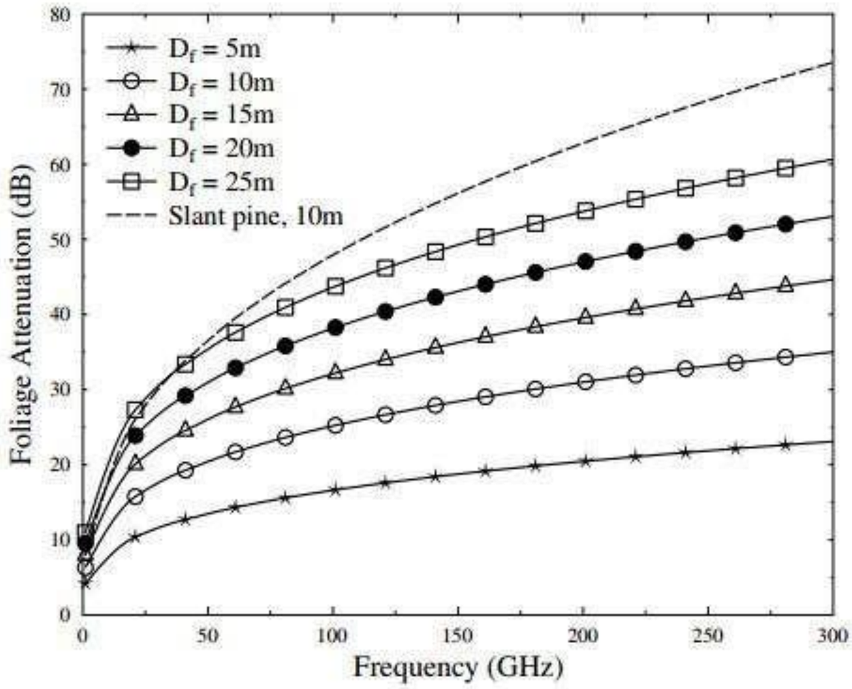

Fig 2.7 Foliage Attenuation vs Frequency *f* [29].

2.5.2 Frequency Licensing

The coordination and licensing of the radio frequency used in various sovereign regions of the world is administered by their corresponding authorities. In some parts of the word, the E-band millimeter wave spectrum has not been opened for public use while in other parts of the world where it has been opened. The details of the licensing scheme are still being worked out.

The licensing scheme is based on a two-tier approach. At first, a non-exclusive nationwide license is acquired from the FCC for the operation of equipment using millimeter wave bands. The FCC license is by itself not a permission to deploy millimeter wave links with impunity, but rather is a prerequisite for the second step. As the second step, a “license” to deploy is obtained by registering individual point- to-point links through an independent link registration system (LRS) developed and maintained by an FCC-appointed database manager. The cost of a nationwide FCC license and the registration of each link is of the order of a few hundred dollars. More recently to a band between 70 [GHz] and 90 [GHz] (also referred to as E-Band), that have been allocated for the purpose of wireless communication in the public domain.

ITU-R selected at the WRC- 15 several frequency bands above 24.25 [GHz] as candidates for 5G networks [45]. It was based on the IMT feasibility study for bands above 6 [GHz] [45]. A number of mmWave bands are currently being considered for global 5G mmWave communications. The 28 and 73[GHz] frequency bands for outdoor scenarios are attractive, as the attenuation loss induced from atmospheric absorption is less than 0.1 dB over a mmWave cell radius of 200 m [36], while it is significantly higher at 60 [GHz] (~4 dB/200 m). Also, the Federal Communications Commission (FCC) has recently issued new rulemakings to bring these bands into service [46]. It is very likely that 28 [GHz] will be used for the first 5G deployments in the South Korea, US and Japan beside that 28, 38, 60 and 73 [GHz] are strong candidate bands for implementing 5G networks [47][48].

2.6 Literature Reviews

5G is the foundation of what's next and the key feature of 5G is millimeter wave (mmWave). mmWave is not just another new radio access standard. Rather, the main novelty of mmWave will be the integration of multiple networks serving diverse sectors, domains, and applications, such as multimedia, virtual reality (VR), augmented reality (AR), Machine-to-Machine (M2M), Internet of Things (IoT), Smart City etc. A recent report shows that data traffic for these new applications are predicted to grow from 2016 to 2021 much larger than the assumed 590% for conventional applications: 770% for mobile video, 950% for mobile VR and 1320% for M2M/IoT [3].

Authors *et al.* [47] presented the motivation for new mm-wave cellular systems, methodology and offer a variety of measurement results that show 28 and 38 [GHz] frequencies can be used when employing steerable directional antennas at base stations and mobile devices. They conducted extensive propagation measurement campaigns at 28 and 38 [GHz] to gain insight on AOA, AOD, RMS delay spread, path loss, and building penetration and reflection characteristics for the design of future mm-wave cellular systems. There are many channel simulators available for different frequencies and different environmental conditions. Various approaches have been proposed for 5G channel modeling. Author in [23] developed a wireless channel using two ray Rayleigh fading. On the basis Clarke's model, Smith developed a simulation tool for indoor and outdoor propagation channel.

There are numerous channel simulators that have been developed and used by earlier researchers. Rappaport and Seidel developed a statistical channel model referred SIRCIM (Simulation of Indoor Radio Channel Impulse Response Models) [44] which is estimated based indoor channel model for the early development of Wireless Fidelity(Wi-Fi). The operating frequency range of SIRCIM was 10 MHz to 60 [GHz].

The model incorporates first- and second-order statistics to characterize the discrete impulse responses of indoor radio channels for both line of-sight (LOS) and obstructed (OBS) topographic. They presented statistical models for wide-band power impulse responses inside open plan buildings. These models were based on propagation measurements from five factory buildings and statistically characterize the impulse responses of open plan building radio channels at 1300 MHz. SMRCIM (Simulation of Mobile Radio Channel Impulse Response Model) channel simulator based on SIRCIM (Simulation of Indoor Radio Channel Impulse Response Model) was developed by Rappaport *et al.* [49] in for operating frequencies up to 60 [GHz].

Fung and Rappaport developed simulation software named BERSIM to simulate mobile radio communications and to estimate average Bit Error Rate [21]. BERSIM was useful for anticipating link quality in the real time of mobile radio communication links without demanding any radio frequency hardware.

Recently, QuaDRiGa [16] was developed at the Fraunhofer Heinrich Hertz Institute to facilitate the modeling of MIMO radio channels for particular network configurations, such as indoor, satellite or heterogeneous arrangements. It is a 3-D multi-cell channel model that can apply to predict the performance for uniform macro cell (UMa) settings with high-gain antennas. QuaDRiGa channel simulator supports many features such as time evolving, scenario transitions etc.

Author in [50] explained one of the early analytical measurement operations done at mmWave frequencies. Here, the channel models were developed for 60-[GHz] indoor, short range communication channels. For the purpose of measurement, a 10-ns resolution sliding correlator was used, with a steerable directional antenna at the transmitter and receiver, having a HPBW of 7˚. With this measurement technique, researchers were able to obtain a large number of Power Delay Profiles (PDP).

Another project known as the COMMINDOR project [51], [54], [55] was carried out in France for the sake of achieving a "very high speed" of 155 Mbit/s, in the early 2000s, for short-range residential scenarios operating at 60 [GHz]. Zhang *et al.* [52] employed the RT technique in order to characterize a directional 60 [GHz] multipath channel based on a 2 × 2 MIMO system. This work was further refined by Torkildson *et al.* in [53] by employing a six-ray channel model for an outdoor scenario in the 60 [GHz] band. Furthermore, the measurements conducted in [44] were used for modeling the path-loss for an indoor scenario associated both with LOS and NLOS environments for transmission over a 60 [GHz] channel using both omni-directional as well as directional transmit and receive antennas.

Rappaport and his team at NYU developed a Novel millimeter wave channel simulator concerning 5G mmWave communication termed NYUSIM [9],[10],[56]. NYUSIM can be used to generate channel impulse response (CIRs) for mmWave systems, perform BER simulation, characterize MIMO channel and obtain MIMO channel condition number. The simulator was developed by NYU Wireless which can receive multipath components in a time cluster arriving from various pointing angles because of high gain MIMO directional antennas and such characteristic has not been available in WINNER [57] and 3GPP models [48]. NYUSIM can provide precision in a rendering of actual channel impulse responses (CIR) in both time and space.

NYUSIM can be utilized to generate sample functions of both temporal and spatial CIRs from both omnidirectional and directional channel models.

The paper [56] explained, in detail, the wideband mmWave measurements conducted in New York City by the NYU wireless laboratory as part of its research scheme to generate 5G mmWave channel models. To accomplish these measurements, a sliding correlator channel sounder was utilized for each measurement campaign. The fundamental principle associated with a sliding correlation method is to generate two identical PN sequences at the Tx and Rx with a small variation in clock speeds or chip rate. In this thesis, NYUSIM [10] is introduced which is a open source channel simulator ,used at multi meter wave (mm Wave) frequencies (28 to 73 [GHz]) in different outdoor environments like UMi, UMa and RMa environments [56]-[58].This simulator provides accurate channel impulse responses in both time and space. NYUSIM supports carrier frequencies in the range 0.5 -100[GHz] and Radio frequency band widths in the range 0 to 800 MHz

2.7 Conclusion

in the literature, there are several channel models and simulators, among these simulators nyusim model and simulator which has been developed based on extensive real-world wideband propagation channel measurements at multiple millimeter-wave (mmWave) frequencies from 28 to 73 GHz in various outdoor environments in urban microcell (UMi), urban macrocell (UMa), and rural macrocell (RMa) environments [11]–[19]. NYUSIM provides an accurate rendering of actual channel impulse responses in both time and space, as well as realistic signal levels that were measured, andis applicable for a wide range of carrier frequencies from 500 MHz to 100 GHz, and RF bandwidths from 0 to 800 MHz.

CHAPTER 3

Statistical Analysis of 5G/6G Millimeter Wave Channels for different scenarios

3 Statistical Analysis of 5G/6G Millimeter Wave Channels for differente scenarios

3.1 INTRODUCTION

Without waiting for the launch of 5G mobile networks around the world, the competition for 6G has already started. Researchers are promised a 6G technology that would further amplify the benefits of 5G for more data rate, more connected devices, and on a more secure network with less intensive energy. In terms of data rates, if 5G brings wireless user terminals into the gigabit era, 6G will propel us a thousand times faster, at speeds reaching 1 Terabit/second [59, 60]. The millimeter waves (mmWaves) and terahertz have been approved for 5G and 6G systems respectively [61,62]. One of the main challenges for the deployment of 5G/ 6G technologies is the spectrum to be adopted which means the necessary to investigate the channels' properties. In fact, mmWaves are adopted by 5G however, experiments to date have focused on frequencies below 100 [GHz], the main work has been concentrated in bands below 60 [GHz], or at most 95 [GHz] [63, 68]. On the other hand, the United States Federal Communications Commission (USFCC) advises the use of the bands from 95 [GHz] to 3 THz for 6G [69]. In such high-frequency bands, many researches are underway to reach extremely high data rates exceeding several Gbps. However, the mmWaves bands faces some propagation phenomena such as atmospheric absorption, penetration loss, human and building blockage, diffuse scattering from coarse materials, shadowing, refraction loss, and loss due to reflection. For the mmWaves propagation, the line of sight (LOS) can be predicted, while the non-LOS (NLOS) is also seen for the real obstacle.

In this chapter, we considered several potential scenarios for analyzing mmWaves and sub-terahertz propagations at frequency bands of 28, 38, 60, 73, 100 and 120 [GHz] for outdoor Urban Microcell (UMi).

It is necessary to note that in the literature, various papers investigated mmWaves channels' properties using different scenarios but not in depth and ignoring the geometric parameters (Co-Pol/X-Pol, SISO/SIMO/MIMO) in the most recent works [63–65, 67–68, 70] for outdoor UMi. Additionally, the effect of multi user–MIMO (MU–MIMO) on channels' properties did not taken into account by numerous researchers, as well as the effect of switching from LOS to NLOS scenarios on millimeter wave bands.

Compared with the existing studies, our key contributions in this work can be summarized as follows:

1. An in-depth study of the propagation of different frequency bands using various scenarios was carried out, especially the geometric parameters (Co-Pol / X-Pol, SISO / SIMO / MIMO).
2. The effect of Multi User MIMO (MU–MIMO) on the mmWaves channel characteristics mainly the impact of switching from 1U-MIMO to 2U-MIMO and 2U-MIMO to 4U-MIMO are discussed where in the literature the most researchers have not investigated this study.
3. The effect of switching from LOS to NLOS.
4. Focusing on the analysis of the propagation of frequency bands around 100 [GHz] (sub-terahertz) that are candidates for 6G systems, taking into account the potential scenarios with additional analysis and details.

3.2 Related Works

The Radio propagation models have a significant impact on decisions made in the field of wireless communications that are developed to assist researchers in the deployment, design, study, and evaluation of various proposed wireless technology solutions. In [23], the authors developed a mathematical hypothesis to demonstrate the statistical performance of the field and the signals encountered in mobile radio communication in terms of a set of separated plane waves, redirected by a scattering and reflecting obstruction, and incident horizontally on the mobile radio reception via the Rayleigh fading channel. Exploiting the Rayleigh fading channel model pioneered by Clarke, Smith *al* in [22], developed simulation software for outdoor and indoor propagation channels.

Rappaport et *al* in [49], developed another simulator named SIRCIM (Simulation of Indoor Radio Channel Impulse Response Models) for radio channel impulse response statistical models for the analysis and design of wireless communication systems. Fung et *al* [71], developed another software simulation named Bit Error Rate Simulator (BERSIM) to evaluate in real time the link quality between a transmitter and receiver in mobile radio communication without resorting to any radio frequency equipment. Latest advances in the mmWaves communication area brought renewed interest to researchers in modeling 5G communication channels [63, 68]. In the literature, many path loss models are presented, but it is mandatory to know which ones are suitable for a given frequency range. The authors in [27], compared the performance of some path loss propagation models at mmWaves and terahertz frequencies which are the single frequency floating-intercept (FI) model, the single-frequency close-in (CI) model, the multi-frequency alpha-beta-gamma (ABG) model, and the multi-frequency close-in frequency dependent (CIF) model. Furthermore, the authors in [73], conducted a thorough review of channel models for the development of 5G radio frameworks, including the overall structure of channel models and the main distinctions among mmWaves and microwave channel models.

It is important to note that all frequency bands must be studied in different scenarios, in some work the survey was specified for a region or a city. The authors in [74], presented a data set for the propagation losses of wireless communications for the bands 28 , 37 and 39 [GHz] for four major Indian cities, based on the corresponding weather conditions, in which the path losses take into account various atmospheric weather conditions. The channel characterization is most often performed in various urban areas, where both LOS and NLOS are considered. Otherwise, due to the scope of millimeter-wave channel modeling and the requirement to operate in frequency bands greater than 6 [GHz] for wireless communication such as 5G/6G, many groups of researches have begun to share their expertise to create mmWaves channel models and establish a performance evaluation platform. Among these groups, the NYU WIRELESS academic research center that developed NYUSIM model and finally simulation software adopted [70, 75].

The NYUSIM model [70] is based on the close-in (CI) model [27, 61] and on field measurements for several years in the 28 to 140 [GHz] range in New York City [36, 75]. NYUSIM model proves its performance in comparison with other models [73]. At New York University, Rappaport and his team developed a channel simulator named NYUSIM [9] for millimeter bands based on expanded real-world for channel propagation measurements. The simulator builds the real time channel response as well as the spatial channel response in order to properly evaluate the 5G physical and link layers. The mentioned model is based on the Statistical Spatial Channel Model (SSCM) involving Spatial Lobes (SL) and Time Clusters (TC) to get the corresponding Angle of Arrival (AoA) and Angle of Departure (AoD) of the power spectrum for the channel responses [30]. In addition, the model received the multi-path components in a time-cluster manner from different pointing angles by means of high-gain MIMO directional antennas. These features are not considered in WINNER [27] and 3GPP models [30]. Asma Ali Budalal et *al* in [76], outlined the impacts of various weather events in tropical areas such as rain on the behavior of the millimeter-wave channel at the carrier frequency 38 [GHz]. Besides, the authors in [77], carried out a NYUSIM simulation of spatial channel modeling characteristics for 5G mmWaves at carrier frequencies (28, 38, 60, and 73 [GHz]). The authors in [78], investigated on the rainfall estimation of backhaul link using mmWaves frequencies (25, 28, and 38 [GHz]) in Beijing. Moreover, the impact of rain on mmWaves communications by an earthly path in tropical areas, is investigated in [79]. In [80], the impact of weather conditions on the channel model characteristics of millimeter wave band frequencies (60 and 73 [GHz]) considering the rainy season and winter season in Bangladesh is discussed. To assist in the modeling and design of the statistical channel model for future 5G and 6G mmWaves/sub-terahertz communications, the contribution of this article is twofold. First, using NYUSIM [70, 75] to provide a new statistical analysis of the effect of degraded environmental factors and number of users in MIMO configuration on channel characteristics of unlicensed 60 [GHz] and licensed 28, 38, and 73 [GHz] mmWaves frequencies and 0.1, 0.120 THz frequencies. Second, and more generally, we consider five scenarios for different channel parameters and antenna configurations.

Comparing our contributions with those of other recent works allows us to draw the conclusions outlined in Table 1. The comparison is made in terms of frequency bands, scenarios and reported parameters. It is easy to observe that the different scenarios adopted in this work are polarization (Co-Pol/X-Pol), antenna patterns (SISO/SIMO/MIMO) and the number of users in MIMO configuration (MU-MIMO) as well as the reported parameters.

Reference	Frequency channel	scenario	Reported parameters
[63] 2020	27/39 [GHz]	MIMO	Gain, efficiency
[64] 2021	60 GHz	RT Outdoor by Ray Tarcing	Path Loss, Received Signal Strength
[65] 2020	Sub-6GHz	Deep learning RT Outdoor	Spectral efficiency
[67] 2021	Sub-6GHz/28GHz		Session drop probability
[68] 2021	28 /60GHz	UMi Indoor	Path loss
[70] 2021	28/140GHz	UMi LOS/NLOS indoor	Path Loss, RMS delay spread
[72] 2017	30/140/300 GHz	Indoor LOS	Path Loss, Path loss Exponent
[74] 2018	28/37/39 GHz	UMi Outdoor	Attenuation due to atmospheric gase, rain and fog
[77] 2019	28/38/60/73 GHz	UMi LOS Outdoor	PL, PLE, RMS Delay Spread
[78] 2019	25/28/38 GHz	Rain senario	PL
Our contribution	28/38/60/73/100/ 120 GHz	UMi LOS/NLOS, Polarisation (Co-Pol/X-Pol), Antenna patterns (SISO/SIMO/MIMO), users in MIMO configuration (MU-MIMO, Rain rate,Température /Humidity	PL, PLE, Received power, RMS Delay Spread

Table 1. Some recent studies related to mmWave/terahertz frequency bands.

3.3 Path Loss Models

The Radio propagation models have a significant impact on decisions made in the field of wireless communications. The 5G/6G wireless communications offers tremendous promise, to the point where users can already expect to have access to ultra-high data rates from anywhere and at any time. However, these new communications are already subject to some criticism. Indeed, field tests have shown that this may only be true in optimal conditions, since 5G/6G systems operate on mmWaves and terahertz frequencies. Furthermore, 5G wireless communications can be severely affected by weather conditions, path loss (PL), attenuation due to atmospheric conditions, reflection loss, building materials, blocking of obstacles and scattering [74, 81].

Industry and academic researchers have attempted to develop competitive wireless technology, but they have been faced with an unprecedented demand for capacity and higher data rates. Therefore, it is necessary to use higher frequencies at 6 [GHz] and above 100 [GHz] for 5G / 6G technologies. Thus, to optimize network efficiency and get more details on some candidate frequency bands for future mobile communication technology.

3.3.1 CI-Path loss model

Based on the NYUSIM platform [70, 75], this section investigates the path loss model, the strength of the received signal and power delay profiles.

A. Path loss

We consider the close-in free space (CI) reference distance path loss model with a reference distance of 1 m taking into account additional atmospheric attenuation factors in NYUSIM, expressed as follows [9, 47, 61]:

$$PL^{CI}\left(f,d\right)\left[\text{dB}\right]=FSPL\left(f,1\text{m}\right)\left[\text{dB}\right]+10n\,log_{10}\left(d\right)+AT\left[\text{dB}\right]+x_{\sigma}^{CI} \tag{1}$$

where $d \geq 1\text{m}$, f indicates the carrier frequency in [GHz], $d\,[\text{m}]$ is the distance between the transmitter (TX) and the receiver (RX), n denotes the Path Loss Exponent (PLE), AT attenuation term caused by the atmosphere, x_{σ}^{CI} is a zero-mean Gaussian random variable with a standard deviation σ in dB, and $FSPL\left(f,1\text{m}\right)$ denotes the free space path loss in dB at the carrier frequency f at a TX-RX separation distance of 1m.

$$FSPL\left(f,1\text{m}\right)[\text{dB}]=10\log_{10}\left(\frac{4\pi f\times 10^{9}}{c}\right)=32.4[\text{dB}]+20\log_{10}\left(f\right) \tag{2}$$

where c is the speed of light in a vacuum, of which f is in [GHz]. The term AT is considered by:

$$AT[\text{dB}]=\alpha[\text{dB/m}]\times d[\text{m}] \tag{3}$$

where α is the attenuation factor in dB/m, that illustrates the collective mitigation effect of water vapor fog, rain and dry air [47]. The parameter d is the 3D TX-RX separation distance in (1).

The PL caused by co-polarized (Co-Pol) TX and RX antennas is expressed as [82]:

$$PL_{V-V}(d) = P_{T-V} - P_{R-V} + G_T + G_R \tag{4}$$

where P_{T-V} (dBm) is the transmitted power into the vertically polarized TX antenna, P_{R-V} denotes the received power at the output of the vertically polarized RX antenna , G_T and G_R are TX and RX antennas gains (dBi) respectively.

The cross polarization (X-Pol) path loss PL_{V-H} is then calculated at the same distance as follows [82]:

$$PL_{V-H}(d) = P_{T-V} - P_{R-H} + G_T + G_R \tag{5}$$

In the above equation, P_{R-H} is the power received at the output of the RX antenna horizontally polarized (dBm). X-Pol link involves transmitting in one polarization and receiving in the orthogonal polarization.

B. Received Signal Power

The received power is given as follows [47]:

$$P_R[\text{dBm}] = P_T[\text{dBm}] + G_T[\text{dB}] + G_R[\text{dB}] - PL(d)[\text{dB}] \tag{6}$$

where P_R, P_T, G_T and G_R designate respectively the signal received power, the signal transmitted power, the gain of the transmitting and receiving antennas. Furthermore, $PL(d)$ represents the average path loss at separation distance d.

C. Power Delay Profile (PDP)

To illustrate the omnidirectional power delay profile (OPDP), the impulse response of the omnidirectional channel can be derived by [31]:

$$h_{omni}\left(t,\vec{\Theta},\vec{\varphi}\right)=\sum_{n=1}^{N}\sum_{m=1}^{Mn}a_{m,n}\exp(j\varphi_{m,n}).\delta\left(t-\tau_{m,n}\right).\delta\left(\vec{\Theta}-\vec{\Theta}_{m,n}\right).\delta\left(\vec{\varphi}-\vec{\varphi}_{m,n}\right) \tag{7}$$

where: t -- Propagation time described by absolute form, $\vec{\Theta}=\left(\theta,\varphi\right)$-- vector features azimuth and elevation angles of departures which characterize TX, $\vec{\varphi}=\left(\theta,\varphi\right)$ -- vector features azimuth and elevation angles of arrivals which characterize RX N, M_n -- the time clusters (TCs) number and the cluster subpaths number, $a_{m,n}$ -- the value of the m^{th} -- subpaths pertaining to the n^{th} TCs, $\tau_{m,n}$ -- the time delays angles, $\varphi_{m,n}$ -- the propagation angles.

3.4 SIMULATION SCENARIOS, ANALYSIS AND DISCUSSION

Based on the CI model, we analyzed and compared the proposed millimeter wave and sub-terahertz channels: 28, 38, 60, 73, 100, and 120 [GHz] for different scenarios. In this context, we have considered different scenarios divided into two categories: First, the geometric parameters: Co-Pol/X-Pol, antenna patterns (SISO/SIMO/MIMO) and number of users in MIMO configuration (MU-MIMO). Second, the environmental conditions: LOS/NLOS, rain rate, temperature and humidity for an urban microcell. In this section, we use the NYUSIM model, which is shown to be more accurate for realistic simulations than other channel models in urban environments [75]. Unlike the 3GPP model [30], which relied on many legacy results below 6 [GHz], NYUSIM emphasizes a more physical basis and relies on massive amounts of real data measured at mmWave frequencies [83]. Simulation parameters evoked in this section are summarized in Table 2. Furthermore, unless otherwise stated, we set the environment scenario to LOS.

Channel Parameters	**Value**	**Antenna Parameters**	**Value**
RF Frequency	28/38/60/73/100/120 ([GHz])	**TX/RX Array Type**	ULA/ULA (Uniform Linear Array)
RF BW MHz	800	**Num TX/RX Elements**	1/1
Scenario	UMi	**TX/RX Antenna Elements Spacing**	0.5λ/0.5λ
Environment	LOS/NLOS	**TX Azimuth/ Elevation HPBW**	10°/10°
T-R Separation (m)	100	**RX Azimuth/ Elevation HPBW**	10°/10°
TX Power (dBm)	30		
Num RX	1		
Press (mbar)	1013		
Hum %	50		
Temp. C°	20		
Pol	Co-Pol		
D Foliage (m)	0		
Rain rate mm/hr	0		

Table 2. LOS/NLOS scenario parameters.

3.4.1 LOS/NLOS scenario

For all considered channels, we consider the LOS and NLOS environments. In this scenario, we have two phases:

In the first phase, we set LOS or NLOS then we investigate the frequency bands. Figs. 3.1-3.3, show the PL, received power, and PLE of both the directional power delay profile DPDP and OPDP in terms of frequency bands. In the case of LOS scenario, for DPDP, the 28 [GHz] channel has lower PL and PLE 102.8 dB, 2.1 respectively, whereas 73 and 120 [GHz] have the highest values (116.1 and 116.3 dB) and vice versa for the received power. For OPDP, the 28 [GHz] channel has lower PL 98.8 dB, while the 100 [GHz] channel has the lowest PLE (1.8) and the 60 and 120 [GHz] channels have the two highest values (110.8 and 112.7 dB) and conversely for received power.

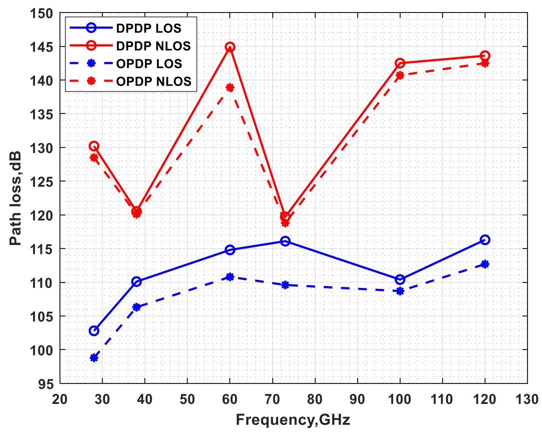

Fig 3.1 Path loss for LOS/NLOS scenarios.

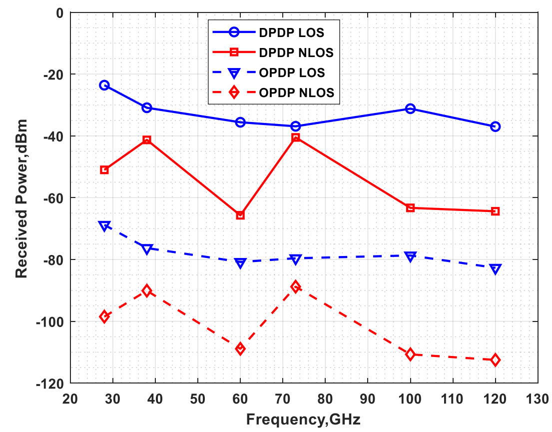

Fig 3.2 Received Power for LOS/NLOS scenarios.

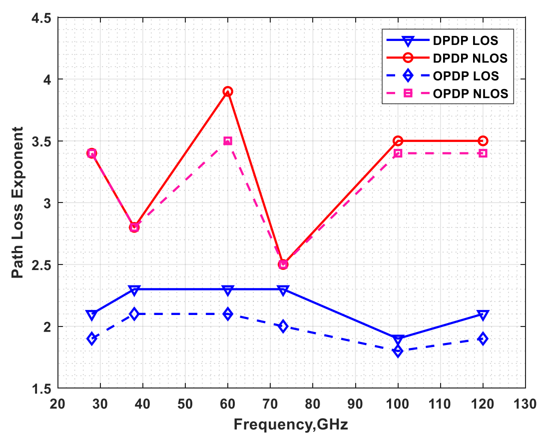

Fig 3.3 Path Loss Exponent for LOS/NLOS scenarios.

In the case of NLOS situation, for DPDP/OPDP, the 38 and 73 [GHz] channels have a lower PL and PLE (120.5, 119.7 dB for PL and 2.8, 2.5 for PLE), whereas for 60 [GHz], it has the two highest values (144.9 dB, 3.9) and conversely for the received power. Nevertheless, the 100 and 120 [GHz] channels have roughly similar statistics for PL, PLE, and received power, while still being better than the 60 [GHz] channel. The authors in [77] confirmed the above results for 28, 38, 60 and 73 [GHz] frequency bands.

As a second phase, we investigate the impact of changing the type of environment from LOS to NLOS on the channel characteristics for DPDP and OPDP. Figures 3.4 and 3.5 show the effect of changing from LOS to NLOS situation on the characteristics of the channel for both DPDP and OPDP respectively. From these figures, we result that 100 [GHz] channel was widely affected by the change from LOS to NLOS (30 dB), besides the channel 73 [GHz] was less affected compared to the other channels (3 dB). While for 60 [GHz], it has the two highest values and conversely for the received power (30 dB). Various works in the literature investigated the mentioned bands in LOS/NLOS scenarios but ignored the effect of changing from LOS to NLOS on channel characteristics as in [77, 84–87].

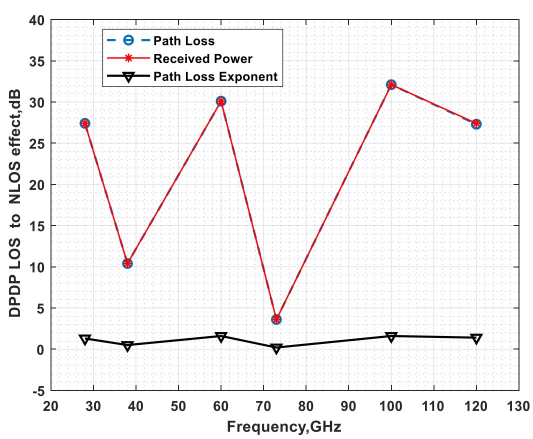

Fig 3.4 Effect of changing the type of environment from LOS to NLOS on the characteristics of the channel for DPDP.

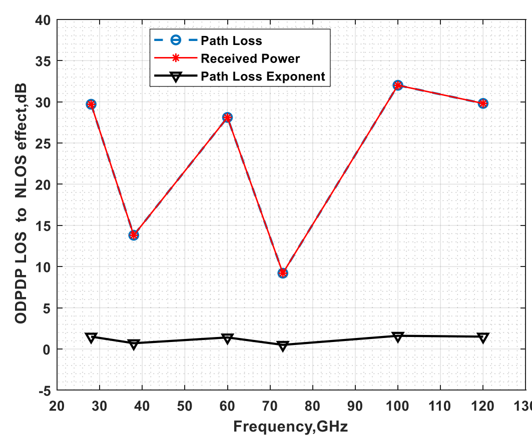

Fig 3.5 Effect of changing the type of environment from LOS to NLOS on the characteristics of the channel for OPDP.

3.4.2 Co-Pol/X-Pol scenario

Switching from Co-Pol to X-Pol (cross-polarization) can affect the channel characteristics and cause a significant path loss. The cross polarization discrimination (XPD) is determined by the difference between the path losses of the Co-Pol (V-V) and X-Pol (V-H) antenna. In this scenario we aim to study the polarization effect on the mentioned frequency bands (28, 38, 60, 73, 100 and 120 [GHz]).

Figures 3.6, 3.7 and 3.8, illustrate the PL, received power, and PLE of both DPDP and OPDP with LOS environment for Co-Pol/X-Pol polarizations. In case DPDP with Co-Pol polarization, the 28 [GHz] channel has a better PL and PLE (102.8 dB , 2.1), while 73 and 120 [GHz] have the two worsts values (116.1 and 116.3 dB 2.3, 2.1) and conversely for the received power.

For OPDP with Co-Pol polarization, the 28 GHz channel has the best PL 98.8 dB, while 120 [GHz] has the higher one 112.7 dB and conversely for the received power, 100 [GHz] has the lower PLE 1.8, whereas 38 and 60 [GHz] have the higher values 2.1. For DPDP and OPDP with X-Pol polarization, the 28 [GHz] has the lowest PL and the PLE (127.6 dB, 3.3), whereas, 120 [GHz] has the two higher values (146.2 dB, 3.6) and conversely for the received power.

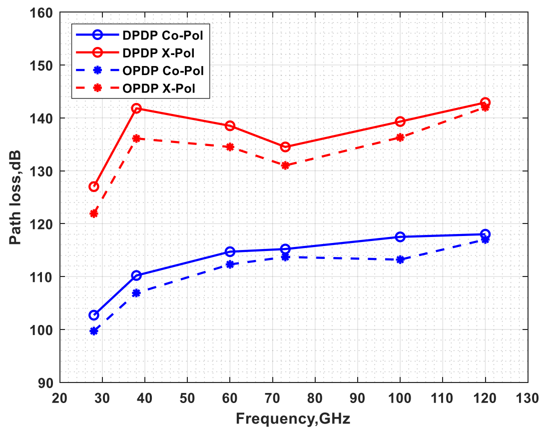

Fig 3.6 Path Loss for Co-Pol/X-Pol scenario.

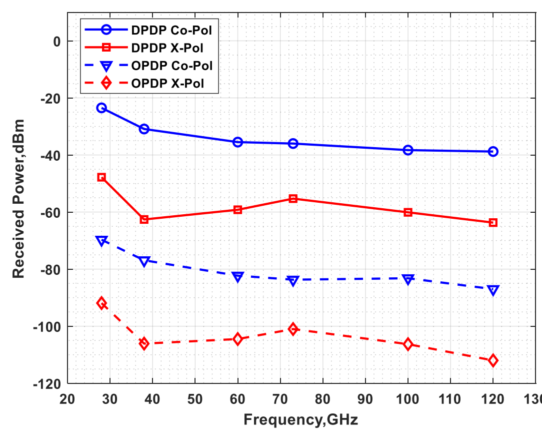

Fig 3.7 Received Power for Co-Pol/X-Pol scenario.

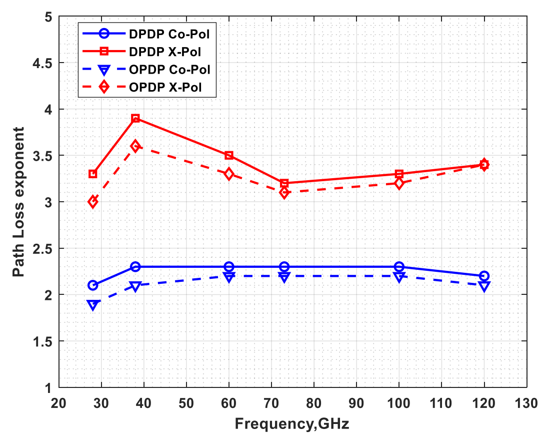

Fig 3.8 Path Loss Exponent for Co-Pol/X-Pol scenario

The remaining channels show approximately the same statistics on their characteristics; however, the 73 [GHz] frequency demonstrates the greatest improvement.

Figures 3.9 and 3.10 show the impact of changing from Co-Pol state to the X-Pol on the characteristics of the channel for both DPDP and OPDP, respectively. From these figures, we can see that the 100 and 120 [GHz] channels are more affected by the change from Co-Pol to X-Pol on PL and received power (XPD= 30 dB). However, the 60 and 73 [GHz] channels experience lesser effects compared to the other channels (XPD= 22 dB). In addition, it is noted that all channels have approximately the similar impact on the PLE. Concerning the comparison with some works of the literature. In [39], the results indicate that the polarization effect on the mmWave communication channel at 73 [GHz] is much significant than 28 [GHz]. Our results indicate the opposite, where the effect depends on TX-RX separation distance (near field and far field). Otherwise, in [89], the authors given a comparison of cross-polarization at 28, 73, and 140 [GHz] for indoor scenario. The results showed that the XPD was constant over the T-R separation distance range from 3 to 6 m. We conclude that the range above 100 m, the outcomes are different where the value of XPD depended on the separation distance.

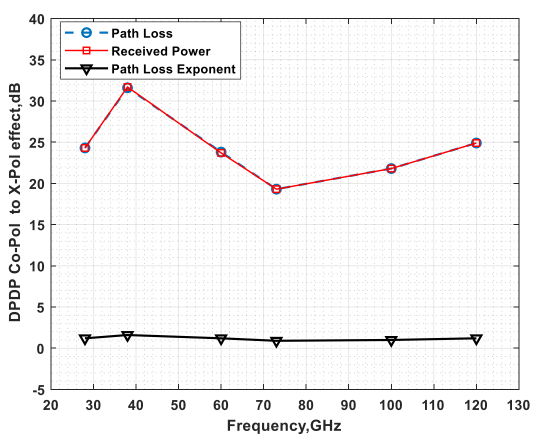

Fig 3.9 Effect of changing from Co-Pol state to the X-Pol state on the characteristics of the channel for DPDP.

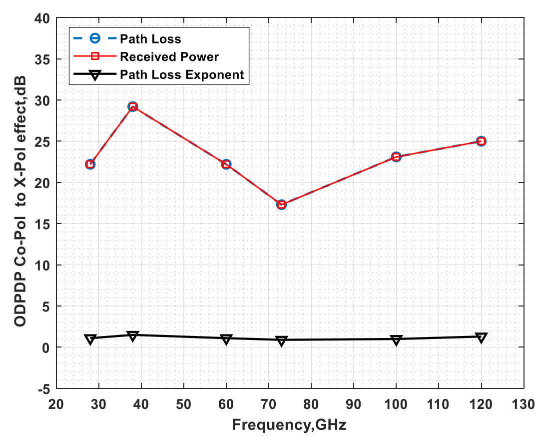

Fig 3.10 Effect of changing from Co-Pol state to the X-Pol state on the characteristics of the channel for OPDP.

3.4.3 Antennas Patterns scenarios

Here, we consider three antenna configurations as: SISO (1×1), SIMO (1×4) and MIMO (4×4).

Figures 3.11, 3.12 and 3.13, show the PL, received power and PLE of both DPDP and OPDP for SISO/SIMO/MIMO configurations.

For the SISO configuration, the 28 [GHz] channel exhibits a lower PL (102.8 dB), while the 73 and 120 [GHz] channels have the highest values (116.1 and 116.3 dB), and conversely for the received power. In addition, the 100 [GHz] channel shows a lower PLE (1.9), whereas the 38 [GHz] channel shows the higher one (2.3). In SIMO mode, channels 28 and 38 [GHz] have the lowest PL (105.2, 106.1dB), meanwhile the channel 120 [GHz] has the highest value (125.8 dB), and conversely for the received power. In the end, the channel 38 [GHz] has the lowest PLE (2.1), while channels 60 and 120 [GHz] have the highest values (2.6). In the MIMO configuration, the 28 and 38 [GHz] channels have the lowest PL (106 , 107.6 dB), while the 100 and 120 [GHz] channels have the highest values (118.1 , 116.5 dB) and conversely for the received power. In addition, channel 73 [GHz] has the lowest PLE (1.9), while channel 60 and 100 [GHz] have the highest values (2.3).

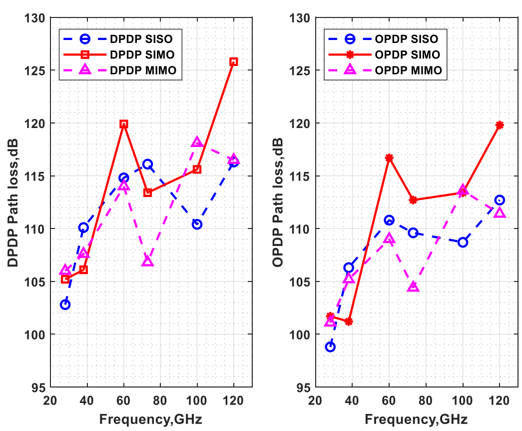

Fig 3.11 Path Loss for antennas patterns scenario in the case of DPDP and OPDP.

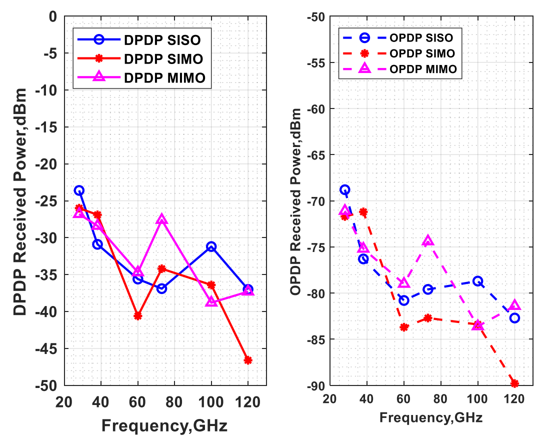

Fig 3.12 Received Power for antennas patterns scenario in the case of DPDP and OPDP.

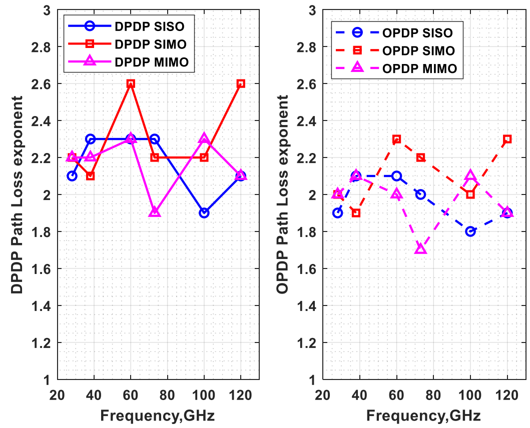

Fig 3.13 Path Loss Exponent for MIMO scenario in the case of DPDP and OPDP.

Figures 3.14 and 3.15 show the impact of switching from SISO to SIMO and SIMO to MIMO configuration on the channel characteristics for DPDP and OPDP, respectively. From Fig 3.14, the 120 and 38 [GHz] channels are more affected by the transition from a SISO to SIMO channel on the PL and received power; however, respectively in the negative and positive way (variation of 9.5dB and 4dB respectively) , while the 28 [GHz] channel is less affected compared to the other channels (2.4 dB). Furthermore, all channels have nearly a similar impact on the PLE.

It can be seen from Fig 3.15 that the 120 and 73 [GHz] channels are most positively affected by the transition from a SIMO to a MIMO channel regarding to PL and received power (9.3 dB and 6.6 dB respectively), whereas the 28 [GHz] channel is less affected compared to the other channels (0.8 dB). All channels have approximately the same effect on the PLE. In [90], a proper selection of a number of antenna elements in 28 [GHz] frequency in NLOS and LOS environment and their performance is presented, by analyzing different channel parameters in urban microcell scenario for Dhaka city. The results indicate that the MIMO with a 4×4 antenna element is giving less path loss, better-received power and less RMS delay spread in comparison with other MIMO (2×2, 3×3, 5×5, 6x6, and 7×7). In our case, we confirm the results of 4x4 MIMO for 28 [GHz], but for the others carriers frequencies (38,60,73,100 and 120 [GHz]) are not conducted.

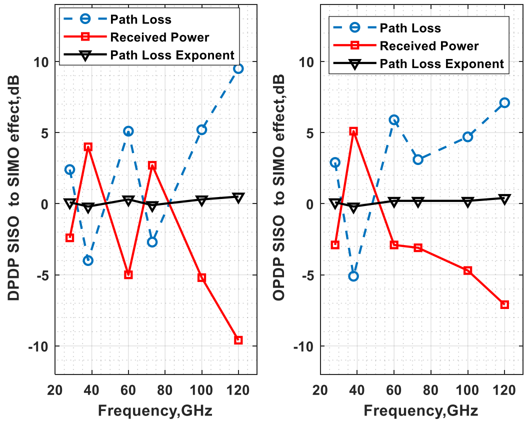

Fig 3.14 Effect of changing from SISO to SIMO channel for DPDP and OPDP.

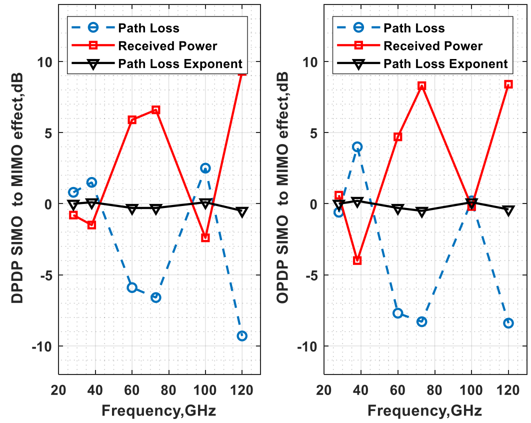

Fig 3.15 Effect of changing from SIMO to MIMO channel for DPDP and OPDP.

3.4.4 Rain scenario

We consider the rain scenario with three precipitation rates: 0 mm/hr, 25 mm/hr and 50 mm/hr. Figs. 3.16, 3.17 and 3.18 show, the PL, received power, and PLE of both DPDP and OPDP for rain rate scenarios.

Based on these figures, for 0 mm/hr rain rate setting, the 28 [GHz] channel has a lower PL (106 dB), while 100 and 120 [GHz] have higher values (118.1 and 116.5 dB respectively) and conversely for the received power. The 73 [GHz] channel has a lower PLE (1.9), while 100 [GHz] has the higher one (2.3). At 25 mm/hr rain rate setting, the 38 [GHz] channel has the lower PL (102.3 dB), while 100 and 120 [GHz] channels have the higher values (120 and 119.4 dB respectively) and conversely for the received power. Moreover, the 38 [GHz] channel has the lower PLE (1.9), while 73 and 100 [GHz] have the higher value (2.4). In the case of 50 mm/hr rain rate setting, the 38 [GHz] channel has the lower PL (107.5 dB), while the 120 [GHz] channel shows the higher one (116.1 dB) and conversely for the received power, the 100 [GHz] channel holds the lower PLE (1.8), while 28 [GHz] has the highest value (2.5).

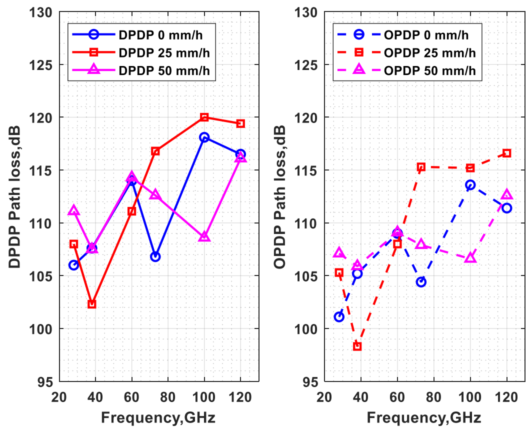

Fig 3.16 Path Loss for rain scenario in the case of DPDP and OPDP.

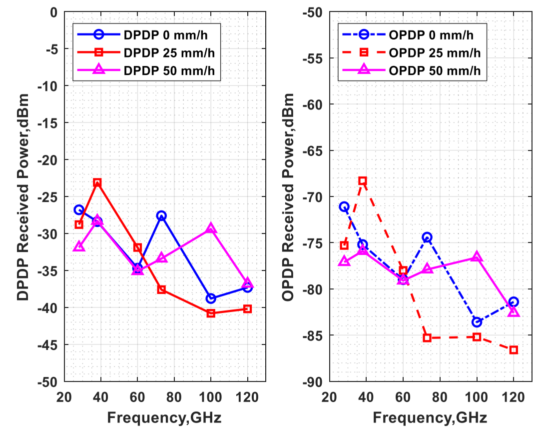

Fig 3.17 Received Power for rain scenario in the case of DPDP and OPDP.

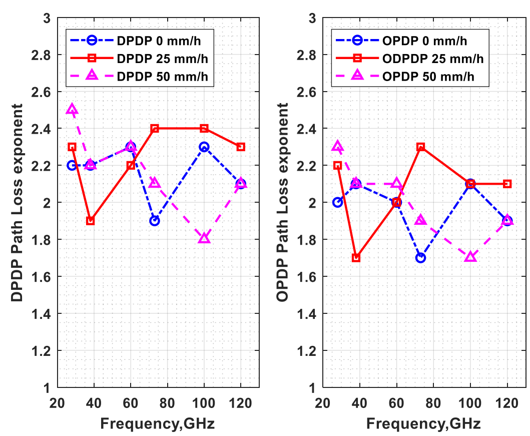

Fig 3.18 Path Loss Exponent for rain scenario in the case of DPDP and OPDP.

Figures 3.19 and 3.20 show the impact of changing from 0 mm/hr to 25 mm/hr rain rate and from 25 mm/hr to 50 mm/hr rain rate on channel characteristics for both DPDP and OPDP, respectively. From Fig. 3.19, the 73 and 38 [GHz] channels are more affected by the change from 0 mm/hr to 25 mm/hr rain rate on PL and received power, however, respectively in the negative and positive way (10dB , 5.3dB respectively) while channels 60 and 100 [GHz] less affected compare to the other channels (2.9dB ,1.9dB respectively). Overall, all channels have approximately the same effect on PLE (between 0.1 and 0.2). Similarly, from Fig 3.20, the 73 and

100 [GHz] channels are most adversely affected by the change from 25 mm/hr to 50mm/hr rain rate on PL and received power (4.2 dB, 11.4 dB respectively), while the 28 and 60 [GHz] channels are the least affected (3.1 dB, 3.2 dB respectively).. In addition, a similar impact on PLE was observed for all channels.

In [74], the results obtained indicate that with an increase in the carrier frequency, the attenuation level increases. The rain fade increase by 7 dB with a variation of the frequency from 28 to 37 [GHz]. Compared to our outcomming the attenuations increase rapidly for the frequencies 60 to 73 [GHz] by 13 dB, whereas 2 dB with a variation of frequencies from 28 to 38 [GHz] as shown in Figs 3.19 and 3.20. This difference depend to the setting parameters of the channel radio link.

In [91], a brief analysis of rain fading was presented based on the simultaneous measurement of one-minute rain rate and its effects on a short experimental link of 38 [GHz]. Rain fade average is observed as high as 6.72 dB for 300 m path at about 30 mm/hr rain intensity. In comparison with our results shown in Figs 3.19 and 3.20, the rain fade is 5 dB for 100 m path with 25 mm/hr rain rate variation, besides for 28, 60, 73, 100 and 120 [GHz] the rain fade are 2, 3 ,10 , 2 and 3 dB respectively .

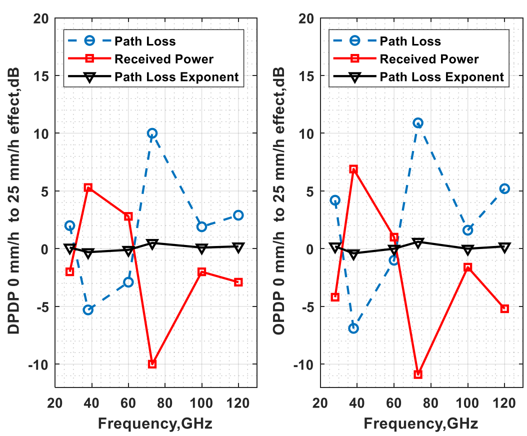

Fig 3.19 Effect of changing from 0 mm/hr to 25 mm/hr rain rate on channel characteristics for DPDP and OPDP.

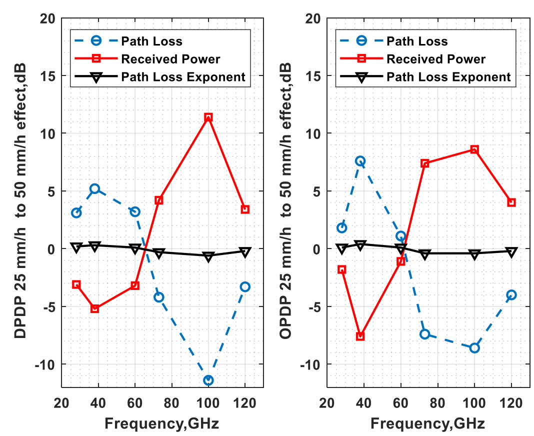

Fig 3.20 Effect of changing from 25 mm/hr to 50mm/hr rain rate on channel characteristics for DPDP and OPDP.

3.4.5 Temperature and Humidity scenario

In this scenario, we adopt three temperature and humidity values:

$T1 = 20°C / H1 = 50\%$, $T2 = 35°C / H2 = 60\%$ and $T3 = 45°C / H3 = 70\%$.

Figs. 3.21, 3.22 and 3.23 show the PL, received power, and PLE of both DPDP and OPDP for temperature and humidity scenarios.

1. For $T1 = 20°C / H1 = 50\%$ scenario, the 28 [GHz] channel has a lower PL (102.8 dB), while 60 and 120 [GHz] have higher values (114.8dB ,116.3dB respectively). and conversely for the received power. For the 100 [GHz] channel, it has a lower PLE (1.9), while 38, 60 and 73 [GHz] channels have the higher values (2.3).
2. For $T2 = 35°C / H2 = 60\%$ scenario, the 28 and 38 [GHz] channels have a lower PL (102.5dB, 104.7dB respectively), while 60 [GHz] has the higher value (122.1 dB) and conversely for the received power. Channel 60 [GHz] has a higher PLE (2.7), while 38 and 100 [GHz] have the lower values (2).
3. For $T3 = 45°C / H3 = 70\%$ scenario, 120 [GHz] has the highest PL value (120 dB) whereas the 28 [GHz] channel has the lower PL (105.2 dB) and conversely for the received power. Channel 38 [GHz] has a low PL and high Received power compare to the others channels. All Channels have roughly the same value of PLE about (2.3).

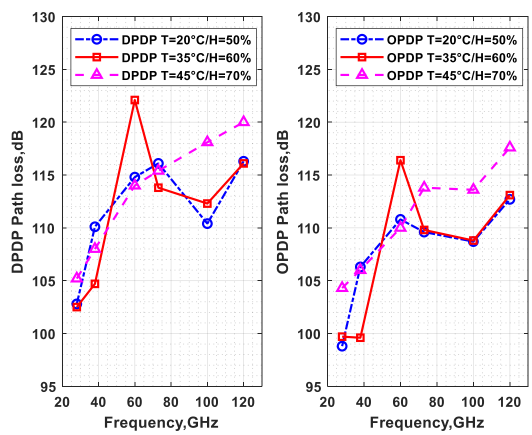

Fig 3.21 Path Loss in case of temperature and humidity scenarios for DPDP and OPDP.

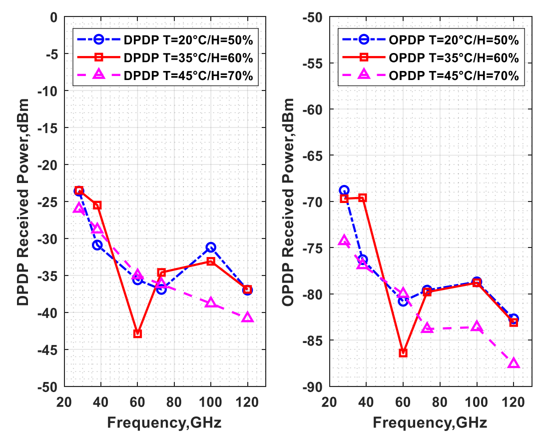

Fig 3.22 Received Power in case of temperature and humidity scenarios for DPDP and OPDP.

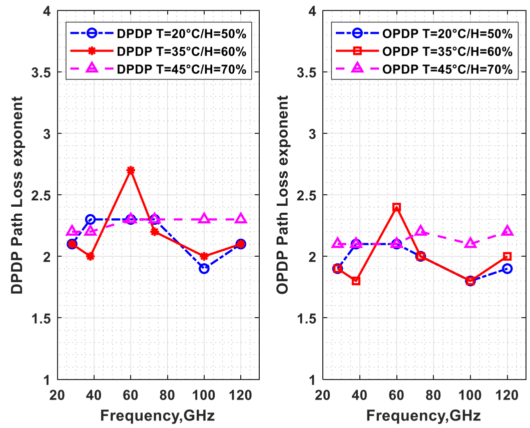

Fig 3.23 Path Loss Exponent in case of temperature and humidity scenarios for DPDP and OPDP.

Figures 3.24 and 3.25 show the impact of changing the weather condition from $T1 = 20°C / H1 = 50\%$ to $T2 = 35°C / H2 = 60\%$ and from $T2 = 35°C / H2 = 60\%$ to $T3 = 45°C / H3 = 70\%$ on channel characteristics for both DPDP and OPDP, respectively.

From Fig. 3.24, channel 38 [GHz] is more affected positively (variation of 5.4 dB) by the change from $T1 = 20°C / H1 = 50\%$ to $T2 = 35°C / H2 = 60\%$ on PL and received power; however, channel 60 [[GHz]] is more affected negatively (variation of 7.3 dB); while the other channels have roughly the same effect (variation of 2 dB). Furthermore, Fig. 3.25 reveals that 38 and 100 [GHz] channels are more adversely affected by $T2 = 35°C / H2 = 60\%$ to $T3 = 45°C / H3 = 70\%$, while 60 [GHz] channels are more positively affected on PL and received power (8.1 dB), while 28 and 73 [GHz] channels are less affected compared to other channels (about 2 dB). The same effect is observed on the PLE for all channels.

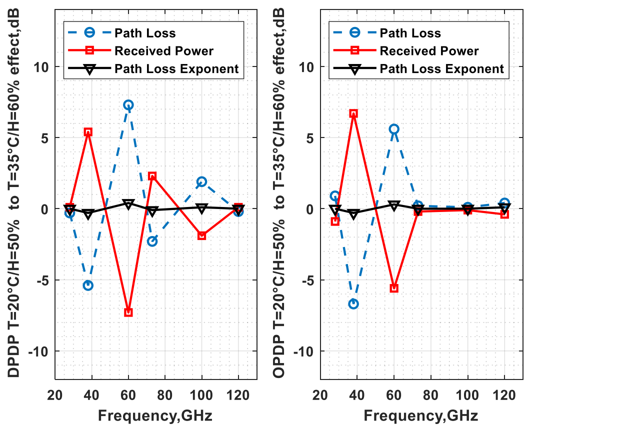

Fig 3.24 Effect of changing of the weather condition from $T1 = 20°C / H1 = 50\%$, $T2 = 35°C / H2 = 60\%$ on channel characteristics for DPDP and OPDP.

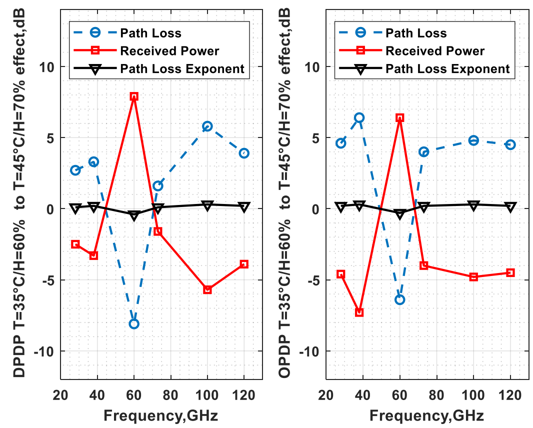

Fig 3.25 Effect of changing of the weather condition from $T2 = 35°C / H2 = 60\%$ to $T3 = 45°C / H3 = 70\%$ on channel characteristics for DPDP and OPDP

In [92], the authors developed a custom model via the generic NYUSIM channel simulator, that fits the properties of mmWave propagation in Iraq environment and also the effect of weather parameters, as temperature and humidity, on link quality is discussed. The results indicate that a rise in the value of humidity causes a "concavity" in the 28 [GHz] subband performance while it has weaker impacts on the remaining bands especially for moderate values of humidity. In comparison with our results, the 38 and 60 [GHz] are more affected by the variation of the humidity and the temperature.

3.4.6 Multi User- MIMO scenario

The evaluation of millimeter wave channels performance considering Multi User-MIMO (MU- MIMO) are ignored in the literature. In this last scenario, we consider three MU-MIMO configurations: 1U-MIMO (2×2), 2U-MIMO (2×2) and 4U-MIMO (2×2).

Figures 3.26, 3.27 and 3.28, show the PL, received power and PLE of both DPDP and OPDP for 1U-MIMO (2×2), 2U-MIMO (2×2) and 4U-MIMO (2×2) configurations.

For the 1U-MIMO configuration, the 28 [GHz] channel exhibits a lower PL 102.7 dB, while the 100 and 120 [GHz] channels have the highest values 118.5 and 119.6 dB respectively and conversely for the received power. In addition, the 73 [GHz] channel shows a lower PLE 1.6, whereas the 38, 100 and 120 [GHz] channels shows the higher one 2.1. In 2U-MIMO mode, channel 28 [GHz] has the lowest PL 102 dB, meanwhile the channel 120 [GHz] has the highest value 125.8 dB, and conversely for the received power. In the end, the channel 28 [GHz] has the lowest PLE 2, while channels 100 and 120 [GHz] have the highest values 2.2 and 2.6 respectively. In the 4U-MIMO configuration, the 28, 60 and 73 [GHz] channels have the lowest PL 105.4, 107.1 and 109.9 dB respectively, while the 100 and 120 [GHz] channels have the highest values 121.6 and 116.3 dB respectively and conversely for the received power. In addition, channel 73 [GHz] has the lowest PLE 2, while channel 100 [GHz] has the highest value 2.5.

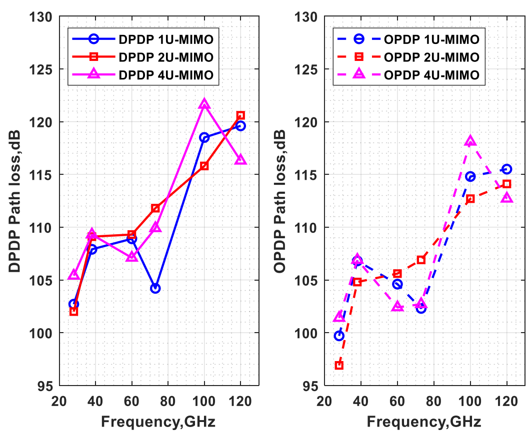

Fig 3.26 Path Loss for MU-MIMO scenario in the case of DPDP and OPDP.

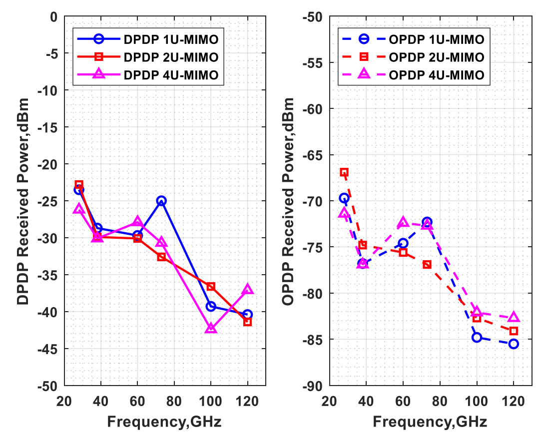

Fig 3.27 Received Power for MU-MIMO scenario in the case of DPDP and OPDP.

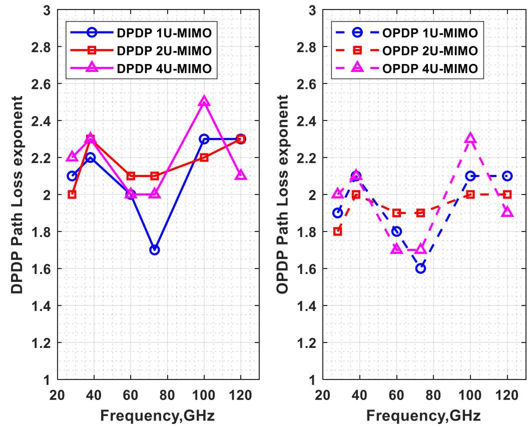

Fig 3.28 Path Loss Exponent for MU-MIMO scenario in the case of DPDP and OPDP.

Figures 3.29 and 3.30 show the impact of switching from 1U-MIMO to 2U-MIMO and 2U-MIMO to 4U-MIMO configuration on the channel characteristics for DPDP and OPDP, respectively. From Fig. 3.29, the 73 [GHz] is attenuated more than the other channels when switching from 1U-MIMO to 2U-MIMO (variation of 7.6 dB), while the 60 [GHz] channel is less affected (variation of 0.4 dB) compared to the other channels. Furthermore, all channels have nearly a similar impact on the PLE (0.1).

It can be seen from Fig.3.30 that the 60 and 73 [GHz] channels are most positively affected by the transition from 2U-MIMO to 4U-MIMO channel in terms of PL and received power (2dB), while the 38 [GHz] channel is less affected compared to the other channels (0.2 dB). All channels have approximately the same effect on the PLE.

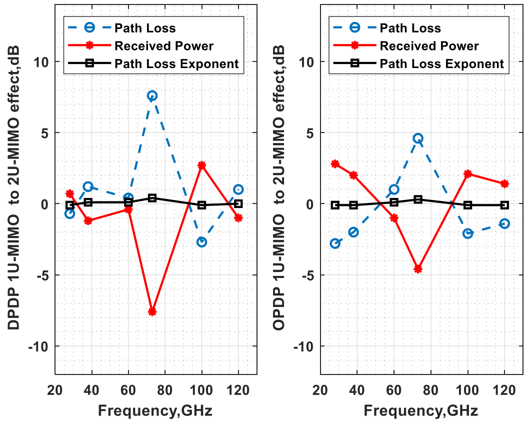

Fig. 3.29 Effect of changing from 1U-MIMO to 2U-MIMO channel for DPDP and OPDP.

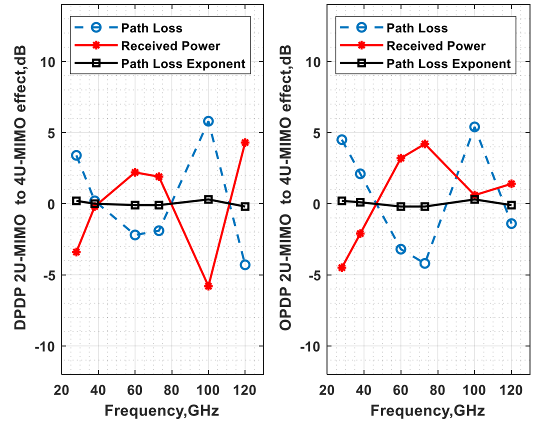

Fig. 3.30 Effect of changing from 2U-MIMO to 4U-MIMO channel for DPDP and OPDP.

3.5 CONCLUSION

Summing up the results, it can be concluded that the parameters of statistical channel modeling are dependent on the geometric parameters (Co-Pol/X-Pol, SISO/SIMO/MIMO) and environmental conditions (LOS/NLOS, rain rate, temperature and humidity). Furthermore, the MU–MIMO scenario affect is investigated, mainly the impact of switching from 1U-MIMO to 2U-MIMO or 2U-MIMO to 4U-MIMO, this scenario is not taken into account in recent works. The study of this work aims to illustrate mmWave characteristics (PL, PLE, Received power) at 28, 38, 60, 73, 100 and 120 [GHz]. Overall observation suggests that mmWave channel with carrier frequencies 28, 60, 100 and 120 [GHz] channels are more affected by the switching from LOS to NLOS. However, 38 [GHz] channel is the least affected, nevertheless, channel 73 [GHz] is more tolerant of the LOS to NLOS effect. Besides, in terms of antenna configurations (SISO/SIMO/MIMO), the results indicated that 120 [GHz] is more affected, while 28 [GHz] is less affected than the other channels, except that 38 [GHz] is more favorable to change this factor. For rain, temperature and humidity factors, it was concluded that the attenuations of 60, 100 and 120 [GHz] are the most important, while 28 and 73 [GHz] channels are less affected, except that 38 channel is the most capable to withstand the change of these factors. After comparing our results with those from the literature, we have concluded that rain fade depends to link length. Finally, the OPDP exhibits a lower attenuation index and attenuation exponent than the DPDP. This proposed work will be highly useful for 5G/6G research and system deployment and expected to help future engineers to design an efficient mmWave channel modeling for new outdoor scenarios.

CHAPTER 04

Analysis of Outdoor to Indoor Penetration Loss for mmWave Channels

4 Analysis of O2I Penetration Loss for mmWave Channels

4.1 Introduction

The 5th Generation Mobile Technology (5G) is expected to connect people, data, applications, transportation systems and cities in an intelligent network communication environment. It should transfer large amounts of data faster, reliably connect a large number of devices, and process large amounts of data with minimal delay. 5G systems use mainly millimeter waves (mmWave), various systems have been proposed for the use of microwave bands in 5G systems, particularly for 28, 38, 60 and 73 [GHz] frequencies. It’s very important to study mmWaves dedicated to 5G systems. In this chapter, we focused on the outdoor to indoor (O2I) propagation path loss. We present an analysis of outdoor to indoor penetration Loss for mmWave channels of 28, 38, 60 and 73 [GHz] for different scenarios using NYUSIM V2.0 simulator developed by researchers at New York University (NYU).

4.2 Related works

For the higher frequency bands of the O2I scenarios, studies are found to cover many frequency bands, such as 10, 28 and 60 [GHz] [93-95]. Reference [93] investigated indoor coverage at different frequencies (10, 30 and 60 [GHz]) in a single building with an externally deployed base station. The work illustrated general trends in the variation of coverage in the frequency range. However, O2I coverage at 60 [GHz] can be quite difficult for some types of buildings and the flow has been seriously affected, depending on the materials of the walls, the interior layout and the size of the building. In [94], the authors presented results for path loss, penetration loss for two different type of housing, including single-family unit and multistory brick building .In [95], the authors presented the results from a 28 [GHz] channel sounding campaign performed to investigate the effects of outdoor to indoor penetration on the channel characteristics for a fixed wireless access scenario.

In [96], the authors studied the 3, 10, 17 and 60 [GHz] radio propagation channel in an O2I (outdoor-indoor) scenario. Measurements were made using a wideband channel sounder to derive channel parameters such as channel delay spread values and building penetration losses.

In [97], the authors proposed a simple model for indoor outdoors (O2I) propagation based on the frequency bands 2 and 5 [GHz]. The proposed model focuses on the variation of the angle of incidence on a vertical plane as microwaves move from an O2I environment.

The industry has a lot of interest in the higher frequency band and proposed a series of technical reports on 3GPP, which contain channel models for frequencies from 0.5 to 100 [GHz] [6-9]. In the meantime, an additional consideration on penetration loss modeling for the 5G system are also studied in [102]. In the academic world, many researchers have also explored the homestead of high frequency channels. In [103], the authors exposed radio propagation measurements and analysis of mmWave transmission in building and urban cellular communications in the 28 [GHz] band bandaged. Based on measurements, spatiotemporal channel characteristics such as multipath delay, angular statistics and path loss were analyzed and modeled.

In [104], the authors examined the modeling of path loss in UMi environments. The authors established a stochastic path loss model by street that could properly describe the LOS path depending to the orientation of the street as well as the great variance observed for the whole way loss model settings.

In [105], the authors clarified the O2I path loss characteristics based on the measurement from 0.8 to 3.7 [GHz] in UMi (urban microcell) scenario, and they are modeled. In addition, extension of conventional O2I models is discussed.

The 38 [GHz] mmWave frequency band is also a powerful candidate for the future deployment of the 5G system. In [106], the authors presented a detailed analysis based on analysis of outdoor urban propagation characteristics and O2I at 38 [GHz]. The results of the measurements confirmed that, at this particular frequency, the propagation in urban scenarios was mainly motivated by LOS and reflection.

4.3 O2I penetration loss models

4.3.1 3rd Generation Partnership Project 3GPP TR 38.901

3rd Generation Partnership: Global models of large-scale path loss may also take into account the loss of penetration into a building and subsequent path loss within the building. The O2I path loss model taking into account building penetration loss according to 3GPP TR 38.901 [30] is as follows:

$$PL[dB] = PL_b + PL_{tw} + PL_{in} + N\left(0, \sigma_P^2\right) \tag{8}$$

where PL_b is the base loss of the outer path, PL_{tw} is the building loss of penetration through the outer wall, PL_{in} is the loss that depends on the depth in the building, and σ_P^2 is the standard deviation for penetration loss. The building penetration loss PL_{tw} can be modeled as:

$$PL_{tw}[dB] = PL_{npi} - 10\log_{10}\sum_{i=1}^{N}\left(p_i \times 10^{\frac{L_{material_i}}{-10}}\right) \tag{9}$$

where PL_{npi} is an additional loss which is added to the external wall loss to account for non-perpendicular incidence, $L_{material_i} = a_{material_i} + b_{material_i} . f_c$ is the penetration loss of material i , f_c is the frequency in [GHz], $a_{material_i}$ and $b_{material_i}$ are constants depend to the material i , p_i is the proportion of i-th materials, where $\sum p_i = 1$, and N is the number of materials. Penetration loss of several materials and the O2I penetration loss models are given in Table 3.

Material	Penetration loss
Standard multi-pane glass	$L_{glass} = 2 + 0.2 \cdot f_c$
IRR glass	$L_{IRRglass} = 23 + 0.3 \cdot f_c$
Concrete	$L_{concrete} = 5 + 4 \cdot f_c$
Wood	$L_{wood} = 4.85 + 0.12 \cdot f_c$

Table 3 O2I penetration loss of different material [30].

Rough models are also provided to estimate the building penetration loss in Table 4. Both the low-loss and high-loss models are applicable to UMa and UMi-street canyon, while only the low-loss model is applicable to RMa. The O2I car penetration loss included in path loss is determined by:

$$PL[dB] = PL_b + N\left(\mu, \sigma_P^2\right) \tag{10}$$

where PL_b is the basic outdoor path loss, and for most cases , $\mu = 9.dB$ and $\sigma_p = 5.dB$. An optional $\mu = 20.dB$ is provided for metalized car windows for frequencies ranging from 0.6 to 60 [GHz] [30].

O2I penetration loss Models	Path loss through external wall : $PL_{tw}[dB]$, f_c is in GHz	Indoor loss $PL_{in}[dB]$, d is in meters	Standard deviations σ_P [dB]
3GPP TR 38.901 Low loss model [30].	$5-10\log_{10}(0.3\cdot10^{-L_{glass}/10}+0.7\cdot10^{-L_{concrete}/10})$	$0.5d_{2D-in}$	4.4
3GPP TR 38.901 High loss model [30].	$5-10\log_{10}(0.7\cdot10^{-L_{IRRglass}/10}+0.3\cdot10^{-L_{concrete}/10})$	$0.5d_{2D-in}$	6.5
Nyusim model Low loss model [6]-[107].	$10\log_{10}\left(5+0.03\cdot f_c^2\right)$	Not specified	4.0
Nyusim model High loss model [6]-[107].	$10\log_{10}\left(10+5\cdot f_c^2\right)$	Not specified	6.0

Table 4 O2I Penetration Loss Parameters

4.3.2 NYUSIM

A parabolic model for building penetration loss from [6,107] is implemented in NYUSIM, which has either a low loss or a high loss form, depending on the type of building surface. The low loss model works for external building materials like standard glass and wood while the high loss model works for external building materials like IRR glass and concrete [6]. The parabolic model for building O2I penetration loss (BPL) is given as [6,107]:

$$BPL[dB] = 10\log_{10}\left(A + b \cdot f_c^2\right) + N\left(0, \sigma_P^2\right) \tag{11}$$

where f_c is the carrier frequency. A = 5, B = 0.03, and $\sigma_P = 4$ for the low loss model. A = 10, B = 5, and $\sigma_P = 6$ for the high loss model.

4.3.3 MmMAGIC

The O2I penetration loss model in mmMAGIC has the form of:

$$O2I[dB] = B_{O2I} + C_{O2I} \cdot \log_{10}(f_c) \approx 8.5 + 11.2\log_{10}(f_c) \tag{12}$$

The advantage of this form is that the coefficients B_{O2I} and C_{O2I} can be added to the existing coefficients in the path loss model of mmMAGIC. A frequency-dependent shadow fading between 8 and 10 dB for the UMi-O2I scenario is presented in [101]:

$$\sum SF[dB] = \sigma_{SF} + \delta_{SF} \cdot 10\log\left(f_c\right) \approx 5.7 + 2.3 \cdot \log_{10}\left(f_c\right) \tag{13}$$

4.4 Simulation and results analysis

In this section, we will simulate the O2I penetration loss for the most used millimeter wave channels (28, 38, 60 and 73 [GHz]) for different scenarios using NYUSIM V2.0.

The simulation with different choice of parameters is carried out in this section. For the simulation, assumptions were made for both channel and antenna properties represented in Table 5. Simulations results for the four scenarios proposed in this study was carried out in the form of figures and organized by type of result.

PARAMETERS/ SCENARIO N°	1	2	3	4
RF BW MHz	800	800	800	800
Scenario	UMi	UMi	UMi	UMi
LOS/NLOS	LOS	LOS	LOS	LOS
T-R Separation (m)	100	100	100	100
TX Power (dBm)	30	30	30	30
Num RX	1	1	1	1
Press (mbar)	1013	1013	1013	1013
Hum %	50	50	50	50
Temp. C°	20	20	20	20
Pol	c-pol	c-pol	c-pol	c-pol
D Foliage (m)	0	0	0	0
Rain rate mm/hr	0	0	0	0
O2I penetration Loss	Yes	Yes	Yes	Yes
O2I penetration Loss Type	Low	High	Low	High
TX/RX Array Type	ULA/ULA	ULA/ULA	ULA/ULA	ULA/ULA
Num TX/RX Elements	1/1	1/1	1/1	1/1
TX/RX Antenna Spacing	0.5λ/0.5λ	0.5λ/0.5λ	0.5λ/0.5λ	0.5λ/0.5λ
TX/RX Elevation/Azimuth	10°/10°	10°/10°	15°/15°	15°/15°

Table 5 Channel and Anntena simulation scenarios parametrs

4.4.1 Directional PDP for O2I penetration loss scenarios

Figures 4.1, 4.2, 4.3 and 4.4 show the Directional PDP output from a NYUSIM run with O2I penetration loss at 28, 38, 60 and 73 [GHz] respectively for the four scenarios. From figure 4.1, 4.2, 4.3 and 4.4 we can summarize results in Table 6.

In scenario 1, channel 38 [GHz] has a lower O2I penetration loss, while 73 [GHz] has the highest value.

In scenario 2, channel 73 [GHz] has a higher O2I penetration loss, while 38, 60 [GHz] have approximately the same values and channel 28 [GHz] has a lower one.

In scenario 3, channel 73 [GHz] has a lower O2I penetration loss, while 60 [GHz] has the highest value.

In scenario 4, channel 38 [GHz] has a higher O2I penetration loss, while 60, 73 [GHz] has the same values and channel 28 [GHz] has a lower one.

At 28 [GHz] channel, the effect of changing the TX/RX HPBW azimuth/Elevation from 10° to 15° is important in case of Low loss O2I penetration type (10,1 dB) while it is careless for the high loss type (1,3 dB). The effect of changing the type of O2I penetration loss from Low to High in case of TX/RX HPBW azimuth/Elevation 15° is twice times in case of HPBW 10°.

At 38 [GHz] channel, the effect of changing the TX/RX HPBW azimuth/Elevation from 10° to 15° is important in case of High loss O2I penetration type (9,2 dB) while it is 3,7dB for the low loss type. The effect of changing the type of O2I penetration loss from Low to High in case of TX/RX HPBW azimuth/Elevation 15° is greeter then case of HPBW 10°.

At 60 [GHz] channel, the effect of changing the TX/RX HPBW azimuth/Elevation from 10° to 15° is approximately the same in the tow cases of High loss O2I penetration type and the low loss type. The effect of changing the type of O2I penetration loss from Low to High in case of TX/RX HPBW azimuth/Elevation 15° is greeter then case of HPBW 10°.

At 73 [GHz] channel, the effect of changing the TX/RX HPBW azimuth/Elevation from 10° to 15° is important in case of Low loss O2I penetration type (10,1 dB) while it is careless for the high loss type (1,3 dB). The effect of changing the type of O2I penetration loss from Low to High in case of TX/RX HPBW azimuth/Elevation 15° is twice times in case of HPBW 10°.

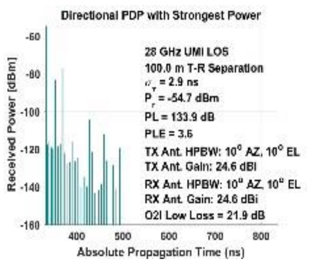

(a) Scenario 1

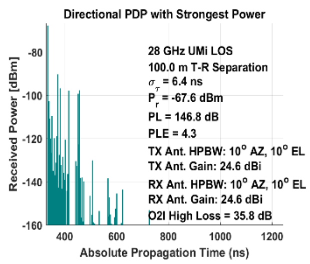

(b) Scenario 2

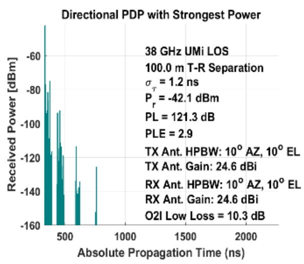

(c) Scenario 3

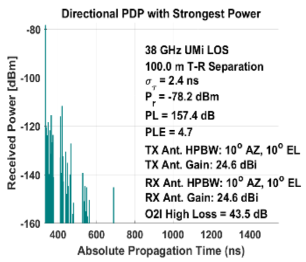

(d) Scenario 4

Fig 4.1 Directional Power Delay Profile channel 28 [GHz]

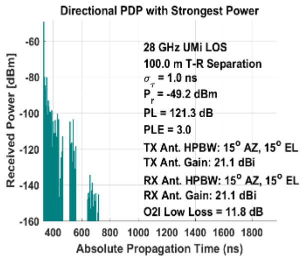

(a) Scenario 1

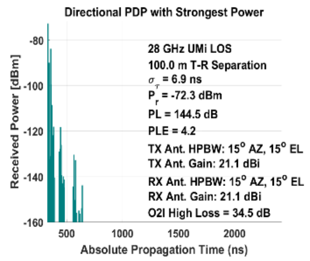

(b) Scenario 2

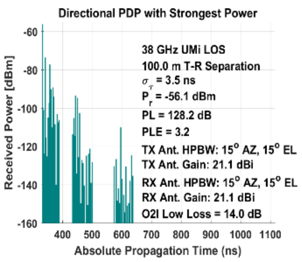

(c) Scenario 3

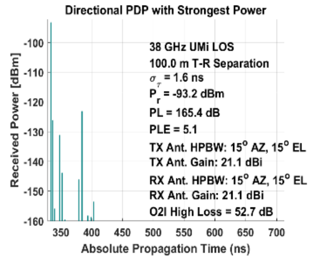

(d) Scenario 4

Fig 4.2 Directional Power Delay Profile channel 38 [GHz]

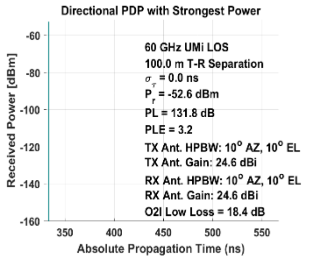

(a) Scenario 1

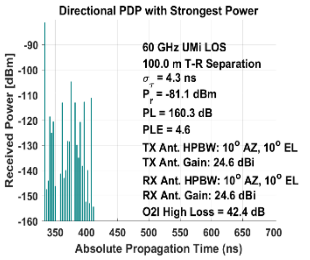

(b) Scenario 2

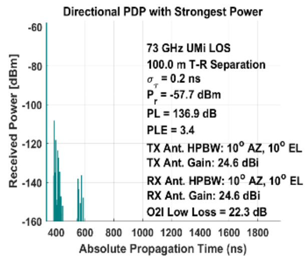

(c) Scenario 3

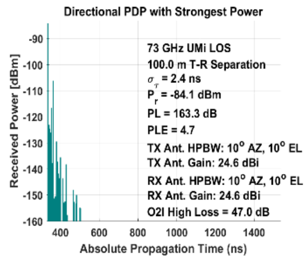

(d) Scenario 4

Fig 4.3 Directional Power Delay Profile channel 60 [GHz]

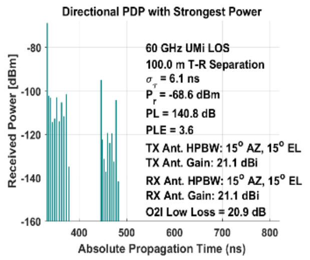

(a) Scenario 1

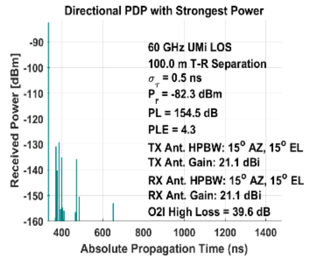

(b) Scenario 2

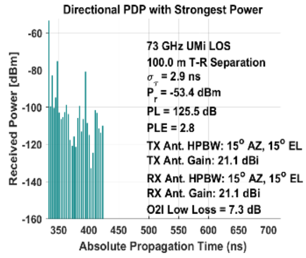

(c) Scenario 3

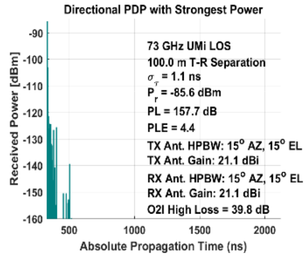

(d) Scenario 4

Fig 4.4 Directional Power Delay Profile channel 73 [GHz]

Freq Channel[GHz]	Scenario	O2I penetration loss [dB]
28	1	21,9
	2	35,8
	3	11,8
	4	34,5
38	1	10,3
	2	43,5
	3	14,0
	4	52,7
60	1	18,4
	2	42,4
	3	20,9
	4	39,6
73	1	22,3
	2	47,0
	3	7,3
	4	39.6

Table 6 Summarize results for Directional PDP

4.4.2 Omni PDP for O2I penetration loss scenarios

Figure 4.5, 4.6, 4.7 and 4.8 show the Omni-directional PDP output from a NYUSIM run with O2I penetration loss at 28, 38, 60 and 73 [GHz] respectively for the four scenarios. From figure 4.5, 4.6, 4.7 and 4.8, we can summarize results in Table 7.

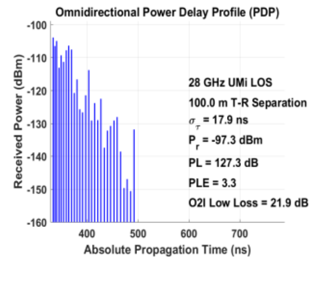

(a) Scenario 1

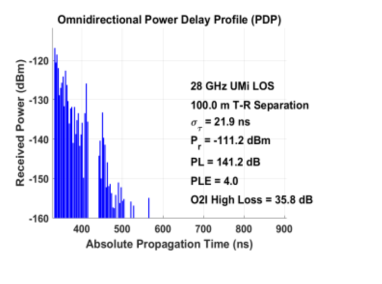

(b) Scenario 2

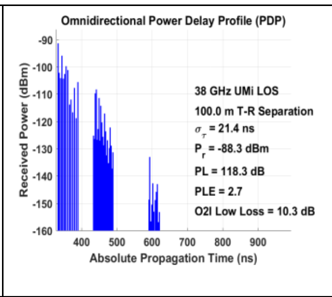

(c) Scenario 3

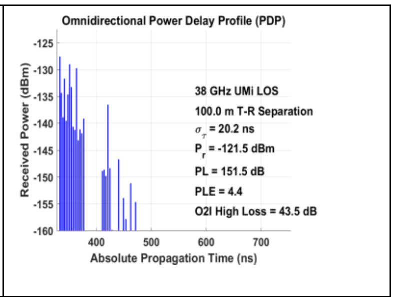

(d) Scenario 4

Fig 4.5 Omnidirectional Power Delay Profile channel 28 [GHz]

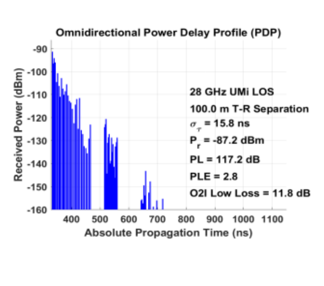

(a) Scenario 1

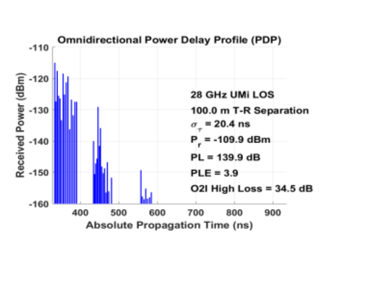

(b) Scenario 2

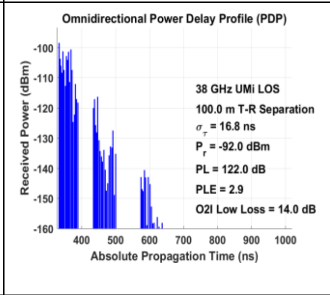

(c) Scenario 3

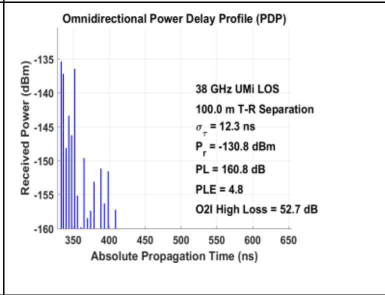

(d) Scenario 4

Fig 4.6 Omnidirectional Power Delay Profile channel 38 [GHz]

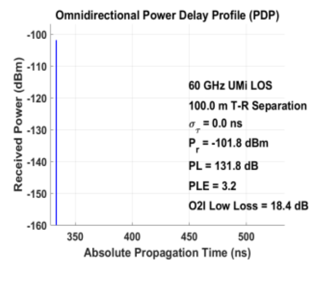

(a) Scenario 1

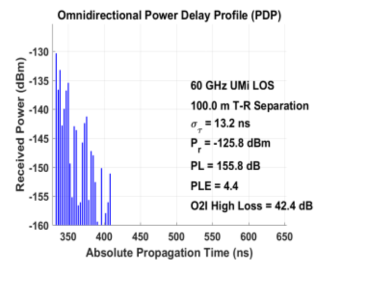

(b) Scenario 2

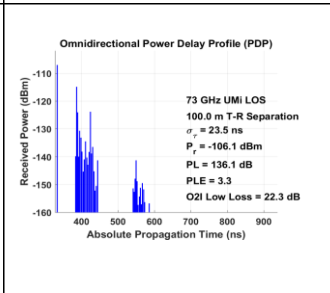

(c) Scenario 3

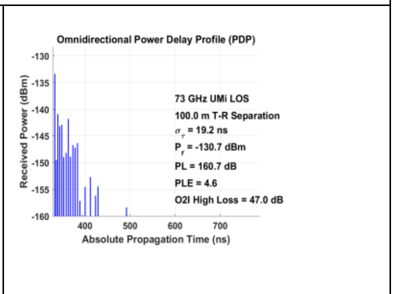

(d) Scenario 4

Fig 4.7 Omnidirectional Power Delay Profile channel 60 [GHz]

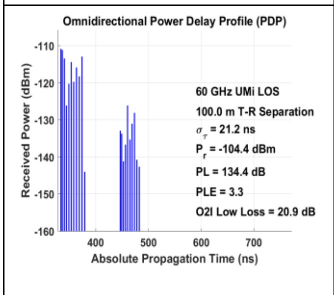

(a) Scenario 1

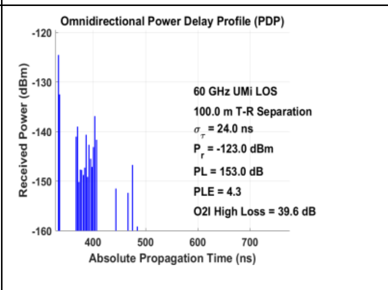

(b) Scenario 2

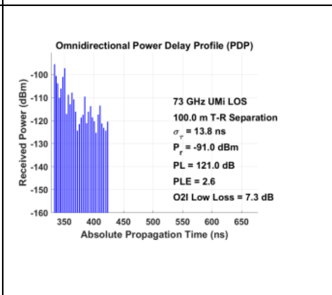

(c) Scenario 3

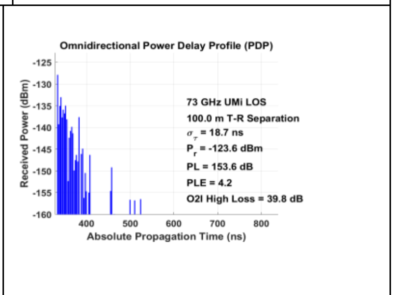

(d) Scenario 4

Fig 4.8 Omnidirectional Power Delay Profile channel 73 [GHz]

Freq Channel [GHz]	Scenario	O2I penetration loss [dB]
28	1	21,9
	2	35,8
	3	11,8
	4	34,5
38	1	10,3
	2	43,5
	3	14,0
	4	52,7
60	1	18,4
	2	42,4
	3	20,9
	4	39,6
73	1	22,3
	2	47,0
	3	7,3
	4	39.6

Table 7 Summarize results for Omnidirectional PDP

All remarks that are reported for the results obtained in the directional PDP are the same for omnidirectional PDP. Directional PDP and Omni-directional PDP have the same values of O2I penetration loss for all channels.

4.5 Conclusion

This chapter presents Analysis of O2I penetration loss of mmWave channels at 28, 38, 60 and 73 [GHz] operating frequency for different scenarios Low loss / High loss and TX/RX Antenna HPBW azimuth/Elevation 10°/15°. The type of building (standard glass, wood, IRR glass and concrete....) and Antenna properties (HPBW) affects channel characteristic O2I penetration loss. After the studies of the channels mentioned above, it was concluded that the channel 73 [GHz] is more affected by the change of the Antenna properties HPBW in case of low loss, the channel 28 [GHz] is less affected than 73 [GHz], but the 38 , 60 [GHz] channels are better for supporting the impact of this change. In case of High loss , channel 38 [GHz] is more affected by the change of the Antenna properties HPBW, the channel 73 [GHz] is less affected than 38 [GHz], but the 28 , 60 [GHz] channels are better for supporting the impact of this change. In case of HPBW=10°, channels 73, 38, 60 [GHz] are more effected by the change of the type of building, but channel 28 is less effected than the other channels. In case of HPBW=15°, channel 38 [GHz] is more effected by the change of the type of building , channels 73, 60, 28 [GHz] is less effected than 38 [GHz]. Directional PDP and Omni-directional PDP have the same values of O2I penetration loss for all channels.

CHAPTER 05

The Impact of azimuth and elevation Half Power Beam Width on Human Blockage scenarios in mmWave Channels

5 Impact of azimuth and elevation Half Power Beam Width on Human Blockage scenarios in mmWave Channels

5.1 Introduction

The 5th Generation Mobile Technology (5G) is expected to connect people, data, applications, transportation systems and cities in an intelligent network communication environment. It should transfer large amounts of data faster, reliably connect a large number of devices, and process large amounts of data with minimal delay. 5G systems use mainly millimeter waves (mmWave), various systems have been proposed for the use of microwave bands in 5G systems, particularly for 28, 38, 60 and 73 [GHz] frequencies. It's very important to study mmWaves dedicated to 5G systems. In this chapter we focused on the human blockage. We present an analysis of human blockage for mmWave channels using NYUSIM V2.0 simulator developed by researchers at New York University (NYU).

5.2 Related works

In [107], the authors proposed a novel and tractable model for characterizing the probability of human-body blockage. The proposed model represents humans as cylinders with arbitrarily distributed heights and radii, whose centers follow the Poisson Point Process (PPP) in two dimensions.

In [94], the authors analyzed mm-wave propagation characteristics at 28[GHz] in a crowded meeting room scenario. They created the simulation scenario by Wireless in Site and carry out simulation by SBR method.

In [108], the authors investigated the impact of using two transmitters to overcome the human blockage and provide direct line of sight (LoS) between transmitters and the receiver to improve coverage, reliability and capacity of the transmission.

In [109], the authors studied the statistical characteristics of this problem is presented. At first, broadband measurements of human blockage are provided. Afterwards, a realistic mobility model for indoor movements of humans is adopted and elliptic cylinders are applied to approximate human bodies in ray-launching simulations

In [110] the authors analyzed the performance of mmWave based wearable networks modeling human bodies as the main source of blockages and developed an analytic approach for computing spatially averaged signal-to-interference-plus-noise-ratio (SINR) performance as seen by a typical user. They assumed the user density is very high and the wearable networks across users are uncoordinated. In this scenario, the users act as both sources of blockages and also carry potentially interfering devices with respect to a typical user's wearable communication link.

In [111], the authors have proposed a novel 3D physical model of human body blockage in outdoor mmWave communications. Compared to traditional models, their model takes the vertical drop between AP and UE into account, and gives different results in the behaviors of HBB phenomena, including self-blockage and pedestrian blockage. Through case studies in a simplified singleuser sidewalk downlink scenario, they have discussed the impacts of pedestrian density, frame length and access point height on the LOS transmission characteristics. Numerical computations have been conducted under different configurations, showing quantitative results.

In [112], the authors conducted human body shadowing (HBS) measurements in three different cases at 28 [GHz] by using a pair of horn antennas. Based on their measurement results, they proposed a simple HBS model, and then used the double-edge and the multiple-edge diffraction method to study the characteristics of HBS.

In [113], the authors conducted a peer-to-peer (P2P) measurement campaign with 7◦, 15◦, and 60◦ half-power beamwidth (HPBW) antenna pairs at 73.5 [GHz] and with 1 [GHz] of RF null-to-null bandwidth in a heavily populated open square scenario in Brooklyn, New York, to study blockage events caused by typical pedestrian traffic.

In [114], the authors presented 73 [GHz] human blockage measurements for a point-to-point link with a 5 m transmitter-receiver separation distance in an indoor environment, with a human that walked at a speed of approximately 1 m/s at a perpendicular orientation to the line between the transmitter and receiver, at various distances between them. The experiment measures the shadowing effect of a moving human body when using directional antennas at the transmitter and receiver for millimeter-wave radio communications. The measurements were conducted using a 500 Megachips-per-second wideband correlator channel sounder with a 1 [GHz] first null-to-null RF bandwidth.

5.3 HUMAN BLOCKAGE SHADOWING LOSS MODELS

Two simple methods are used here to model blocking events:

1) a two-state method with unshadowed and shadowed states;

2) a four-state method with unshadowed, decaying signal level, shadowed, and rising signal level states.

5.3.1 Two-State Blockage Modeling

A two-state Markov model can be employed to describe unshadowed and shadowed states for a wireless link in the presence of walker made variations in the strength of the received signal [115],

[116]. Fig. 5.1 indicates a presentation of a two-state Markov model where P_{unshad} and P_{shad} denote the change probabilities of going from a shadowed to unshadowed state and inversely, respectively. A predefined threshold is designated in order to characterize a shadowed or unshadowed state and is usually 0 dB to -10 dB from the zero intersections just before and after the fading event.

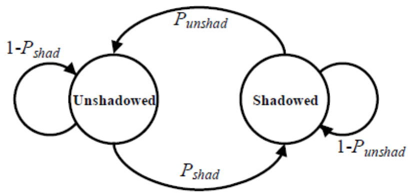

Fig 5.1 Two-state Markov model for blockage events [113].

5.3.2 Four-State Blockage Modeling

A four-state piecewise linear modeling method is alsouseful for describing blockage with the following regions : unshadowed, shadowed, a decaying signal level region from unshadowed to shadowed, and a rising signal level region from shadowed to unshadowed [117]. The blockage event signal level (in dB) as a function of time, $SE(t)$ is expressed as [117], [118] :

$$SE(t) = \begin{cases} r_{\text{decay}} \cdot t, & \text{for } 0 \le t \le \frac{SE_{\text{mean}}}{r_{\text{decay}}} \\ SE_{\text{mean}}, & \text{for } \frac{SE_{\text{mean}}}{r_{\text{decay}}} \le t \le t_D - \frac{SE_{\text{mean}}}{r_{\text{rise}}} \\ SE_{\text{mean}} - r_{\text{rise}} \cdot t, & \text{for } t_D - \frac{SE_{\text{mean}}}{r_{\text{rise}}} \le t \le t_D \\ 0, & \text{otherwise} \end{cases} \quad (14)$$

where r_{decay} is the signal strength decay rate in dB/ms, t is the time in ms from the onset (t = 0 ms) of the blockage event, SE_{mean} is the blockage event mean signal attenuation in dB, r_{rise} is the blockage event signal strength rise rate in dB/ms, and t_D is the shadowing event fade time duration in ms [119].

Fig. 5.2 indicates a presentation of a four-state Markov model where P_{decay}, P_{rise} denotes the changing probabilities from an unshadowed state to a state of decaying signal levels, and from a shadowed state to a rising signal level, respectively state, P_{unshad} and P_{shad} are the changing probabilities, from a rising signal state to an unshadowed state and from a decaying signal state to an shadowed state, respectively.

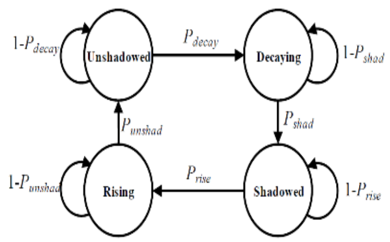

Fig 5.2 Four-state Markov model for unshadowed, decaying, shadowed, and rising regions for modeling blockage events [8] .

NYUSIM provides both a default setting as a linear fit of different beamwidths based on [120], but also permits the user to input different setting of Markov model parameters for different human shadowing models.

The default linear fit of transition rates is adopted in the NYUSIM channel model and given by [75]

$$\begin{aligned} \lambda_{\text{decay}} &= 0.2 \\ \lambda_{\text{shad}} &= 0.065 * \text{HPBW}(\ \ ^\circ) + 7.425 \\ \lambda_{\text{rise}} &= 0.05 * \text{HPBW}(\ \ ^\circ) + 7.35 \\ \lambda_{\text{unshad}} &= 6.7 \end{aligned} \qquad (15)$$

5.4 SIMULATION AND RESULTS ANALASIS

In this section, we will simulate the humane blockage for the most used millimeter wave channels (28, 38, 60 and 73 [GHz]) for different scenarios using NYUSIM V2.0.

The simulation with different choice of parameters is carried out in this section. For the simulation, assumptions were made for both channel and antenna properties represented in Table 8 and Table 9 with activation of human blockage event using the default linear fit of transition rates. Simulations results for the four scenarios proposed in this study was carried out in the form of figures and organized by type of result.

PARAMETERS/ SCENARIO N°	1	2	3	4
RF BW MHz	800	800	800	800
Scenario	UMi	UMi	UMi	UMi

LOS/NLOS	LOS	LOS	LOS	LOS
T-R Separation (m)	100	100	100	100
TX Power (dBm)	30	30	30	30
Num RX	1	1	1	1
Press (mbar)	1013	1013	1013	1013
Hum %	50	50	50	50
Temp. C°	20	20	20	20
Pol	c-pol	c-pol	c-pol	c-pol
D Foliage (m)	0	0	0	0
Rain rate mm/hr	0	0	0	0

TABLE 8. Channel simulation scenarios parameters

PARAMETERS/ SCENARIO N°	1	2	3	4
TX/RX Array Type	ULA/ULA	ULA/ULA	ULA/ULA	ULA/ULA
Num TX/RX Elements	1/1	1/1	1/1	1/1
TX/RX Antenna Spacing	0.5λ/0.5λ	0.5λ/0.5λ	0.5λ/0.5λ	0.5λ/0.5λ
TX/RX Elevation/Azimuth	7°/7°	10°/10°	15°/15°	30°/30°

TABLE 9. Antenna Simulation Parameters

5.4.1 DPDP for human blockage loss senarios:

Figs. 5.3-5.5, show the PL, received power, and PLE of the directional power delay profile DPDP with human blockage event at 28, 38, 60 and 73 [GHz] respectively for the four scenarios.

From Figs 5.3-5.5, we see that:

In all scenarios, channel 73 [GHz] has a lower received power, while 28 [GHz] has the higher one.
In all scenarios, channel 38 [GHz] has a received power greeter than 60 [GHz].

Scenario1 (HPBW=7°) has the higher value of received power while scenario 4 (HPBW =30°) has lower one and vice versa for path loss.

In all scenarios, all channels have approximately the same path loss exponent values.

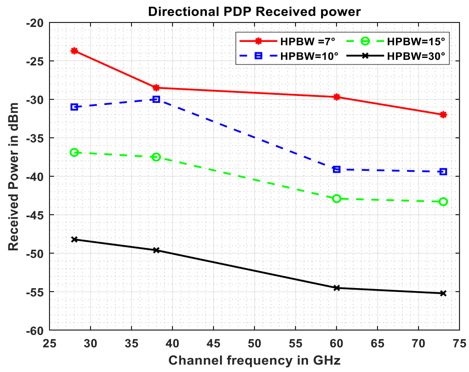

Fig 5.3 Received Power of DPDP.

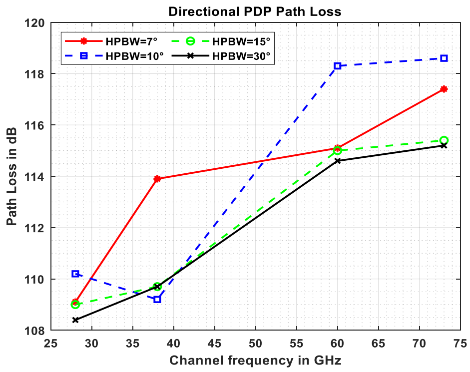

Fig 5.4 Path Loss of DPDP.

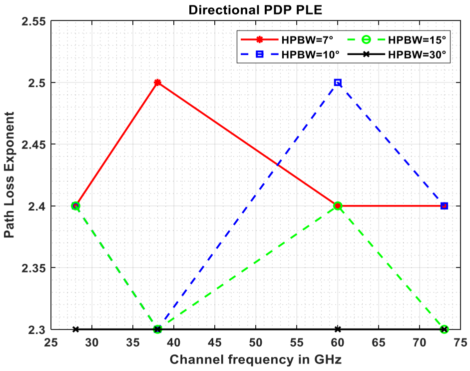

Fig 5.5 Path Loss Exponent for DPDP.

Figs. 5.6-5.8, show the impact of HPBW on the PL, received power, and PLE of the directional power delay profile DPDP for 28, 38, 60 and 73 [GHz] channels.

From Figs 5.6-5.8, we see that:

For all channel, when HPBW increase the received power decrease, and vice versa for the path loss.The parameter HPWB have the same impact in Channels (28, 38 [GHz]) and in channels (60, 73 [GHz]).

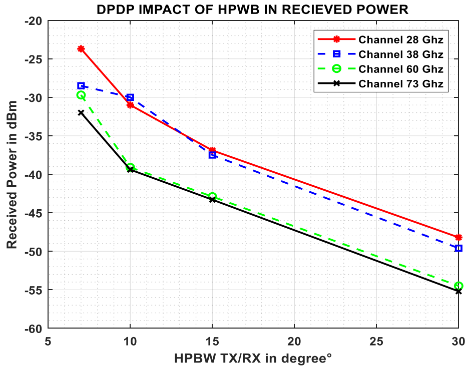

Fig 5.6 Impact of HPBW in Received Power of DPDP.

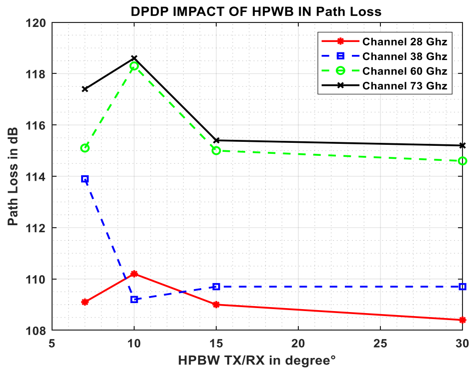

Fig 5.7 Impact of HPBW in Path Loss of DPDP.

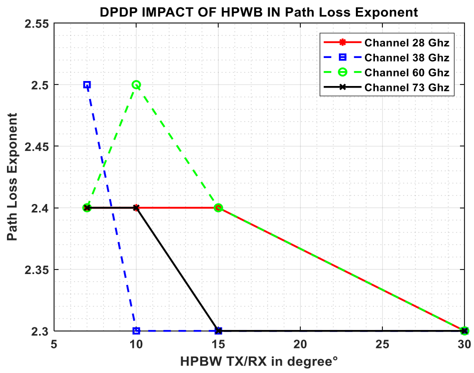

Fig 5.8 Impact of HPBW in Path Loss Exponent for DPDP.

5.4.2 OPDP for human blockage loss scenarios:

Figs. 5.9-5.11, show the PL, received power, and PLE of the omnidirectional power delay profile OPDP with human blockage event at 28, 38, 60 and 73 [GHz] respectively for the four scenarios.

From Figs 5.9-5.11, we see that:

In all scenarios, channel 73 [GHz] has a lower received power, while 28 [GHz] has the higher one.

In all scenarios, for each channel the received power is the same.

In all scenarios, for each channel the path loss is the same.

Scenario1 (HPBW=7°) has the higher value of received power while scenario 4 (HPBW =30°) has lower one and vice versa for path loss.

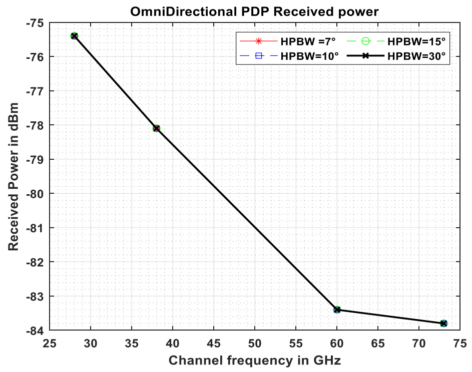

Fig 5.9 Received Power of OPDP.

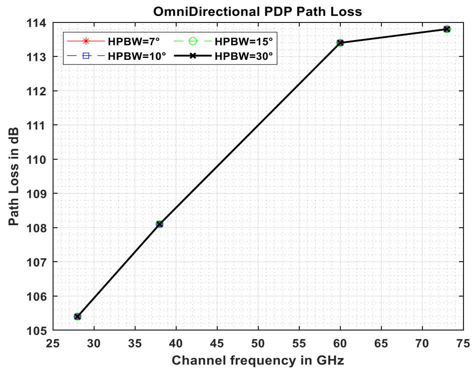

Fig 5.10 Path Loss of OPDP.

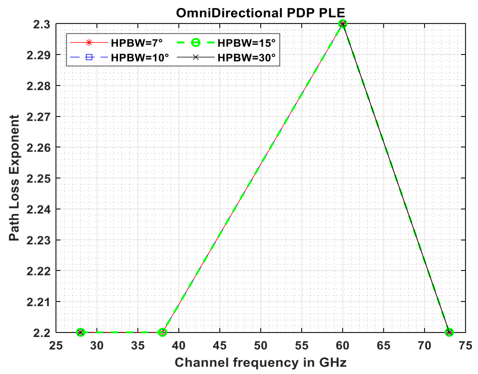

Fig 5.11 Path Loss Exponent for OPDP.

Figs. 5.12-5.14, show the impact of HPBW on the PL, received power, and PLE of the omnidirectional power delay profile DPDP for 28, 38, 60 and 73 [GHz] channels.

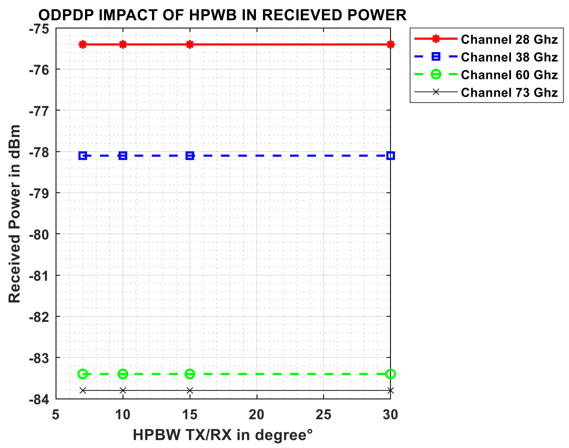

Fig 5.12 Impact of HPBW in Received Power of OPDP.

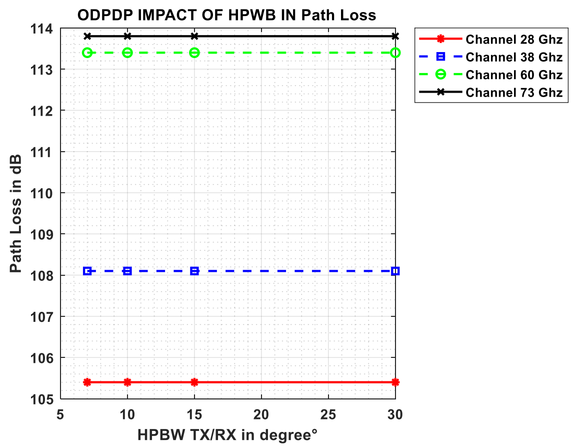

Fig 5.13 Impact of HPBW in Path Loss of OPDP.

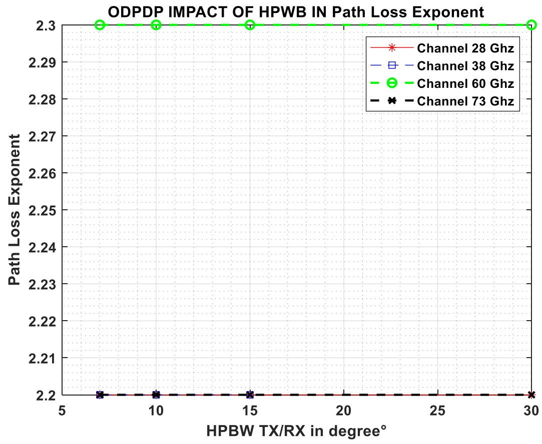

Fig 5.14 Impact of HPBW in Path Loss Exponent for OPDP.

From Figs 5.12-5.14, we see that:

For all channel, when HPBW increase the received power decrease, and vice versa for the path loss.

The parameter HPWB have the same impact in Channels (28, 38 [GHz]) and in channels (60, 73 [GHz]).

All remarks that are reported for the results obtained in the directional PDP are the same for omnidirectional PDP.

Directional PDP has higher path loss, path loss exponent and received power compare to Omni-directional PDP for all channels. In the same Channel Omni-directional PDP have the same values of path loss, path loss exponent and received power for all scenarios.

5.5 CONCLUSION

This chapter presents Analysis of the impact of human blockage for the mmWave channels at 28, 38, 60 and 73 [GHz] operating frequency for different scenarios especially for different TX/RX Antenna HPBW azimuth/Elevation 7°, 10°, 15°, 30°. After the studies of the channels mentioned above, it was concluded that the channel 73 [GHz] is more affected by the human blockage event but the 28, 38 and 60 [GHz] channels are better for supporting it. In same channel, the impact of human blockage events are more important when using widebeam antennas compared to narrow beam antennas. The beam width antenna has no effect on the channel parameters for omnidirectional PDP. Omnidirectional PDP more affected by the human blockage compare to Directional PDP.

CHAPTER 6

Effect of Spatial Consistency Parameters on 5G Millimeter Wave Channel Characteristics

6 Effect of Spatial Consistency Parameters on 5G Millimeter Wave Channel Characteristics

6.1 Introduction

Wireless channel modeling has been extensively studied for several millimeter waves (mmWave) frequencies under different scenarios and environmental conditions for 5G networks, thereby making it increasingly important [61]. Spatial consistency scenario is a major issue in the field of statistical analysis of mmWaves channel propagation [70, 75,121-123]. Overall, the spatial consistency channel model is defined by when the user moves along a given track and produces a correlated and sequential channel impulse response at successive sample points on the track [123]. Therefore, in the context of channel modeling, spatial consistency refers to similar and correlated scattering environments in both large and small scale settings [124]. In general, we can classify channel model scenarios into indoor/outdoor and therefore urban microcells (UMi), macro urban (UMa), and macro rural (RMa) for LOS/NLOS environments [61].

Statistical channel models often use wide variables as well as shadow fading (SF), propagation delay, time groups, and angular spreads, which moreover depend on small-scale parameters such as time excess delay, received power, angle of arrival (AoA), and the angle of departure (AoD) for each multipath component measurement. This work presents the results of several analyses for various environments and spatial variables performed with NYUSIM model [121] and associated simulator (established by the New York university as open-source software) used by the authors in [61, 71, 121]. NYUSIM model exploits the Close In (CI) path loss channel model to perform all channel measurements [70, 75,121-123].

The primary basis for choosing this model is the use of a purely geometric multiple reflection surface approach to produce spatially correlated and time-varying channel coefficients. These modeling skills generate realistic data when being performed using the Monte Carlo method, thus making this model an excellent measurement-based channel simulator for the design and evaluation of the 5G mmWave bands. Although in the literature, there are many deterministic and statistical channel models which are presented as 5GCM [124], mmMAGIC [101], METIS [11], MiWEBA [125], and 3GPP [30], NYUSIM [121] is still the most suitable model. This model is extended from a static drop-based channel model to a dynamic time-varying channel model that fits well through the natural evolution of NYUSIM and other statistical drop-based models [121].

Given the small number of experiments and studies conducted on spatial consistency analysis, we focus on an in-depth analysis of the effect of different parameters on received power, path loss (PL), and path loss exponent (PLE) for both directional power delay profile (DPDP) and omnidirectional power delay profile (OPDP). Moreover, this study considers spatial consistency [75] and omnidirectional/directional power delay profile (PDP) for the case of a mobile terminal with spatial consistency and a static user terminal (UT) without spatial consistency. The considered diverse parameters are: correlation distance, LOS/NLOS, moving distance, the user's velocity, and user track-type for UMi scenario of the 5G system.

6.2 Related work

Along with channel modeling tools (SMRCIM [126] and SIRCIM [49]), statistical channel impulse response models have been developed for multi-path components corresponding to microwave frequencies with respect to temporal and spatial correlation. In particular, these simulators investigated the motion, Doppler propagation, and the phase shift resulting from the multivariate components in a limited zone. Some works focus on spatial consistency analysis; however, they are insufficient since some channel characteristics (PL, PLE, received power) are not studied in detail and in depth, especially regarding spatial consistency parameters [71,75,122,123]. Using the NYUSIM channel simulator platform, the authors in [123] studied the spatial modeling properties at 73 [GHz] frequency but considering only one spatial consistency tuning parameter. In [104], the authors developed a modified PL model for spatial consistency analysis, but without examining the spatial consistency effect on various channel characteristic parameters. The authors in [127] compared a geometry-based spatially consistent channel model with a deterministic ray-tracing model to evaluate the properties of the strongest multipath components as a function of the azimuth/elevation angles of arrival and delay of successive spatial locations in 5G UMi. In [128], the authors proposed a model that improves geometry-based stochastic channel models with spatial consistency by selecting the standardized 3GPP 3-dimensional (3D) channel model. This improved model is characterized by a single parameter called decorrelation distance where simulation was done at low frequencies 2 [GHz] and 28 [GHz].

The main contribution of this paper is to investigate the effect of various spatial consistency parameters on the modeling of 5G mmWave channels. The objective is to study channel characteristics in the 5G mmWave band for typical spatial consistency scenarios: correlation distance LOS/NLOS, moving distance, velocity of the user, and user track type in UMi environment. At each 1 m step, the channel coefficients are updated using a spatial coherence process along the UT track (Linear/Hexagonal) in a local area of the cell, considering a channel portion spitted into diverse channel snapshots. However, the characteristics of millimeter wave dynamics can be the subject of further work.

In general, the received power decreases with distance for the small-scale spatial autocorrelation coefficient [75]. Since the scattering environment is not significantly varied in a local area, the large-scale parameters have a greater correlation distance. In effect, the scattering environment is not significantly varied in a local area.

6.3 STATISTICAL ANALYSIS OF 5G MILLIMETER WAVE CHANNEL MODELING

A major problem in statistical channel modeling is the consideration of spatial consistency scenario, which results in a time-varying channel impulse response in a local environment. To overcome this problem, a rigorous channel modeling is therefore necessary. In this section, based on NYUSIM model, we analyze the impact of different spatial consistency parameters as a function of received power, PL and PLE of DPDP and OPDP considering absolute delay and tracking of the user's localization distance on 28, 38, and 73 [GHz] millimeter wave channels.

Considering a spatial consistency scenario, Figure 6.1 describes the LOS and NLOS mmWave connection for moving mobile station (MBS) also called user terminal (UT). The base station transfers traffic to the core network under LOS/NLOS communication, where NLOS is caused by edifice obstacles between the transceiver and the core network.

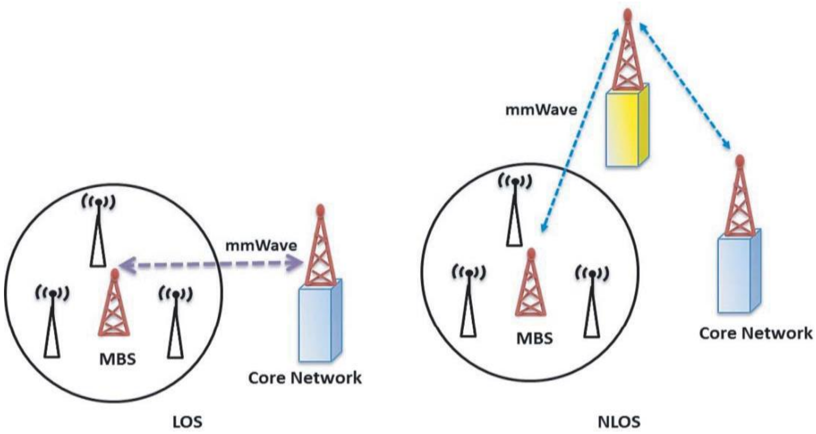

Fig 6.1 LOS/NLOS scenarios for 5G mmWave networks considering spatial consistency.

6.3.1 Spatial consistency

Spatial consistency continuously describes the real evolution of the channels along the track of the user terminal (UT) in a determined zone. Toward carrying out spatial consistency, shadow fading (SF) and LOS/NLOS condition maps are established. The correlation distance identifies the notion of "a local zone", which limits the channel portion length (channel portion is about: 10–15 m long).

The channels are well thought-out to be extremely correlated and are updated using a spatial consistency process within a channel portion that can be separated within diverse channel snapshots. We define the updating distance (eg. $1m$) by the distance between two-channel snapshots consecutive, where the channel coefficients are updated for each $1m$ step along the user's terminal track. Figure 6.2 shows a shadow fade map spatially correlated across base station (BS) and user positions. Furthermore, the spatially correlated SF map is created through filtering an independent SF map using an exponential function in Eq (14). Let's take here: $SF\ [dB] \sim N\ (0,\ 7)$ in an UMi NLOS environment. TX/RX separation distance is $100\ m$. UT has a hexagonal track with $40m$ of moving distance on four portions of $10\ m$.

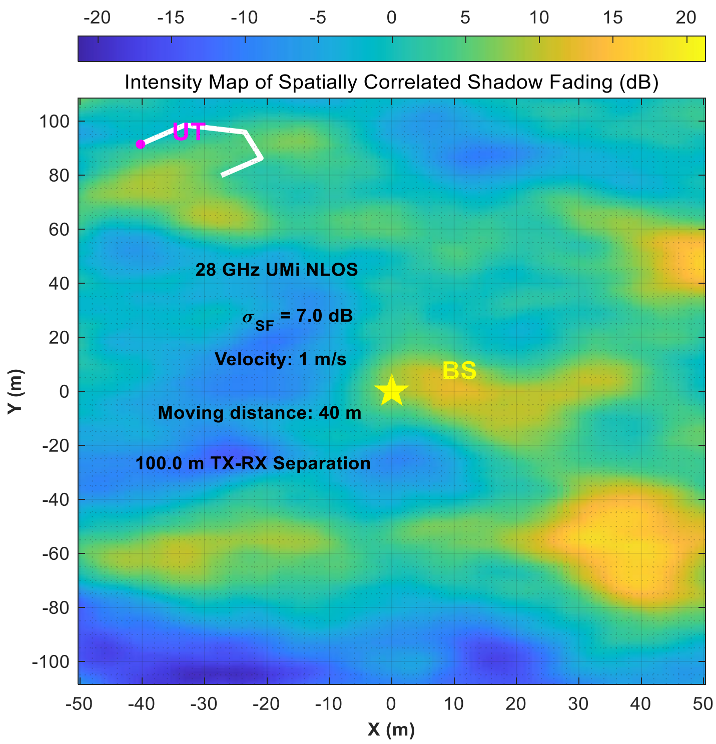

Fig 6.2 Spatial correlated Shadow Fading Map.

Figure 6.3 shows the UT track in the SF map in which the UT moves clockwise in a partial hexagonal track. Here we consider that the displacement is 40 m, and the length of each side of the hexagon is 10 m. Moreover, the spatially correlated SF and LOS/NLOS condition values are created in the same form.

In terms of SF, a 2-dimensional (2D) grid map is created to hold the spatially correlated SF gains in the simulated zone. The SF is a random variable that follows a log-normal distribution with zero mean and σ standard deviation as described in Eq. (1). At each grid, the map of SF is initialized by assigning independent and identically distributed random variables (i.i.d) fitting normal distribution. An exponential 2-D filter is used with the map, and it is formulated by [129]:

$$h(x,y) = \exp(-\frac{\sqrt{x^2+y^2}}{d_{co}}) \tag{14}$$

Fig 6.3 User Terminal track in SF map

x, y represent the coordinates of UT with respect to the center of the filter.

$\sqrt{x^2+y^2}$: represents the distance of the filter.

d_{co}: is the correlation distance of SF.

It is worth noting that the LOS/NLOS condition is significant in estimating the performance of wireless communication systems, especially at mmWave frequencies. These conditions define the PLE and shadow fade deviation, while the user's movements between the LOS and NLOS conditions result in a dramatic change in received signal power. Usually, when a UT moves in a local zone, LOS/NLOS condition is the same inside the correlation distance of LOS/NLOS.

By generating a spatially correlated LOS/NLOS condition map, a UT will encounter the same visibility conditions in a local area. Within each channel portion, the visibility condition is kept constant, indicating that the large-scale parameters are spatially consistent. As soon as a UT moves from one channel portion to the next channel portion and its visibility state is changed according to the position of the UT in the map, different parameter values for LOS or NLOS are used to initialize the channel coefficients for the new channel portion. This implies that the LOS/NLOS shift can be applied to the spatially correlated map.

The LOS probability model $Pr_{LOS}(d)$ used in NYUSIM for 5G UMi scenario is given by [75]:

$$Pr_{LOS}(d) = (\min(d_1/d, 1)(1-\exp(-d_2/d)) + \exp(-d_2/d))^2 \tag{15}$$

NLOS condition. The size of a UMi cell for mmWave communication systems is typically 200 m [75]. So, the simulated zone is fixed to 200 m 100 m. The correlation distance is 10 m. The granularity of the map is 1 m. The heights of the BS and UT where d is the 2D Euclidean distance between BS and UT and (d_1, d_2) = (22 m, 100 m).

Figure 6.4 shows a spatially correlated LOS and NLOS environment map in UMi scenari In addition, the “white zone” represents LOS condition while the “black zone” represents are 10 m and 1.50 m, respectively.

The LOS and NLOS conditions change can affect the UT’s track depending on the UT’s location on the map.

In line with the NYUSIM channel model [75,121], the authors of [129] proposed an efficient and dynamic extension for spatial consistency using a modified flowchart-described scheme, which made it possible to achieve spatial consistency and extend a static and drop-based channel model to a dynamic and time-variant one. Figure 5 describes the procedure for generating the spatial coherence parameters using the NYUSIM platform [129]. The new NYUSIM platform aims to update channel coefficients in an iterative way along the UT trajectory. The main steps in the modified flowchart are illustrated as follows [129]:

- Set TX-RX separation distance, UT’s velocity, and direction: The update UT distance is less than 1 m so that small changes can be captured compared to the correlation distance of 15 m from large-scale settings. The period to be updated is 0.25 s when the UT speed is 1 m/s [129].
- Assign propagation conditions to spatial correlation (LOS and NLOS): It is obvious that a moving user terminal can take various LOS/NLOS in a selected zone, where the propagation environments at several situations are correlated. Thus, NYUSIM model took into account correlation parameters. The model followed a process similar to that illustrated in [27] by generating the large-scale correlation parameters based on a spatial filter to independent exponential random values.

Calculate the path loss of time-variant: The path loss is carried out from the UT updated position in each update. Otherwise, the usual variation SF is judged as constant and varied at the propagation condition (LOS and NLOS) deviation.

- Produce time-variant cluster and sub-path excess delays: Initially NYUSIM generates the initial sub-path with cluster delays, where UT is at the start of a half hexagon direction. The excess time delays is updated based on speed, direction, and the time varying AOA/AOD when the UT progresses along the path.

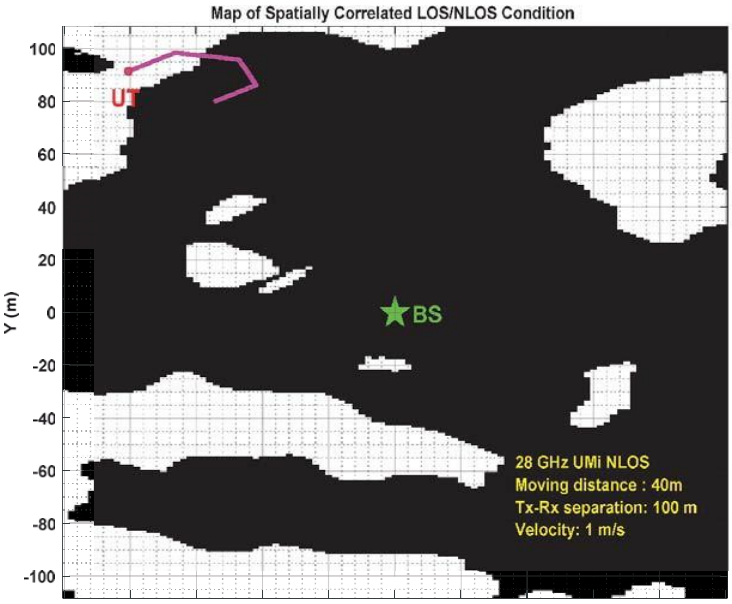

Fig 6.4 Spatial correlated LOS/NLOS condition map.

(a)

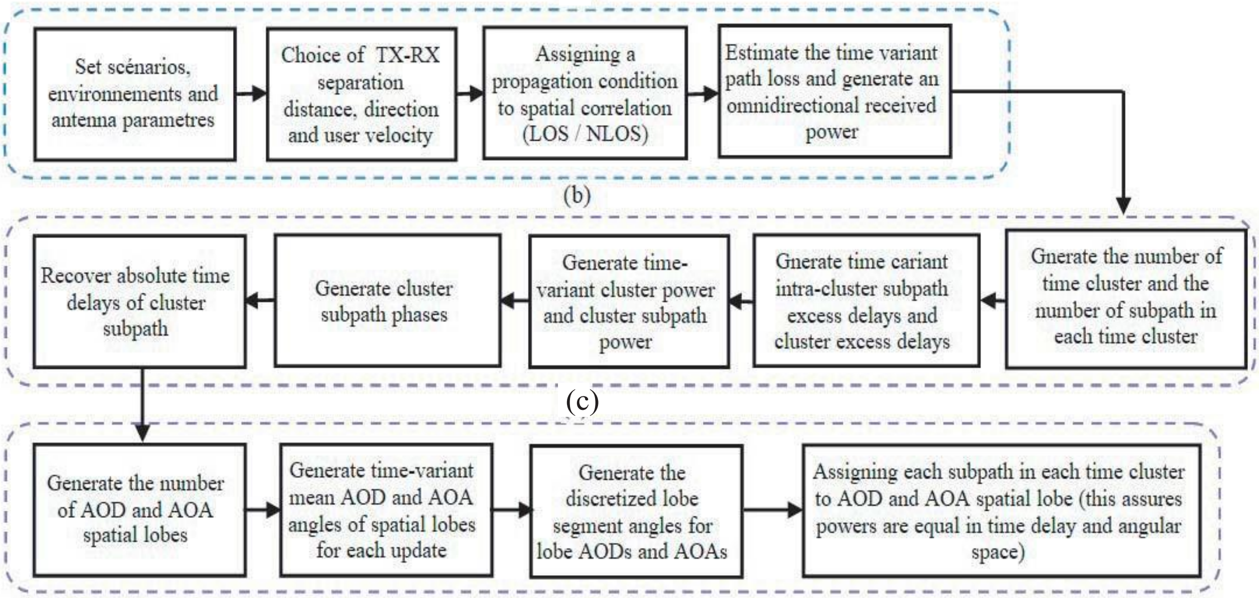

Figure 6.5 Process for generating spatially consistent channel coefficients. (a) General parameters. (b) Time cluster parameters. (c) Spatial lobe parameters [129].

- Produce time-variant cluster powers and sub-path powers: Clearly, the entire expected power to be captured as well varies due to the time-varying path loss. In addition, the power of each sub-path of each cluster must be allocated during the update in a correlated and continuous manner. The two key parameters in this step are the shadow factors (SFs) for a cluster and for a sub-path. An exponential spatial filter similar to the one adopted to guarantee the probability of correlated LOS

is used to build the SFs correlated.

- Produce time-variant sub-path AODs and AOAs: One of the fundamental principles of spatial consistency implementation is to reduce the computational complexity. In fact, spatial consistency algorithms mainly suffer from a high computational complexity. Thus, the extension NYUSIM proposed by authors in [129] related to spatial consistency considers a linear approximation of angles that is introduced before in [130].

The previous steps cited above allowed generating the appropriate statistics for powers, delays, and excessive angles to introduce spatial consistency within NYUSIM model. The use of the new platform showed that the generated channel impulse responses evolved smoothly along the UT track, which confirmed the physical expectation [129]. In this work all the results (Figures and Tables) will be carried out using the NYUSIM model proposed in [129].

6.4 SIMULATION SCENARIOS AND ANALYSIS OF RESULTS

In this section, we compare some candidate mmWave channels, namely 28, 38, and 73 [GHz], for various spatial consistency scenarios using the NYUSIM model. Using the well-known NYUSIM platform, we were able to create realistic changes in the temporal and spatial characteristics of broadband channel impulse responses for a mobile terminal. For this purpose, five scenarios are developed based on the properties of the spatial consistency channels (LOS/NLOS correlation distance, moving distance, user's terminal velocity, user's track type). We followed the process to generate spatially consistent channel coefficients as described in Figure 6.5.

6.4.1 Correlation Distance LOS/NLOS Scenarios

In the first scenario, a simulation was performed by applying the parameters summarized in Table 10, in which we considered three values (10 m, 15 m, and 20 m) of the LOS/NLOS correlation distance for all studied channels. Table 11 summarizes the directional and omnidirectional power delay statistics at 28, 38, and 73 [GHz] for correlation distance LOS and NLOS environments. In addition, Figures 6.6–6.11

Channel Parameters		Antenna Parameters	
RF Frequency	28/38/73 [GHz]	**TX/RX Array Type**	ULA/ULA
RF BW MHz	800	**Num TX/RX Elements**	1/1
Scenario	UMi	**TX/RX Antenna Elements Spacing**	$0.5\lambda/0.5\lambda$
Environment	LOS/NLOS	**TX Azimuth/Elevation HPBW**	$10^{\circ}/10^{\circ}$
T-R Separation (m)	100	**RX Azimuth/Elevation HPBW**	$10^{\circ}/10^{\circ}$
TX Power (dBm)	30	**Spatial consistency Parameters**	
Num RX	1	**Moving distance (m)**	40
Press (mbar)	1013	**Correlation distance LOS/NLOS (m)**	10/15/20
Hum %	50	**Update distance (m)**	1
Temp. C°	20	**Velocity (m/s)**	1
Pol	Co-Pol	**Track type**	Linear
D Foliage (m)	0	**Moving direction (°)**	45°
Rain rate mm/hr	0		

Table 10. Spatial consistency parameters in correlation distance LOS/NLOS scenarios.

Freq Channel [GHz]	Scenario	Correlation distance (m)	Directional Power Delay Profile				Omnidirectional Power Delay Profile			
			RMS DS (ns)	Received Power [dBm]	PL [dB]	PLE	RMS DS (ns)	Received Power [dBm]	PL [dB]	PLE
28	LOS	10	28.98	−57.15	136.51	3.56	22.89	−64.27	94.27	1.56
	LOS	15	25.3	−57.83	137.05	3.95	22.68	−69.01	99.01	1.96
	LOS	20	33.07	−48.82	128.03	3.84	15.08	−68.73	98.73	2.15
	NLOS	10	129.08	−88.84	167.55	5.87	29.52	−84.06	104.06	2.91
	NLOS	15	45.67	−66.06	145.27	4.25	49.53	−91.01	121.01	3.02
	NLOS	20	194.02	−95.57	174.78	5.31	13.7	−102.45	132.45	3.32
38	LOS	10	21.61	−53.37	132.58	3.42	18.65	−97.2	127.2	2.25
	LOS	15	8.48	−50	129.21	3.41	14.41	−71.09	101.09	1.93
	LOS	20	16.58	−56.48	135.69	3.35	22.2	−83.75	113.75	2.32
	NLOS	10	56.8	−69.22	148.43	4.21	24.39	−107.16	137.16	3.65
	NLOS	15	16.76	−75.18	154.39	4.53	11.67	−101.38	131.38	3.38
	NLOS	20	28.05	−57.29	136.5	4.01	43.16	−91.44	121.44	3.18
73	LOS	10	4.3	−52.75	131.96	3.26	17.23	−78.03	108.03	2
	LOS	15	22.02	−57.48	136.69	3.16	11	−80.67	110.67	1.93
	LOS	20	24.39	−46.32	125.53	2.62	18.22	−81.48	111.48	1.96
	NLOS	10	75.23	−90.27	169.48	4.74	35.11	−112.5	142.5	3.46
	NLOS	15	95.43	−86.5	165.71	4.94	59.66	−99.22	129.22	3.06
	NLOS	20	127.79	−99.31	178.53	5.67	16.66	−106.16	136.16	3.46

Table 11. Directional and omnidirectional power delay statistics for correlation distance LOS/NLOS scenarios.

present the PL, received power, and PLE of both DPDP and OPDP in LOS /NLOS environment for correlation distance LOS/NLOS scenarios.

In the case of the directional power delay profile (DPDP) with LOS scenario, the change in correlation distance has a greater impact on the 73 [GHz] channel in terms of PL, received power, and PLE, while the impact is very limited on the 28 and 38 [GHz] channels. For the omnidirectional power delay profile (OPDP) with LOS scenario, this impact is more significant on the 38 [GHz] channel in PL, received power, however, in terms of PLE the 28 [GHz] channel is more affected, on the other hand the 38 and 73 [GHz] channels show the same impact. Finally, for DPDP and OPDP with NLOS, this impact is more significant on the 28 [GHz] channel.

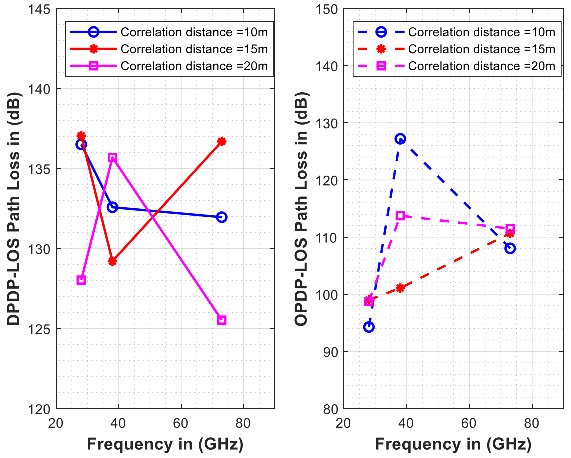

Fig 6.6 Path loss for DPDP and OPDP LOS on correlation distance LOSNLOS scenarios.

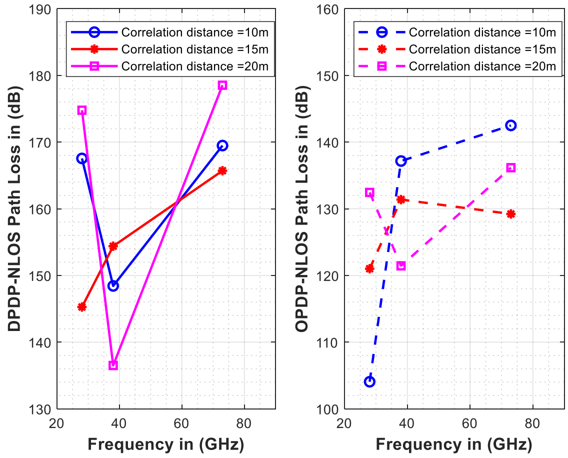

Fig 6.7 Path loss for DPDP and OPDP NLOS on correlation distance LOS/NLOS scenarios.

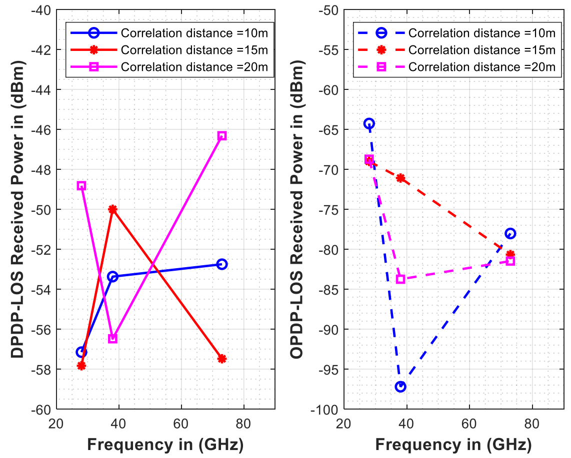

Fig 6.8 Received Power for DPDP and OPDP LOS on correlation distance LOS/NLOS scenarios.

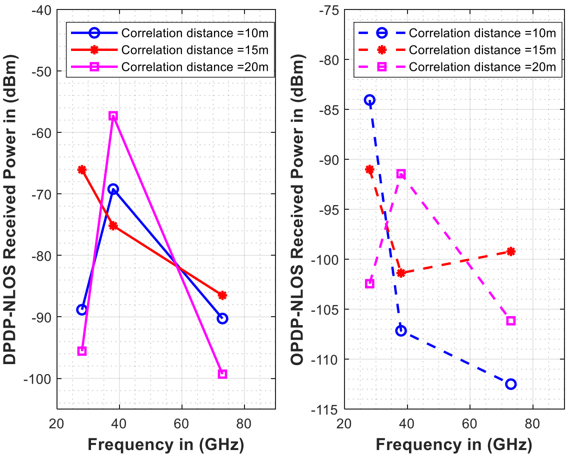

Fig 6.9 Received Power for DPDP and OPDP NLOS on correlation distance LOS/NLOS scenarios

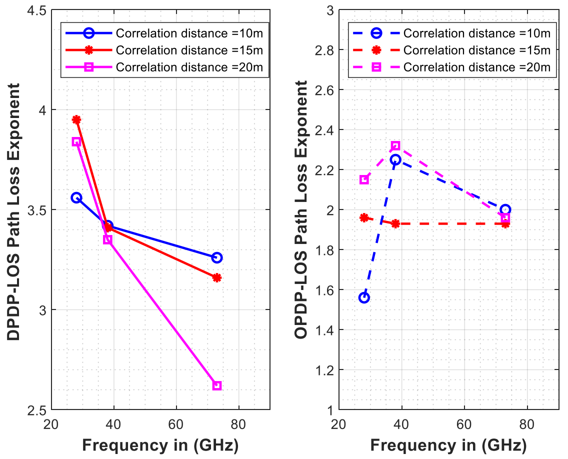

Fig 6.10 Path Loss Exponent for DPDP and OPDP LOS on correlation distance LOS/NLOS scenarios.

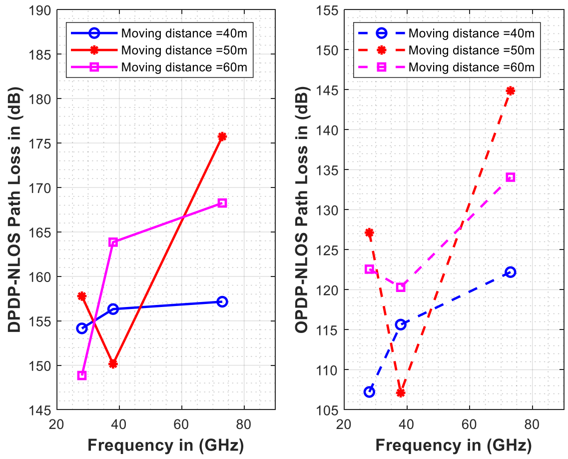

Fig 6.11 Path loss for DPDP and OPDP NLOS on correlation distance LOS/NLOS scenarios.

6.4.2 Moving Distance Scenarios

For LOS and NLOS environments, with the parameters listed in Table 12, we performed a simulation considering three values (40 m, 50 m, and 60 m) of the moving distance for all studied channels. Table 13 summarizes the results of the directional and omnidirectional Power Delay statistics at 28, 38, and 73 [GHz] for moving scenario. Figures 6.12– 6.17 illustrate the PL, received power, and PLE of both DPDP and OPDP in LOS /NLOS environment for moving distance scenarios. Similarly, the effect of the moving distance yields results analogous to those of varying the correlation distance, for both DPDP and OPDP with LOS and NLOS.

Channel Parameters			**Antenna Parameters**	
RF Frequency	28/38/73 [GHz]		**TX/RX Array Type**	ULA/ULA
RF BW MHz	800		**Num TX/RX Elements**	1/1
Scenario	UMi		**TX/RX Antenna Elements Spacing**	0.5λ/0.5λ
Environment	LOS/NLOS		**TX Azimuth/Elevation HPBW**	10°/10°
T-R Separation (m)	100		**RX Azimuth/Elevation HPBW**	10°/10°
TX Power (dBm)	30		**Spatial consistency Parameters**	
Num RX	1		**Moving distance (m)**	40/50/60
Press (mbar)	1013		**Correlation distance LOS/NLOS (m)**	10
Hum %	50		**Update distance (m)**	1
Temp. C°	20		**Velocity (m/s)**	1
Pol	Co-Pol		**Track type**	Linear
D Foliage (m)	0		**Moving direction (°)**	45°
Rain rate mm/hr	0			

Table 12. Spatial consistency parameters used within moving distance scenarios.

Freq Channel [GHz]	Scenario	Moving distance (m)	Directional Power Delay Profile				Omnidirectional Power Delay Profile			
			RMS DS (ns)	Received Power [dBm]	PL [dB]	PLE	RMS DS (ns)	Received Power [dBm]	PL [dB]	PLE
28	LOS	40	30,23	-59,12	138,33	3,61	26,72	-76,62	106,62	2,12
	LOS	50	19,83	-56,33	135,54	3,48	9,09	-69,18	99,18	1,77
	LOS	60	24,26	-56,26	135,47	3,56	24,02	-77,37	107,37	2,21
	NLOS	40	40,34	-74,93	154,15	4,92	46,79	-77,22	107,22	2,43
	NLOS	50	35,25	-78,57	157,78	4,46	15,04	-97,14	127,14	3,04
	NLOS	60	69,84	-69,64	148,85	4,68	41,76	-92,57	122,57	3,28
38	LOS	40	23,96	-57,09	136,3	3,66	18,55	-67,2	97,2	1,68
	LOS	50	0,35	-41,98	121,19	2,66	5,6	-75,47	105,47	1,93
	LOS	60	24,53	-54,04	135,25	3,88	23,85	-69,99	99,99	2,01
	NLOS	40	75,97	-77,11	156,32	5,1	49,15	-85,64	115,64	2,88
	NLOS	50	70,87	-70,94	150,15	4,87	16,13	-77,12	107,12	2,43
	NLOS	60	109,79	-84,64	163,85	4,67	26,79	-90,3	120,3	2,63
73	LOS	40	25,36	-56,37	135,58	3,1	22,14	-89,48	119,48	2,34
	LOS	50	24,21	-57,8	137	3,31	12	-80,7	110,7	2,01
	LOS	60	56,54	-74,05	153,26	4,6	15,04	-73,24	103,24	1,84
	NLOS	40	39,95	-77,94	157,15	4,26	14,95	-102,2	122,2	3,05
	NLOS	50	239,2	-96,52	175,73	4,98	19,16	-114,86	144,86	3,46
	NLOS	60	106,79	-89,04	168,25	4,51	34,22	-104,06	134,06	2,95

Table 13. Results obtained from directional and omnidirectional power delay statistics for moving distance scenarios

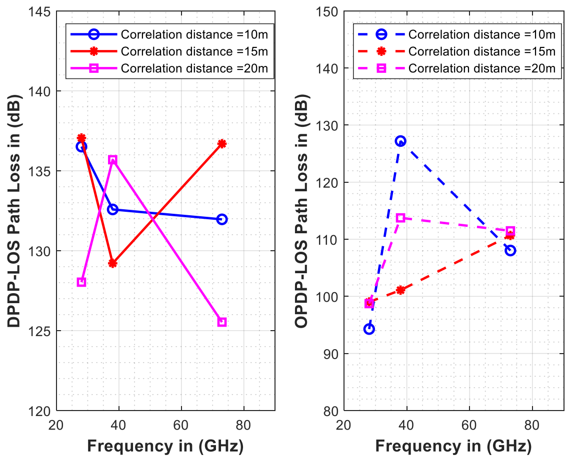

Fig 6.12 Path loss for DPDP and OPDP LOS on correlation distance LOSNLOS scenarios.

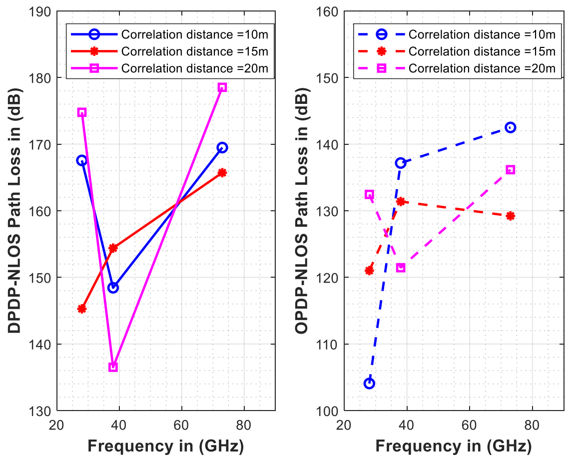

Fig 6.13 Path loss for DPDP and OPDP NLOS on correlation distance LOS/NLOS scenarios.

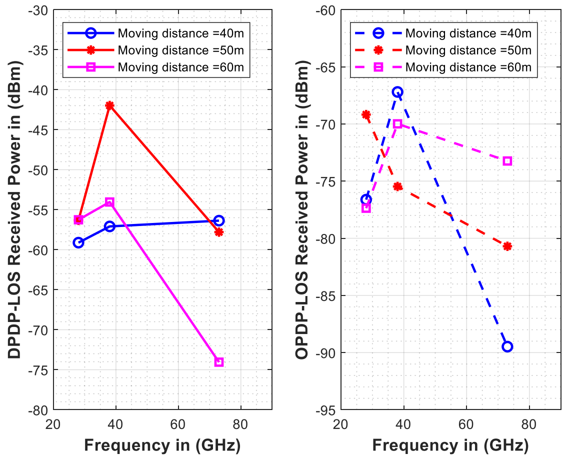

Fig 6.14 Received Power for DPDP and OPDP LOS on moving distance scenarios

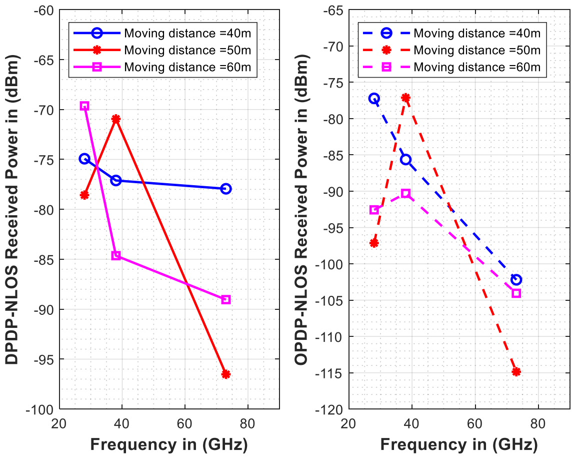

Figure 6.15 Received Power for DPDP and OPDP NLOS on moving distance scenarios.

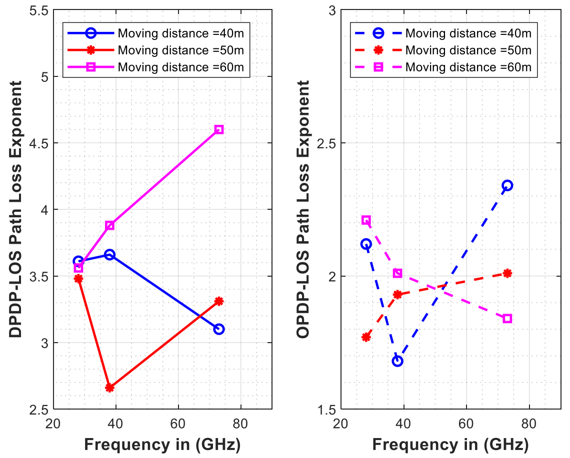

Figure 6.16 Path Loss Exponent for DPDP and OPDP LOS on moving distance scenarios.

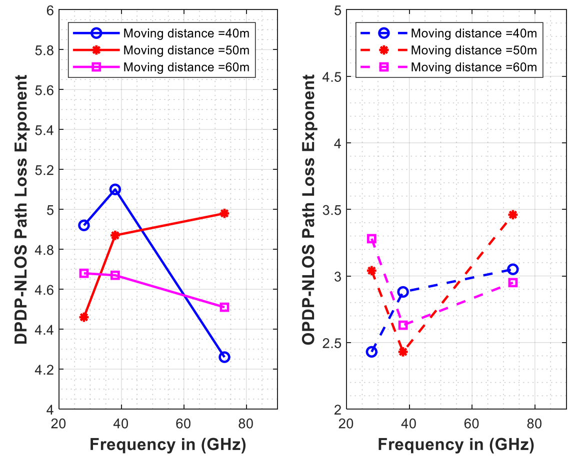

Figure 6.17 Path Loss Exponent for DPDP and OPDP NLOS on moving distance scenarios

6.4.3 Velocity Scenarios

In this scenario, we performed a simulation with the parameters summarized in Table 14 where we considered three values (1 m/s, 2 m/s, and 5 m/s) of the user's velocity for all studied channels in both LOS and NLOS environments

Table 15 summarizes the results of the OPDP and DPDP statistics at 28, 38, and 73 [GHz] for velocity scenario. Figures 6.18–6.23 present the PL, received power, and PLE of both DPDP and OPDP within LOS/NLOS environment for velocity scenarios. Based on these figures, regarding the DPDP and OPDP scenario with LOS, the impact of the velocity variation on the PL and PLE received power is more significant on the 38 [GHz] channel, while this impact is very low on the 28 and 73 [GHz] channels. Furthermore, for the DPDP scenario with NLOS, the velocity variation has a stronger impact on the 38 [GHz] channel in terms of path loss, received power, and path loss exponent, although this impact is roughly the same on the 28 and 38 [GHz] channels. Finally, for OPDP with NLOS, the impact is more significant on 28 and 73 [GHz] channels in terms of PL, received power, but in terms of PLE, it is more significant on 38 and 73 [GHz] channels.

Channel Parameters		**Antenna Parameters**	
RF Frequency	28/38/73 [GHz]	**TX/RX Array Type**	ULA/ULA
RF BW MHz	800	**Num TX/RX Elements**	1/1
Scenario	UMi	**TX/RX Antenna Elements Spacing**	0.5λ/0.5λ
Environment	LOS/NLOS	**TX Azimuth/Elevation HPBW**	10°/10°
T-R Separation (m)	100	**RX Azimuth/Elevation HPBW**	10°/10°
TX Power (dBm)	30	**Spatial consistency Parameters**	
Num RX	1	**Moving distance (m)**	40
Press (mbar)	1013	**Correlation distance LOS/NLOS (m)**	10
Hum %	50	**Update distance (m)**	1
Temp. C°	20	**Velocity (m/s)**	1/2/5
Pol	Co-Pol	**Track type**	Linear
D Foliage (m)	0	**Moving direction (°)**	45°
Rain rate mm/hr	0		

Table 14. Spatial consistency settings used for the case of user terminal velocity scenarios.

Freq Channel [GHz]	**Scenario**	**Velocity (m/s)**	**Directional Power Delay Profile**				**Omnidirectional Power Delay Profile**			
			RMS DS (ns)	**Received Power [dBm]**	**PL [dB]**	**PLE**	**RMS DS (ns)**	**Received Power [dBm]**	**PL [dB]**	**PLE**
28	LOS	1	8,7	-39,88	119,09	2,75	10,39	-72,33	102,33	1,95
	LOS	2	32,36	-54,34	133,56	3,38	27,96	-76,01	106,01	2
	LOS	5	21,78	-45,47	125,08	3,28	23,68	-72,11	102,11	2,1
	NLOS	1	18,55	-66	145,21	4,56	36,79	-89,89	119,89	3,18
	NLOS	2	56,36	-68,55	147,56	4,28	45,84	-99,19	129,19	3,36
	NLOS	5	41,69	-67,61	146,82	4,2	22,62	-95,92	125,92	3,17
38	LOS	1	22,33	-44,4	123,61	2,79	17,5	-74,74	104,74	1,91
	LOS	2	12,2	-49,63	128,84	3,26	16,78	-72,44	102,44	1,93
	LOS	5	0,07	-26,48	105,7	2,28	3,15	-65,92	95,92	1,75
	NLOS	1	58,72	-79,43	158,64	4,89	14,19	-102,25	132,25	3,53
	NLOS	2	46,55	-62,89	132,1	3,9	30,81	-104,93	134,93	3,54
	NLOS	5	59,46	-96,21	155,42	4,38	31,94	-99,93	129,93	3,15
73	LOS	1	19,9	-51,21	130,42	2,84	20,29	-81,21	111,21	1,94
	LOS	2	5,12	-50,85	130,56	3,43	15,65	-74,15	104,15	1,95
	LOS	5	19,45	-64,77	143,98	3,64	15,07	-81,01	111,01	2,02
	NLOS	1	31,01	-75,83	155,4	4,1	27,32	-116,75	146,75	3,7
	NLOS	2	126,2	-87,05	166,27	4,51	56,17	-110,04	140,04	3,28
	NLOS	5	102,38	-84,36	163,57	4,75	33,98	-106,45	136,45	3,3

Table 15 Directional and omnidirectional power delay statistics for user terminal velocity scenarios

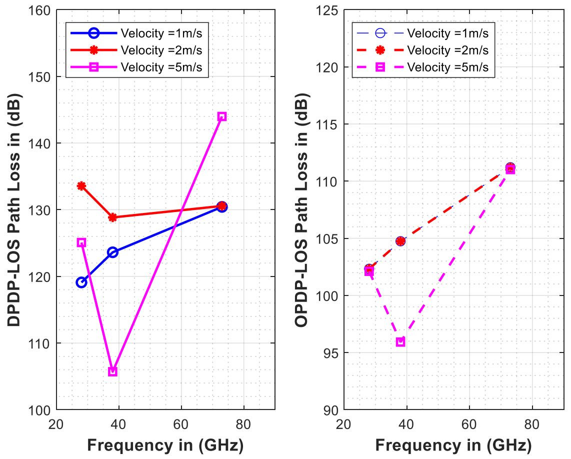

Fig 6.18 Path loss for DPDP and OPDP LOS on velocity of user terminal scenarios.

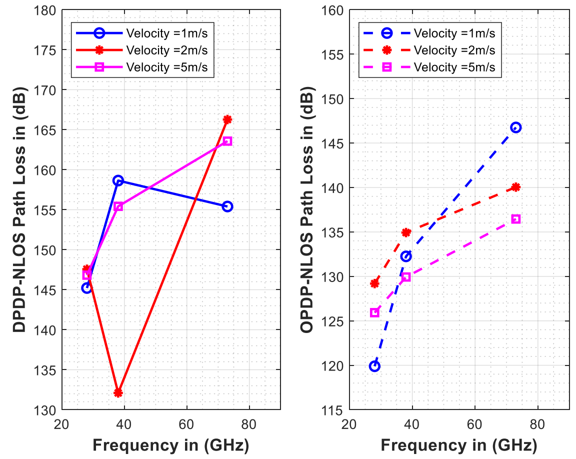

Fig 6.19 Path loss for DPDP and OPDP NLOS on velocity of user terminal scenarios.

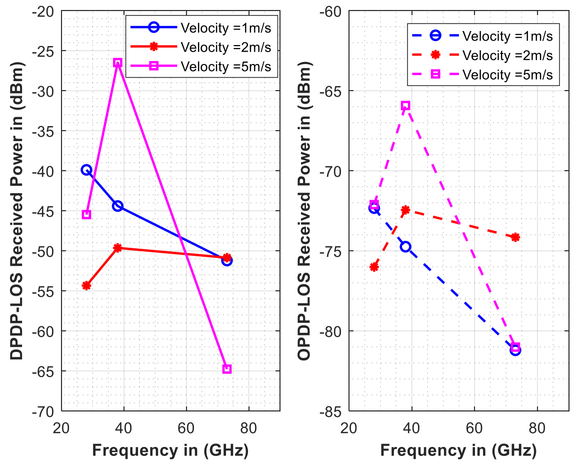

Fig 6.20 Received Power for DPDP and OPDP LOS on velocity of user terminal scenarios.

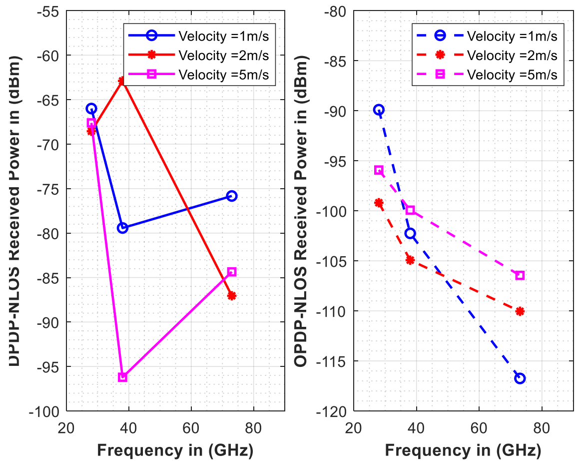

Fig 6.21 Received Power for DPDP and OPDP NLOS on velocity of user terminal scenarios.

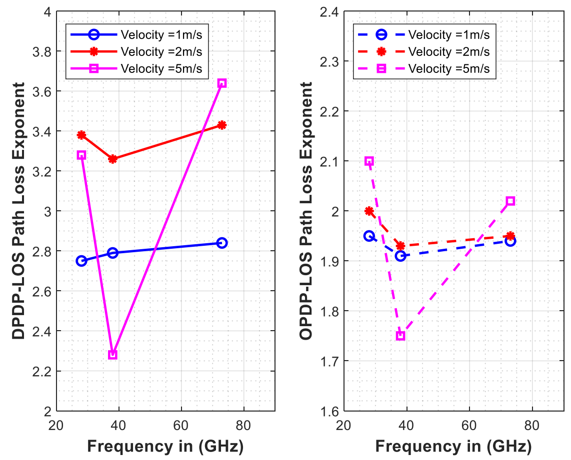

Fig 6.22 Path Loss Exponent for DPDP and OPDP LOS on velocity of user terminal scenarios

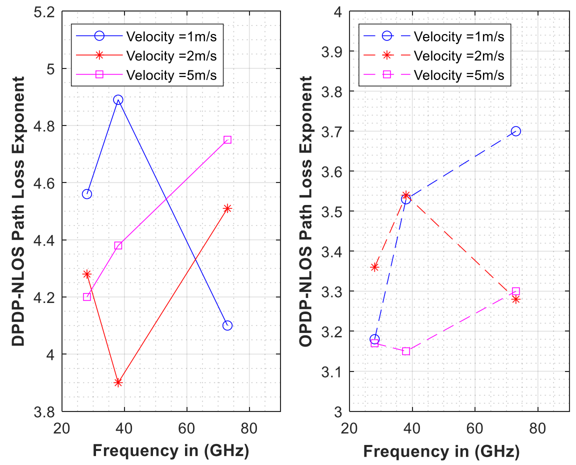

Fig 6.23 Path Loss Exponent for DPDP and OPDP NLOS on velocity of user terminal scenarios

6.4.4 User Track Type Scenarios

In the last set of simulations, we investigated the impact of changing the user track type on the spatial consistency channels properties. The parameters used in simulations are summarized in Table 16, where we considered two types of user track (Linear/Hexagonal) and for all the channels studied in both LOS and NLOS environments.

Channel Parameters		Antenna Parameters	
RF Frequency	28/38/73 [GHz]	**TX/RX Array Type**	ULA/ULA
RF BW MHz	800	**Num TX/RX Elements**	1/1
Scenario	UMi	**TX/RX Antenna Elements Spacing**	$0.5\lambda/0.5\lambda$
Environment	LOS/NLOS	**TX Azimuth/Elevation HPBW**	$10^{\circ}/10^{\circ}$
T-R Separation (m)	100	**RX Azimuth/Elevation HPBW**	$10^{\circ}/10^{\circ}$
TX Power (dBm)	30	**Spatial consistency Parameters**	
Num RX	1	**Moving distance (m)**	40
Press (mbar)	1013	**Correlation distance LOS/NLOS (m)**	10
Hum %	50	**Update distance (m)**	1
Temp. C°	20	**Velocity (m/s)**	1
Pol	Co-Pol	**Track type**	Linear/Hexagonal
D Foliage (m)	0	**Moving direction (°)**	45°
Rain rate mm/hr	0		

Table 16. Spatial consistency parameters used in user track type scenarios

Freq Channel [GHz]	Scenario	Track type	Directional Power Delay Profile				Omnidirectional Power Delay Profile			
			RMS DS (ns)	Received Power [dBm]	PL [dB]	PLE	RMS DS (ns)	Received Power [dBm]	PL [dB]	PLE
28	LOS	Linear	32.33	−52.33	131.54	3.29	17.16	−76.34	106.34	2.11
	LOS	Hexagonal	35.18	−63.86	143.07	4.29	23.88	−78.49	108.49	2.47
	NLOS	Linear	38.57	−76.43	155.64	4.43	54.63	−94.26	124.26	2.95
	NLOS	Hexagonal	44.36	−69.76	148.97	4.57	24.53	−92.01	122.01	3.16
38	LOS	Linear	26.89	−34.33	113.54	2.66	22.76	−66	96	1.72
	LOS	Hexagonal	28.51	−55.25	134.47	3.5	12.43	−79.82	109.82	2.28
	NLOS	Linear	39.89	−72.58	151.79	4.13	35.44	−103.03	133.03	3.24
	NLOS	Hexagonal	127.53	−92.87	172.08	5.34	22.95	−103.83	133.83	3.45
73	LOS	Linear	25.53	−55.76	134.97	3.42	18.92	−76.02	106.02	1.9
	LOS	Hexagonal	26.24	−58.79	138	3.53	23.33	−74.07	104.07	1.77
	NLOS	Linear	185.18	−86.51	165.72	4.4	14.67	−109.66	139.66	3.26
	NLOS	Hexagonal	193.72	−91.25	170.46	5.24	17.36	−95.3	125.3	2.89

Table 17. Directional and omnidirectional power delay statistics for user track type scenarios.

Table 17 summarizes the results of the DPDP and OPDP statistics at 28, 38, and 73 [GHz] for the user track type scenario. Figures 6.24–6.29 illustrate the PL, received power, and PLE of both DPDP and OPDP in LOS/NLOS environment for the user track type scenarios. As illustrated in these figures, for the DPDP and OPDP using LOS scenarios, the impact of switching channel user type is more significant on the 38 [GHz] channel with respect to both PL and received power; however in terms of PLE, the impact is more significant on the 28 and 38 [GHz] channels, whilst on the 73 [GHz] channel there is very limited impact.

Also, for the DPDP scenario with NLOS, the switch in the user channel type has a more significant impact on the 38 [GHz] channel with respect to PL, received power and PLE; however, there is an insignificant impact on the 28 [GHz] channel. Lastly, for OPDP with NLOS, the impact is more significant on the 73 [GHz] against of PL, received power, and path PLE, but the impact is insignificant on 28 [GHz]

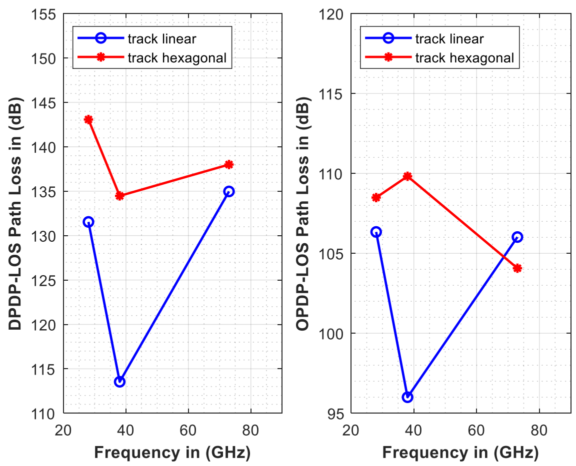

Figure 6.24 Path loss for DPDP and OPDP LOS on track type scenarios.

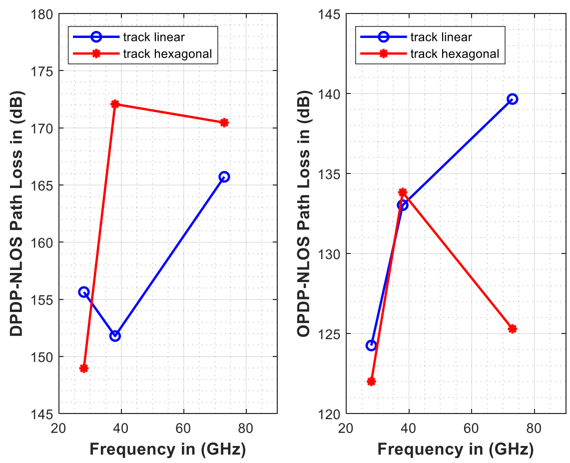

Figure 6.25 Path loss for DPDP and OPDP NLOS on track type scenarios.

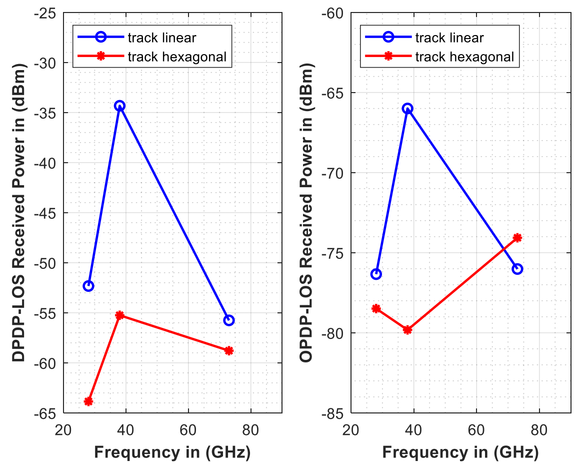

Figure 6.26 Received Power for DPDP and OPDP LOS on track type scenarios.

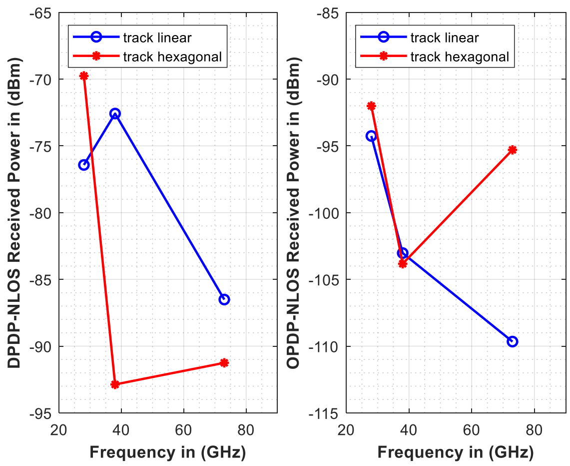

Figure 6.27 Received Power for DPDP and OPDP NLOS on track type scenarios.

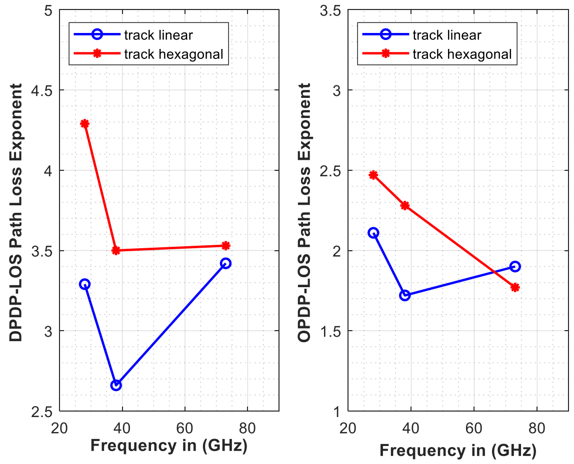

Figure 6.28. Path Loss Exponent for DPDP and OPDP LOS on track type scenarios.

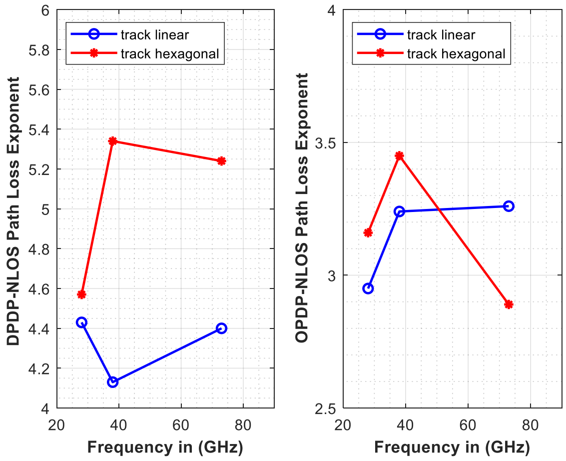

Figure 6.29 Path Loss Exponent for DPDP and OPDP NLOS on track type scenarios...

6.5 CONCLUSION

This chapter statistically modeled the 28, 38, and 73 [GHz] millimeter wave bands intended to be employed by the 5G network considering spatial consistency scenarios: LOS/NLOS correlation distance, travel distance, user speed, user track type, for 5G UMi in LOS and NLOS scenarios. Besides, an extensive simulation was performed using the CI model adopted by the NYUSIM to analyze the impact of different spatial consistency parameters on the statistical characteristics of the channel such as path loss, received power, path loss exponent for directional power delay profile and omnidirectional power delay profile. The results showed that the performance of mmWave channels could be influenced by changing the spatial consistency parameters. This spatial analysis would be useful for exposing and developing the measurable channel model for 5G millimeter-wave communications.

7 General Conclusion

This thesis provides an in-depth statistical study of millimeter wave propagation candidates for 5G/6G systems based on different scenarios for outdoor Urban Microcell (UMi) channels,

Summing up the results, it can be concluded that the parameters of statistical channel modeling are dependent on the geometric parameters (Co-Pol/X-Pol, SISO/SIMO/MIMO) and environmental conditions (LOS/NLOS, rain rate, temperature and humidity). Furthermore, the MU–MIMO scenario affect is investigated, mainly the impact of switching from 1U-MIMO to 2U-MIMO or 2U-MIMO to 4U-MIMO, this scenario is not taken into account in recent works. The study aims to illustrate mmWave characteristics (PL, PLE, Received power) at 28, 38, 60, 73, 100 and 120 [GHz]. Overall observation suggests that mmWave channel with carrier frequencies 28, 60, 100 and 120 [GHz] channels are more affected by the switching from LOS to NLOS. However, 38 [GHz] channel is the least affected, nevertheless, channel 73 [GHz] is more tolerant of the LOS to NLOS effect. Besides, in terms of antenna configurations (SISO/SIMO/MIMO), the results indicated that 120 [GHz] is more affected, while 28 [GHz] is less affected than the other channels, except that 38 [GHz] is more favorable to change this factor. For rain, temperature and humidity factors, it was concluded that the attenuations of 60, 100 and 120 [GHz] are the most important, while 28 and 73 [GHz] channels are less affected, except that 38 channel is the most capable to withstand the change of these factors. After comparing our results with those from the literature, we have concluded that rain fade depends to link length.

By Analyzing the O2I penetration loss of mmWave channels at 28, 38, 60 and 73 [GHz] operating frequency for different scenarios Low loss / High loss and TX/RX Antenna HPBW azimuth/Elevation 10°/15°. The type of building (standard glass, wood, IRR glass and concrete....) and Antenna properties (HPBW) affects channel characteristic O2I penetration loss. After the studies ,the results indicate that the channel 73 [GHz] is more affected by the change of the Antenna properties HPBW in case of low loss, the channel 28 [GHz] is less affected than 73 [GHz], but the 38 , 60 [GHz] channels are better for supporting the impact of this change. In case of High loss , channel 38 [GHz] is more affected by the change of the Antenna properties HPBW, the channel 73 [GHz] is less affected than 38 [GHz], but the 28 , 60 [GHz] channels are better for supporting the impact of this change. In case of HPBW=10°, channels 73, 38, 60 [GHz] are more effected by the change of the type of building, but channel 28 is less effected than the other channels. In case of HPBW=15°, channel 38 [GHz] is more effected by the change of the type of building , channels 73, 60, 28 [GHz] is less effected than 38 [GHz].

By Analyzing the impact of human blockage for the mmWave for different scenarios especially for different TX/RX Antenna HPBW azimuth/Elevation 7°, 10°, 15°, 30°. After the studies, it was concluded that the channel 73 [GHz] is more affected by the human blockage event but the 28, 38 and 60 [GHz] channels are better for supporting it. In same channel, the impact of human blockage events are more important when using widebeam antennas compared to narrow beam antennas. The beam width antenna has no effect on the channel parameters for omnidirectional PDP. Omnidirectional PDP more affected by the human blockage compare to Directional PDP.

Finaly, statistically modeled the 28, 38, and 73 [GHz] millimeter wave bands intended to be employed by the 5G network considering spatial consistency scenarios: LOS/NLOS correlation distance, travel distance, user speed, user track type, for 5G UMi in LOS and NLOS scenarios. Besides, an extensive simulation was performed using the CI model adopted by the NYUSIM to analyze the impact of different spatial consistency parameters on the statistical characteristics of the channel such as path loss, received power, path loss exponent for directional power delay profile and omnidirectional power delay profile. The results showed that the performance of mmWave channels could be influenced by changing the spatial consistency parameters. This spatial analysis would be useful for exposing and developing the measurable channel model for 5G millimeter-wave communications.

Power delay profile (OPDP) showed improved performance over the directional power delay profile (DPDP) for all channels**.**

This proposed work will be highly useful for 5G/6G research and system deployment and expected to help future engineers to design an efficient mmWave channel modeling for new outdoor scenarios.

References

[1] Rappaport, Theodore S., et al. *Millimeter wave wireless communications*. Pearson Education, 2015.

[2] Khan, Farooq, and Zhouyue Pi. "mmWave mobile broadband (MMB): Unleashing the 3–300[GHz] spectrum." 34th IEEE Sarnoff Symposium. IEEE, 2011.

[3] Index, Cisco Visual Networking. "Global mobile data traffic forecast update, 2016–2021." *white paper* 7 (2017).

[4] Pietraski, Phil, et al. "Millimeter wave and terahertz communications: Feasibility and challenges." ZTE Communications 10.4 (2012): 3-12.

[5] IC1004, C. O. S. T. "White paper on channel measurements and modeling for 5G networks in the frequency bands above 6 [GHz]." Eur. Cooperation in Sci. and Technol.(COST), Tech. Rep (2016).

[6] Haneda, Katsuyuki, et al. "5G 3GPP-like channel models for outdoor urban microcellular and macrocellular environments." *2016 IEEE 83rd vehicular technology conference (VTC spring)*. IEEE, 2016.

[7] Haneda, Katsuyuki, et al. "Indoor 5G 3GPP-like channel models for office and shopping mall environments." *2016 IEEE international conference on communications workshops (ICC)*. IEEE, 2016.

[8] Sun, Shu, et al. "Investigation of prediction accuracy, sensitivity, and parameter stability of large-scale propagation path loss models for 5G wireless communications." *IEEE transactions on vehicular technology* 65.5 (2016): 2843-2860.

[9] Sun, Shu, George R. MacCartney, and Theodore S. Rappaport. "A novel millimeter-wave channel simulator and applications for 5G wireless communications." *2017 IEEE International Conference on Communications (ICC)*. IEEE, 2017.

[10] New York University, NYUSIM, 2016. [Online]. Available: http://wireless.engineering.nyu.edu/5gmillimeter-wave-channelmodeling-software/

[11] Nurmela, Vuokko, et al. "Deliverable D1. 4 METIS channel models." *Proc. Mobile Wireless Commun. Enablers Inf. Soc.(METIS)* (2015): 1.

[12] mmMAGIC. 6-100 [GHz] Channel Modelling for 5G: Measurement and Modelling Plans in mmMAGIC. ***European Commission H2020***. (2015, July) [Online]. Available: https://5g-mmmagic.eu/results/#deliverables

[13] Halbauer, Hardy, et al. *Architectural aspects of mm-wave radio access integration with 5G ecosystem*. 5G PPP mmMAGIC, 2016.

[14] Liu, Lingfeng, et al. "The COST 2100 MIMO channel model." *IEEE Wireless Communications* 19.6 (2012): 92-99.

[15] Seidel, Scott Y., Koichiro Takamizawa, and Theodore S. Rappaport. "Application of second-order statistics for an indoor radio channel model." *IEEE 39th Vehicular Technology Conference*. IEEE, 1989.

[16] Jaeckel, Stephan, et al. "QuaDRiGa: A 3-D multi-cell channel model with time evolution for enabling virtual field trials." *IEEE transactions on antennas and propagation* 62.6 (2014): 3242-3256.

[17] Yu, Yu, et al. "Propagation model and channel simulator under indoor stair environment for machine-to-machine applications." *2015 Asia-Pacific Microwave Conference (APMC)*. Vol. 2. IEEE, 2015.

[18] Rappaport, Theodore S., Scott Y. Seidel, and Koichiro Takamizawa. "Statistical channel impulse response models for factory and open plan building radio communicate system design." *IEEE transactions on communications* 39.5 (1991): 794-807.

[19] Wireless Valley Communications, Inc. *SMRCIM Plus 4.0 (Simulation of Mobile Radio Channel Impulse Response Models) Users Manual*, Aug. 1999.

[20] Rajendran, Vinodh K., et al. "Concepts and implementation of a semantic web archiving and simulation system for rf propagation measurements." *2011 IEEE Vehicular Technology Conference (VTC Fall)*. IEEE, 2011.

[21] Fung, Victor, Theodore S. Rappaport, and Berthold Thoma. "Bit error simulation for pi/4 DQPSK mobile radio communications using two-ray and measurement-based impulse response models." *IEEE journal on selected areas in communications* 11.3 (1993): 393-405.

[22] Smith, John I. "A computer generated multipath fading simulation for mobile radio." *IEEE Transactions on Vehicular Technology* 24.3 (1975): 39-40.

[23] Clarke, Richard Hedley. "A statistical theory of mobile-radio reception." *Bell system technical journal* 47.6 (1968): 957-1000.

[24] Krauss, Thomas P., and Michael D. Zoltowski. "Oversampling diversity versus dual antenna diversity for chip-level equalization on CDMA downlink." *Proceedings of the 2000 IEEE Sensor Array and Multichannel Signal Processing Workshop. SAM 2000 (Cat. No. 00EX410)*. IEEE, 2000.

[25] Molisch, Andreas F., et al. "The COST259 directional channel model-part I: Overview and methodology." *IEEE Transactions on Wireless Communications* 5.12 (2006): 3421-3433.

[26] Weiler, Richard J., et al. "Quasi-deterministic millimeter-wave channel models in MiWEBA." *EURASIP Journal on Wireless Communications and Networking* 2016.1 (2016): 1-16.

[27] Kyosti, Pekka. "WINNER II channel models." *IST, Tech. Rep. IST-4-027756 WINNER II D1. 1.2 V1. 2* (2007).

[28] "Test environments and channel models," tech. rep., Annex 1 to section 5.11, chapter 5, Doc 5D/Temp/238, 17, Nov. 2016.

[29] Mondal, Bishwarup, et al. "3D channel model in 3GPP." *IEEE Communications Magazine* 53.3 (2015): 16-23.

[30] 3GPP, "Study on channel model for frequencies from 0.5 to 100 [GHz]," TR 38.901 V14.3.0, 3rd Generation Partnership Project (3GPP), Dec. 2017.

[31] Samimi, Mathew K., and Theodore S. Rappaport. "3-D millimeter-wave statistical channel model for 5G wireless system design." *IEEE Transactions on Microwave Theory and Techniques* 64.7 (2016): 2207-2225.

[32] Rappaport, Theodore S., et al. "Wideband millimeter-wave propagation measurements and channel models for future wireless communication system design." *IEEE transactions on Communications* 63.9 (2015): 3029-3056.

[33] El Ayach, Omar, et al. "Spatially sparse precoding in millimeter wave MIMO systems." *IEEE transactions on wireless communications* 13.3 (2014): 1499-1513.

[34] MacCartney Jr, George R., et al. "Millimeter wave wireless communications: New results for rural connectivity." *Proceedings of the 5th workshop on all things cellular: operations,*

applications and challenges. 2016.

[35] MacCartney, George R., and Theodore S. Rappaport. "Rural macrocell path loss models for millimeter wave wireless communications." *IEEE Journal on selected areas in communications* 35.7 (2017): 1663-1677.

[36] Rappaport, Theodore S., et al. "Millimeter wave mobile communications for 5G cellular: It will work!." *IEEE access* 1 (2013): 335-349.

[37] Intelligence, G. S. M. A. "Understanding 5G: Perspectives on future technological advancements in mobile." *White paper* (2014): 1-26.

[38] L. DMC R&D Center, Samsung Electronics Co., "5G vision," Feb. 2015, ***White Paper.*** [Online]. Available at http://www.samsung.com/ global/business-images/insights/2015/Samsung-5G-Vision-0.pdf.

[39] Pi, Zhouyue, and Farooq Khan. "An introduction to millimeter-wave mobile broadband systems." *IEEE communications magazine* 49.6 (2011): 101-107.

[40] Khan, Farooq, and Zhouyue Pi. "mmWave mobile broadband (MMB): Unleashing the 3–300[GHz] spectrum." *34th IEEE Sarnoff Symposium*. IEEE, 2011.

[41] Marcus, Michael, and Bruno Pattan. "Millimeter wave propagation: spectrum management implications." *IEEE Microwave Magazine* 6.2 (2005): 54-62

[42] Rappaport, Theodore S., and Sijia Deng. "73 [GHz] wideband millimeter-wave foliage and ground reflection measurements and models." *2015 IEEE International Conference on Communication Workshop (ICCW)*. IEEE, 2015.

[43] Schotten, Hans D., et al. "Intermediate description of the spectrum needs and usage principles." (2013).

[44] Wei, Lili, et al. "Key elements to enable millimeter wave communications for 5G wireless systems." *IEEE Wireless Communications* 21.6 (2014): 136-143.

[45] Series, Radiowave Propagation. "Characteristics of precipitation for propagation modelling." *Recommendation ITU-R* (2012): 837-6.

[46] Access, E. U. T. R. "Further advancements for E-UTRA physical layer aspects." *3GPP Technical Specification TR* 36 (2010): V2.

[47] Rappaport, Theodore S., et al. "Wideband millimeter-wave propagation measurements and channel models for future wireless communication system design." *IEEE transactions on Communications* 63.9 (2015): 3029-3056.

[48] Federal Communications Commission. "Report and order and further notice of proposed rulemaking." *the Matter of Revision of the Commission's Rules to Ensure Compatibility with Enhanced* 911 (2016): 94-102.

[49] Rappaport, Theodore S., Scott Y. Seidel, and Koichiro Takamizawa. "Statistical channel impulse response models for factory and open plan building radio communicate system design." *IEEE transactions on communications* 39.5 (1991): 794-807.

[50] Xu, Hao, Vikas Kukshya, and Theodore S. Rappaport. "Spatial and temporal characteristics of 60-[GHz] indoor channels." *IEEE Journal on selected areas in communications* 20.3 (2002): 620-630.

[51] Collogne, S., Gheorghe Zaharia, and Ghais El Zein. "Experimental investigation of the spatial and temporal characteristics of the 60 [GHz] radio propagation within residential environments." *Signals, Circuits and Systems, 2003. SCS 2003. International Symposium on*. Vol. 2. IEEE, 2003.

[52] Zhang, Hong, Sriram Venkateswaran, and Upamanyu Madhow. "Channel modeling and MIMO capacity for outdoor millimeter wave links." *2010 IEEE Wireless Communication and Networking Conference*. IEEE, 2010.

[53] Torkildson, Eric, Hong Zhang, and Upamanyu Madhow. "Channel modeling for millimeter wave MIMO." *2010 Information Theory and Applications Workshop (ITA)*. IEEE, 2010.

[54] Lostanlen, Yves, et al. "Comparison of measurements and simulations in indoor environments for wireless local networks at 60 [GHz]." *Vehicular Technology Conference. IEEE 55th Vehicular Technology Conference. VTC Spring 2002 (Cat. No. 02CH37367)*. Vol. 1. IEEE, 2002.

[55] Collogne, S., and G. E. Zein. "Characterization and modelisation of the 60 [GHz] electromagnetic waves propagation in indoor environment." *Theses, INSA de Rennes, Dec* (2003).

[56] Rappaport, Theodore S., et al. "Wideband millimeter-wave propagation measurements and channel models for future wireless communication system design." *IEEE transactions on*

Communications 63.9 (2015): 3029-3056.

[57] Samimi, Mathew K., and Theodore S. Rappaport. "Statistical channel model with multi-frequency and arbitrary antenna beamwidth for millimeter-wave outdoor communications." *2015 IEEE Globecom Workshops (GC Wkshps)*. IEEE, 2015.

[58] MacCartney, George R., and Theodore S. Rappaport. "Study on 3GPP rural macrocell path loss models for millimeter wave wireless communications." *2017 IEEE International Conference on Communications (ICC)*. IEEE, 2017.

[59] Saad, Walid, Mehdi Bennis, and Mingzhe Chen. "A vision of 6G wireless systems: Applications, trends, technologies, and open research problems." *IEEE network* 34.3 (2019): 134-142.

[60] Chowdhury, Mostafa Zaman, et al. "6G wireless communication systems: Applications, requirements, technologies, challenges, and research directions." *IEEE Open Journal of the Communications Society* 1 (2020): 957-975.

[61] Rappaport, Theodore S., et al. "Overview of millimeter wave communications for fifth-generation (5G) wireless networks—With a focus on propagation models." *IEEE Transactions on antennas and propagation* 65.12 (2017): 6213-6230.

[62] Giordani, Marco, et al. "Toward 6G networks: Use cases and technologies." *IEEE Communications Magazine* 58.3 (2020): 55-61.

[63] Ali, Wael, et al. "Planar dual-band 27/39 GHz millimeter-wave MIMO antenna for 5G applications." *Microsystem Technologies* 27.1 (2021): 283-292.

[64] Kamboh, Usman Rauf, et al. "Path loss modelling at 60 GHz mmWave based on cognitive 3D ray tracing algorithm in 5G." *Peer-to-Peer Networking and Applications* 14.5 (2021): 3181-3197.

[65] Sim, Min Soo, et al. "Deep learning-based mmWave beam selection for 5G NR/6G with sub-6 GHz channel information: Algorithms and prototype validation." *IEEE Access* 8 (2020): 51634-51646.

[66] Ullah, Hidayat, and Farooq A. Tahir. "A high gain and wideband narrow-beam antenna for 5G millimeter-wave applications." *IEEE Access* 8 (2020): 29430-29434.

[67] Begishev, Vyacheslav, et al. "Performance analysis of multi-band microwave and millimeter-wave operation in 5G NR systems." *IEEE Transactions on Wireless Communications* 20.6 (2021): 3475-3490.

[68] Saha, Rony Kumer. "Spectrum allocation and reuse in 5G new radio on licensed and unlicensed millimeter-wave bands in indoor environments." *Mobile Information Systems* 2021 (2021).

[69] FC Commission. "FCC takes steps to open spectrum horizons for new services and technologies." *FC Commission: Washington, DC, USA* (2019).

[70] Ju, Shihao, et al. "Millimeter wave and sub-terahertz spatial statistical channel model for an indoor office building." *IEEE Journal on Selected Areas in Communications* 39.6 (2021): 1561-1575.

[71] Fung, Victor, Theodore S. Rappaport, and Berthold Thoma. "Bit error simulation for pi/4 DQPSK mobile radio communications using two-ray and measurement-based impulse response models." *IEEE journal on selected areas in communications* 11.3 (1993): 393-405.

[72] Cheng, Chia-Lin, Seunghwan Kim, and Alenka Zajić. "Comparison of path loss models for indoor 30 GHz, 140 GHz, and 300 GHz channels." *2017 11th European Conference on Antennas and Propagation (EUCAP)*. IEEE, 2017.

[73] Sun, Shu, et al. "Propagation models and performance evaluation for 5G millimeter-wave bands." *IEEE Transactions on Vehicular Technology* 67.9 (2018): 8422-8439.

[74] Agrawal, S. K., and Kapil Sharma. "5th generation millimeter wave wireless communication propagation losses dataset for indian metro cities based on corresponding weather conditions." *Data in brief* 23 (2019): 103564.

[75] Ju, Shihao, et al. "A millimeter-wave channel simulator NYUSIM with spatial consistency and human blockage." *2019 IEEE global communications conference (GLOBECOM)*. IEEE, 2019.

[76] Budalal, Asma Ali, et al. "Millimeter wave channel modeling–present development and challenges in tropical areas." *2018 7th International Conference on Computer and Communication Engineering (ICCCE)*. IEEE, 2018.

[77] Hasan, Rifat, et al. "A statistical analysis of channel modeling for 5g mmwave communications." *2019 International Conference on Electrical, Computer and Communication Engineering (ECCE)*. IEEE, 2019.

[78] Han, Congzheng, et al. "Rain rate retrieval test from 25-GHz, 28-GHz, and 38-GHz millimeter-wave link measurement in Beijing." *IEEE Journal of Selected Topics in Applied Earth Observations and Remote Sensing* 12.8 (2019): 2835-2847.

[79] Nandi, Dalia, and Animesh Maitra. "The effects of rain on millimeter wave communication for tropical region." *2019 URSI Asia-Pacific Radio Science Conference (AP-RASC)*. IEEE, 2019.

[80] Dutty, Hussnin Binte Hamid, and Md Munjure Mowla. "Weather impact analysis of mmwave channel modeling for aviation backhaul networks in 5g communications." *2019 22nd International Conference on Computer and Information Technology (ICCIT)*. IEEE, 2019.

[81] Rudd, Richard, et al. "Building materials and propagation." *Final Report, Ofcom* 2604 (2014).

[82] Xing, Yunchou, et al. "Verification and calibration of antenna cross-polarization discrimination and penetration loss for millimeter wave communications." *2018 IEEE 88th Vehicular Technology Conference (VTC-Fall)*. IEEE, 2018.

[83] Rappaport, Theodore S., Shu Sun, and Mansoor Shafi. "Investigation and comparison of 3GPP and NYUSIM channel models for 5G wireless communications." *2017 IEEE 86th vehicular technology conference (VTC-Fall)*. IEEE, 2017.

[84] Kumari, M. Sheeba, and Navin Kumar. "Channel model for simultaneous backhaul and access for mmWave 5G outdoor street canyon channel." *Wireless Networks* 26.8 (2020): 5997-6013.

[85] Momo, Sumaiya Haq Aftabi, and Md Munjure Mowla. "Statistical analysis of an outdoor mmWave channel model at 73 GHz for 5G networks." *2019 International Conference on Computer, Communication, Chemical, Materials and Electronic Engineering (IC4ME2)*. IEEE, 2019.

[86] Shamsan, Zaid Ahmed. "A Statistical Channel Propagation Analysis for 5G mmWave at 73 GHz in Urban Microcell." *International Conference of Reliable Information and Communication Technology*. Springer, Cham, 2020.

[87] Dutty, Hussnin Binte Hamid, Md Munjure Mowla, and Muhosina Aktar Mou. "Millimeter wave channel modeling for aviation backhaul networks in 5g communications." *2019 22nd International Conference on Computer and Information Technology (ICCIT)*. IEEE, 2019.

[88] Hasan, Rifat, Md Munjure Mowla, and Mahfuza Khatun. "The Impact of Linear Polarization on Channel Modeling in 5G Cellular Communications: A Statistical Approach." *2019 5th International Conference on Advances in Electrical Engineering (ICAEE)*. IEEE, 2019.

[89] Rappaport, Theodore S., et al. "Wireless communications and applications above 100 GHz: Opportunities and challenges for 6G and beyond." *IEEE access* 7 (2019): 78729-78757.

[90] Kamrul, MD Imtiaz, Kazi Mazharul Haque, and Muhammad Mostafa Amir Faisal. "Performance Evaluation of MIMO in Urban Microcell for Dhaka City at 28 GHz Frequency." *2018 International Conference on Innovations in Science, Engineering and Technology (ICISET)*. IEEE, 2018.

[91] Budalal, Asma Ali, et al. "The effects of rain fade on millimetre wave channel in tropical climate." *Bulletin of Electrical Engineering and Informatics* 8.2 (2019): 653-664.

[92] Al-Shuwaili, Ali, and Thamer M. Jamel. "5G Channel Characterization at Millimeter-Wave for Baghdad City: An NYUSIM-based Approach." *2021 18th International Multi-Conference on Systems, Signals & Devices (SSD)*. IEEE, 2021.

[93] Semaan, Eliane, et al. "Outdoor-to-indoor coverage in high frequency bands." *2014 IEEE Globecom Workshops (GC Wkshps)*. IEEE, 2014.

[94] Bas, Celalettin Umit, et al. "Outdoor to indoor penetration loss at 28 GHz for fixed wireless access." *2018 IEEE International Conference on Communications (ICC)*. IEEE, 2018

[95] . Ahumada, L., et al. "Studying the dynamics of outdoor-indoor wireless links at 60 GHz." *2018 IEEE-APS Topical Conference on Antennas and Propagation in Wireless Communications (APWC)*. IEEE, 2018.

[96] Diakhate, Cheikh AL, et al. "Millimeter-wave outdoor-to-indoor channel measurements at 3, 10, 17 and 60 GHz." *2017 11th European Conference on Antennas and Propagation (EUCAP)*. IEEE, 2017.

[97] Mizuno, Yuta, Kentaro Nishimori, and Ryotaro Taniguchi. "A study on outdoor to indoor penetration path loss at 2 and 5 GHz." *IEICE Communications Express* (2019).

[98] 3GPP Radio Access Network Working Group. *Study on New Radio Access Technology; RF and co-existence aspects (Release 14)*. Vol. 14. 3GPP TR 38.803.

[99] ITU, *Prediction of Building Entry Loss, Recommendation ITU-R P.2109-0*, ITU, Geneva, Switzerland, 2017.

[100] ITU, “Compilation of measurement data relating to building entry loss,” Report ITU-R P.2346-2, ITU, Geneva, Switzerland, 2017.

[101] mmMAGIC, “Measurement results and final mmMAGIC channel models,” H2020-ICT-671650-mmMAGIC/D2.2 v2.0,2017, https://5g-ppp.eu/mmmagic/

[102] Zhong, Zhimeng, Jianyao Zhao, and Chao Li. "Outdoor-to-Indoor Channel Measurement and Coverage Analysis for 5G Typical Spectrums." *International Journal of Antennas and Propagation* 2019 (2019).

[103] Ko, Junghoon, et al. "Millimeter-wave channel measurements and analysis for statistical spatial channel model in in-building and urban environments at 28 GHz." *IEEE Transactions on* Wireless Communications 16.9 (2017): 5853-5868.

[104] Karttunen, Aki, et al. "Spatially consistent street-by-street path loss model for 28-GHz channels in micro cell urban environments." *IEEE Transactions on Wireless Communications* 16.11 (2017): 7538-7550.

[105] Imai, T., et al. "Outdoor-to-Indoor path loss modeling for 0.8 to 37 GHz band." *2016 10th European Conference on Antennas and Propagation (EuCAP)*. IEEE, 2016.

[106] Rodriguez, Ignacio, et al. "Analysis of 38 GHz mmWave propagation characteristics of urban scenarios." *Proceedings of European Wireless 2015; 21th European Wireless Conference*. VDE, 2015.

[107] 5GCM, “5G channel model for bands up to 100 GHz,” Oct. 21, 2016.

[108] Gapeyenko, Margarita, et al. "Analysis of human-body blockage in urban millimeter-wave cellular communications." *2016 IEEE International Conference on Communications (ICC)*. IEEE, 2016.

[109] Bilgin, Bilgesu A., Hamideh Ramezani, and Ozgur B. Akan. "Human Blockage Model for Indoor Terahertz Band Communication." *2019 IEEE International Conference on Communications Workshops (ICC Workshops)*. IEEE, 2019.

[110] Peng, Bile, et al. "Statistical Characteristics Study of Human Blockage Effect in Future Indoor Millimeter and Sub-millimeter Wave Wireless Communications." *2018 IEEE 87th Vehicular Technology Conference (VTC Spring)*. IEEE, 2018.

[111] Venugopal, Kiran, Matthew C. Valenti, and Robert W. Heath. "Analysis of millimeter wave networked wearables in crowded environments." *2015 49th Asilomar Conference on Signals, Systems and Computers*. IEEE, 2015.

[112] Han, Bin, Longbao Wang, and Hans D. Schotten. "A 3D human body blockage model for outdoor millimeter-wave cellular communication." *Physical Communication* 25 (2017): 502-510.

[113] Chen, Xubin, et al. "Modelling of human body shadowing based on 28 ghz indoor measurement results." *2016 IEEE 84th Vehicular Technology Conference (VTC-Fall)*. IEEE, 2016.

[114] MacCartney, George R., Theodore S. Rappaport, and Sundeep Rangan. "Rapid fading due to human blockage in pedestrian crowds at 5G millimeter-wave frequencies." *GLOBECOM 2017-2017 IEEE Global Communications Conference*. IEEE, 2017.

[115] MacCartney, George R., et al. "Millimeter-wave human blockage at 73 GHz with a simple double knife-edge diffraction model and extension for directional antennas." *2016 IEEE 84th Vehicular Technology Conference (VTC-Fall)*. IEEE, 2016.

[116] I. Kashiwagi, T. Taga, and T. Imai, "Time-varying path-shadowing modelfor indoor populated environments," *IEEE Transactions on Vehicular Technology*, vol. 59, no. 1, pp. 16–28, Jan. 2010.

[117] S. Dehnie, "Markov chain approximation of Rayleigh fading channel," in *2007 IEEE International Conference on Signal Processing and Communications*, Nov. 2007, pp. 1311–1314.

[118] M. Jacob, C. Mbianke, and T. K¨urner, "A dynamic 60 GHz radio channel model for system level simulations with MAC protocols for IEEE802.11ad," in *IEEE International Symposium on Consumer Electronics (ISCE 2010)*, June 2010, pp. 1–5.

[119] M. Peter *et al.*, "Analyzing human body shadowing at 60 GHz: Systematic wideband MIMO measurements and modeling approaches," in *2012 6th European Conference on Antennas and Propagation (EuCAP)*, Mar. 2012, pp. 468–472.

[120] M. Jacob *et al.*, "Modeling the dynamical human blockage for 60 GHz WLAN channel models," in doc.: IEEE 802.11-10/0090r0, Jan. 2010.

[121] G. R. MacCartney, Jr. and T. S. Rappaport, "A flexible millimeter wave channel sounder with absolute timing", IEEE Journal on Selected Areas in Communications, vol. 35, no. 6, pp. 1402–1418, Jun. 2017.

[122] Ju, S., and T. S. Rappaport, "Millimeter-wave Extended NYUSIM Channel Model for Spatial Consistency," *2018 IEEE Global Communications Conference (GLOBECOM)*, Abu Dhabi, UAE, Dec. 2018, pp. 1-6.

[123] S. Ju, Y. Xing, O. Kanhere and T. S. Rappaport, "3-D Statistical Indoor Channel Model for

Millimeter-Wave and Sub-Terahertz Bands," 2020 *IEEE Global Communications Conference* (GLOBECOM), Dec. 2020, pp. 1-7

[124] Zaman, Kasfia, and Md Munjure Mowla. "A millimeter wave channel modeling with spatial consistency in 5G systems." *2020 IEEE Region 10 Symposium (TENSYMP)*. IEEE, 2020.

[125] N. T. T. Docomo, "5G channel model for bands up to100 GHz," *Tech. Report*, Oct. 2016.

[126] Maltsev, A., et al., "WP5: Propagation, antennas and multiantenna techniques—D5.1: Channel modeling and characterization," *Millim.-Wave Evol. Backhaul Access* (MiWEBA), Jun. 2014

[127] Nuckols, J. E., Nuckols, "Implementation of geometrically based single-bounce models for simulation of angle-of- arrival of multipath delay components in the wireless channel simulation tools, SMRCIM and SIRCIM," *Virginia Tech Library, Master of Science,* 1999.

[128] F. Ademaj and S. Schwarz, "Spatial Consistency of Multipath Components in a Typical Urban Scenario," 2019 *13th European Conference on Antennas and Propagation* (EuCAP), 2019, pp. 1-5.

[129] Ademaj, Fjolla, et al. "A spatial consistency model for geometry-based stochastic channels." *IEEE access* 7 (2019): 183414-183427.

[130] Ju, Shihao, and Theodore S. Rappaport. "Simulating motion-incorporating spatial consistency into NYUSIM channel model." *2018 IEEE 88th vehicular technology conference (VTC-Fall)*. IEEE, 2018.

[131] Wang, Yi, et al. "An extension of spatial channel model with spatial consistency." *2016 IEEE 84th Vehicular Technology Confe*